Neonatal Porcine Islet Xenotransplantation: Non-invasive in vivo imaging and basic islet biology

by

Kieran Creighton Purich

A thesis submitted in partial fulfillment of the requirements for the degree of

Master of Science

Department of Surgery

University of Alberta

ABSTRACT

Islet transplantation has been proven as a successful clinical therapy for diabetes; however, its widespread use is limited by multiple factors including a shortage of human donors, the need for long term immunosuppression and difficulty with graft monitoring post transplantation. Pig islet xenotransplantation is a promising solution to several problems faced by islet transplantation as it would directly address the limited number of islets available for transplantation and provide a tissue source deemed more appropriate for genetic experimentation. Significant research has been completed on genetic modification of pigs to optimize their tissues for transplantation; however, minimal previous work has been completed looking at the basic biology and development of pig islets, limiting the transition from animal models to the clinical realm.

In this thesis, we perform two series of experiments exploring some of the aforementioned challenges. In Chapter 2 we study a novel synthetic polymer, polyvinylpyrrolidone (PVP), which is used in the imaging of islets following transplantation. Polyvinylpyrrolidone has previously proven useful in the coating of superparamagnetic iron oxide (SPIO) nanoparticles (deemed PVP-SPIO nanoparticles) which can then be utilized in the labelling of cells, including mouse islets. These labelled islets allow for greater resolution on MRI, allowing the ability to follow islet grafts post transplantation in animal models. We are the first to experiment with PVP-SPIO in pig islets, and we show that it can be used to label neonatal pig islets, improving their contrast on MRI imaging. We also demonstrate that PVP-SPIO can be used to improve contrast on MRI imaging when the islets are situated under the kidney capsule in a diabetic mouse model, while not impacting the islet's ability to reverse diabetes. Furthermore, our data demonstrates an expansion of PVP-SPIO labelled islet grafts on MRI

following graft rejection, suggesting PVP-SPIO nanoparticles may hold promise in the ability to non-invasively detect graft rejection.

In Chapter 3, the primary chapter of this thesis, we assess the gene and protein expression of neonatal pig islets in the early post-natal period by quantitative reverse transcription polymerase chain reaction (RT-qPCR) and Western immunoassay. Primary pathways of interest span cell-cell adhesion and insulin secretion. Specific molecules of interest include: adhesion molecules E and VE-cadherin as well as glucose transporter GLUT-2, GTPase RAC1 and SNAP25 a protein involved in insulin exocytosis. We perform an exploratory analysis identifying trends seen in different ages of neonatal pigs across different days in culture.

Following gene and protein assessment, we assess islet function, demonstrating differences in the insulin secretory capacity of islets obtained from different ages of neonatal pigs. We examine islet function in vitro as well as in vivo using a diabetic mouse model. Specifically, we compare islets obtained from 1-day-old neonatal pigs to those obtained from 3 and 7-day-old neonatal pigs, identifying differences in function, highlighting the potential of dysregulated function in islets obtained from 1-day-old pigs, suggesting that they may not be the optimal age for neonatal pig islet recovery. Finally, in an attempt to connect cell-cell adhesion and the insulin secretion pathway, we demonstrate the loss of islet function at high glucose conditions when islets are treated with anti E-cadherin monoclonal antibody, suggesting its importance in stimulated insulin secretion. As far as we are aware, the importance of E-cadherin in neonatal pig islets has not been previously reported.

This study serves as a starting point, and further studies to investigate the physiologic pathways which direct early neonatal pig islet cell development are warranted.

PREFACE

This thesis consists of work performed by Kieran Purich, the collaborators listed in the Acknowledgements section and the co-authors stated in Chapters 2 and 3. The research within this thesis has been approved by the University of Alberta's Research Ethics Board under the AUP of 00000326, titled: "Pancreatic islet cell transplantation and breeding colony", which was initially approved on April 18, 2013 and has been kept up to date throughout the project.

Chapter 2 is adapted from: Purich, K, Cai, H, Yang, B, et al. MRI monitoring of transplanted neonatal porcine islets labeled with polyvinylpyrrolidone-coated superparamagnetic iron oxide nanoparticles in a mouse model, *Xenotransplantation*. 2022; 29:e12720. https://doi.org/10.1111/xen.12720 which was published in January 2022.

Kieran Purich compiled, reviewed and analyzed the data, and was the primary author of the manuscript. Haolei Cai, Bin Yang, Zhihao Xu, Anthony G. Tessier, Adnan Black, Ryan Hung, Eric Boivin, Baoyou Xu, Ping Wu, Bo Zhang and Dong Xin all contributed by performing experiments and collecting data. Biagio Gino Fallone, Ray V. Rajotte, Yulian Wu and Gina R. Rayat were involved in study concept, design and supervision. All co-authors approved the final version of the manuscript.

Chapter 3 describes the primary project of this thesis and is adapted from the manuscript titled: "Exploring the postnatal development of pig islets: an in vitro model" which is in preparation for submission to the journal Xenotransplantation. Kieran Purich was involved in the planning and performance of all experiments, collection and analysis of data and was the primary author of the manuscript. Josue R. Silva, Wenlong Huang, Jim Wickware, Thomas Williams and Adnan Black provided assistance performing experiments and analyzing data. Gina R. Rayat created the research question, assisted with experimental design and data collection and was the primary supervisor for the project. Dan Schiller and Dave Bigam were involved in critical appraisal of the work and supervision. All co-authors will approve the final version of the manuscript before submission.

ACKNOWLEDGEMENTS

I would first like to extend my deepest gratitude to my supervisory committee consisting of: Dr. Gina Rayat, Dr. Dan Schiller and Dr. David Bigam. I would not have been able to complete my graduate studies without your support. Thank you for being role models and mentors during my academic journey.

I would also like to thank Dr. Jeevan Nagendran for serving as my examiner. I appreciate your time and you giving me the opportunity to discuss my findings in a formal setting.

To my lab members: Josue Silva, Jim Wickware, Daniel Skubleny, Thomas Williams and Adnan Black, thank you for all your assistance with my experiments and scientific discussion which has been instrumental in my learning. I would also like to extend my appreciation to the support staff outside the lab, specifically, Tracey Zawalusky and Nicole Lahutton who have helped me navigate the many demands of my graduate degree.

Finally, I would like to thank my funding sources including the Clinical Investigator Program, the University of Alberta's Masters Entrance Scholarship, the Canadian Institutes of Health Research Canadian Graduate Scholarship and the Alberta Graduate Excellence Scholarship. Without the generosity of these sources, I would not have been able to pursue my graduate degree.

TABLE OF CONTENTS

LIST OF TABLES

LIST OF FIGURES

LIST OF ABBREVIATIONS

AHXR – Acute humoral xenograft rejection

BPA – Bisphenol A

CAMs – Cell adhesion molecules

CK7 – Cytokeratin 7

CTLA4 – Cytotoxic T-lymphocyte associated protein 4

DKA – Diabetic ketoacidosis

DM – Diabetes mellitus

EDC – Endocrine disrupting chemicals

EDTA – Ethylenediaminetetraacetic acid

ESRD – End stage renal disease

GWAS – Genome wide association studies

T2DM – Type 2 diabetes mellitus

IBMIR – Instant blood mediated inflammatory reaction

IDDM – Insulin dependent diabetes mellitus

IHC – Immunohistochemistry

IL2RA – Interleukin 2 receptor subunit alpha

IXA – International Xenotransplantation Association

MHC – Major histocompatibility complex

MRI – Magnetic resonance imaging

NHP – Nonhuman primate

NPI – Neonatal pig islets

NOD – Non obese diabetic

PERV – Porcine endogenous retrovirus

PET – Positron emission tomography

PM – Plasma membrane

PVP – Polyvinylpyrrolidone

shRNA – Short hairpin RNA

SKP – Simultaneous kidney pancreas

SNAP25 – Synaptosomal associated protein of 25 kDA

SNARE – **SNA**p **Re**ceptor

SPECT – Single-photon emission computerized tomography

SPIO - Superparamagnetic iron oxide

T1DM – Type 1 diabetes mellitus

TF – Tissue factor

VEGFR – Vascular endothelial growth factor receptor

WHO – World Health Organization

Chapter 1 General Introduction

1.1 Diabetes mellitus

Diabetes mellitus (DM) or diabetes, is a group of common metabolic disorders that result in hyperglycemia[1]. The physiology behind diabetes is complex, but is primarily defined by a deficiency in the production or function of insulin[1]. Patients with diabetes have altered sugar, lipid and protein metabolism, leading to a persistent state of hyperglycemia, which places them at risk for acute and chronic life altering complications affecting multiple organ systems[2]. Beyond the impact on the individual, diabetes has a profound effect on society, as approximately 400 million people worldwide are affected by diabetes, leading to significant individual and societal costs[2,3]. In Canada alone, the estimated cost of diabetes and its associated complications amount to billions of dollars every year[4].

1.1.1 Pancreas anatomy, embryology and physiology

The human pancreas is a primarily retroperitoneal organ found in the upper abdomen. It is a blind ended structure with numerous narrow matrices converging at a central collecting duct, known as the Duct of Wirsung, which joins the common bile duct and releases pancreatic secretions into the duodenum through the ampulla of Vater[5] (**Figure 1.1**). The pancreas provides both vital exocrine and endocrine functions[6].

Embryologically, the pancreas forms from common progenitor cells that bud from gut endoderm. Upon exposure to different chemical stimuli these cells differentiate into ductal, endocrine (islets) and exocrine (acinar) cells[7]. Basic pancreas and islet biology have been described in the academic literature for both humans and rodents; however, details are lacking for most other mammalian species, including pigs, our model of interest. In humans, pancreatic endocrine cell development, known as isletogenesis, is known to primarily occur in the second trimester, with the first endocrine cells appearing at around 8-9 weeks of development and remodeling of these clusters of cells continues through late gestation and early childhood[7]. Early islet cells are closely associated with ductal epithelium, suggesting the presence and differentiation of precursor cells[8]. We suspect a similar process takes place in other mammals

and this hypothesis is supported by previous work identifying endocrine precursor cells in pigs through immunohistochemistry (IHC) using the primary antibody cytokeratin 7 (CK7)[9,10].

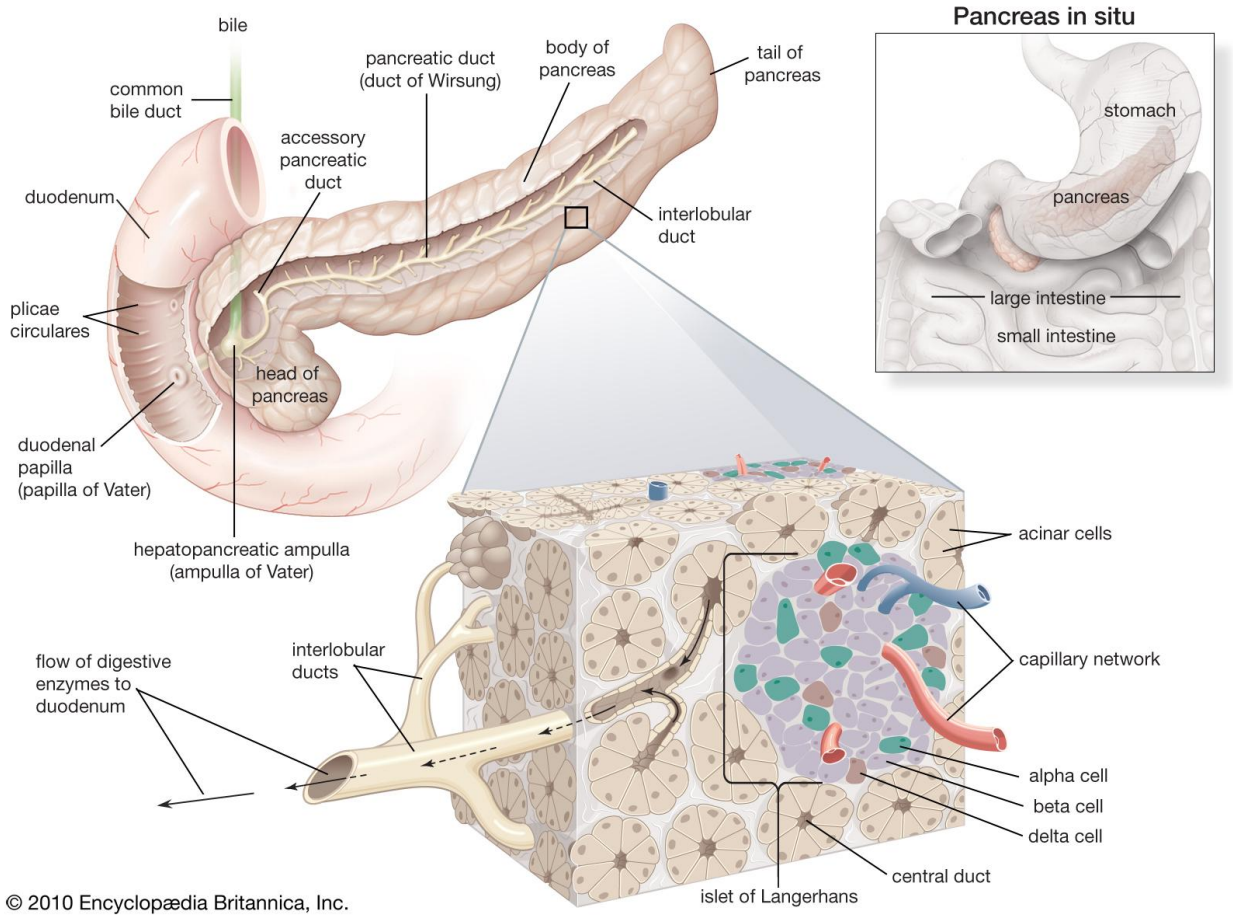

Figure 1.1: Macro and microstructure of the human pancreas and islet cells. Image obtained from Encyclopaedia Britannica[5]

Looking at the pancreas from a functional standpoint, it is separated into two main physiologic groups of cells, endocrine and exocrine. The islets of Langerhans, also known as islets, are clusters of endocrine cells in the pancreas, named after the German pathologist, Paul Langerhans, who first identified them in 1869[7,11,12]. There are five main types of islet cells, characterized by the hormone they produce. These being: alpha cells, which secrete glucagon, beta cells, which secrete insulin, delta cells, which secrete somatostatin, gamma cells, which secrete pancreatic polypeptide and the epsilon cells, which secrete ghrelin[7]. Islets are highly interconnected, allowing for tight regulation of blood glucose and other metabolic functions. Islets can influence each other by paracrine and autocrine functions[13]. As mentioned earlier, the

pancreas also hosts key exocrine (acinar) cells, which make up at least 80% of the volume of the pancreas, and secrete a variety of enzymes for digestive purposes[7].

1.1.2 Classifications and presentations of diabetes mellitus

Diabetes covers a heterogeneous group of metabolic diseases which all exhibit the hallmark feature of elevated blood glucose. Diagnostically, diabetes is defined by the World Health Organization (WHO) as a hemoglobin A1C value of greater than 6.5%, a fasting plasma glucose of >7mmol/L or a two hour plasma glucose level of >11.1mmol/L after an oral glucose tolerance test consisting of a 75 gram oral glucose load[3]. Clinically, due to the hyperglycemia, these patients present with symptoms including weight loss, fatigue, polyuria, polydipsia and polyphagia[14,15]. Patients with diabetes are further classified based on the etiology and physiology behind their disease[1]. The majority of patients with DM are separated into two categories: type 1 diabetes mellitus (T1DM) and type 2 diabetes mellitus (T2DM), characterized by the absolute deficiency of insulin and the relative deficiency of insulin respectively[1]. It is estimated that in between 5 and 10% of patients with diabetes are affected by T1DM, which is the focus of this thesis[2].

T1DM, colloquially and previously known as insulin dependent diabetes (IDDM), or juvenile onset diabetes, is generally classified as an autoimmune disease in which the beta cells of the pancreas have been destroyed by the patient's own immune system[1]. Alternatively, T2DM is caused by insulin resistance or a relative insulin deficiency[1]. Patients with T2DM do not have the significant loss of insulin producing beta cells seen in T1DM[14]. T2DM and other, less commonly encountered forms of diabetes go beyond the scope of this thesis and will not be discussed further.

1.1.3 Etiology of type 1 diabetes

The trigger behind the autoimmune destruction of beta cells seen in T1DM is likely multifactorial, encompassing genetic, environmental and immunologic components. Previous literature supports such and demonstrates that certain ethnic groups are predisposed to T1DM due to their genetics, and the penetrance of these T1DM associated genes appear to be directed

by environmental factors[16–18]. This multifaceted etiology is further supported by twin studies which demonstrate that both genetic and environmental components impact an individual's likelihood to express a diabetic phenotype[19].

With the increase in genetic processing over the past decade, several genome wide association studies (GWAS) have been completed in the attempt to define genes associated with increased diabetic risk[20,21]. Multiple specific immune related genes have been associated with diabetes including major histocompatibility complex (MHC) class 2 region genes, cytotoxic T-lymphocyte associated antigen 4 (CTLA-4) and interleukin-2 receptor alpha chain (IL2RA). It appears that the genetic influence in the etiology of T1DM span beyond the systemic immune system, as many identified genes of interest are expressed directly within the beta cells, suggesting their influence on the function and response of beta cells to the immune system[21–24].

In addition, multiple environmental triggers have been correlated with the incidence of T1DM. Areas of interest include: endocrine disrupting chemicals (EDCs), viral infections and gut microbiota[21,25–27]. EDCs are compounds which have been found to cause interference and changes within the endocrine system[25]. The most common EDC is bisphenol (BPA) which is found in plastics and appears to impair macrophage phagocytosis and promote development of T1DM in mouse models[25]. Enteroviruses also appear to play a role in triggering T1DM, and studies have shown a higher prevalence of enterovirus RNA in the blood of recently diagnosed T1DM patients[26]. Currently it is felt that microbes likely act as modifiers towards the development of T1DM, possibly through the generation of inflammation and immune cell infiltration within the islets known as insulitis[21]. Looking beyond acutely infectious microbes, recent study has also shown that individuals with T1DM have less diverse gut microbiota than their unaffected counterparts, and this difference exists prior to the development of T1DM, suggesting its potential to play a role in T1DM onset[21]. Most studies on EDCs, viruses and gut microbiota yield heterogeneous results making it difficult to draw conclusions with confidence.

1.1.4 Complications of diabetes

Diabetic complications can be divided into two main categories, these being acute and chronic complications. Acute complications occur due to uncontrolled elevated blood glucose levels and can cause sudden metabolic deterioration[14]. In T1DM, absolute insulin deficiency

leads to the inability to process glucose to be used as fuel for the cell[14]. To maintain cell function, the body utilizes other pathways to create energy including lipolysis which if prolonged can lead to diabetic ketoacidosis (DKA). These patients present with severe, life threatening electrolyte abnormalities, acidosis, hypovolemic shock and cerebral edema[14,28].

Individuals with diabetes also suffer from chronic complications largely due to the toxic effects of hyperglycemia[29,30]. Microvascular complications include: nephropathy which can progress to end stage renal disease (ESRD) requiring dialysis, retinopathy which can lead to blindness and neuropathy which can lead to chronic ulcers requiring surgical management or amputation[14]. Macrovascular complications include ischemic heart disease, peripheral vascular disease and cerebrovascular disease[31]. Patients with diabetes are also immunocompromised and at risk for atypical infections. The reason for this immunocompromised status is multifactorial, and some of the involved mechanisms can be seen in **Figure 1.2**[32]. The impact on survival of these acute and chronic complications are significant and patients affected by diabetes have an 11 year reduced life expectancy compared to the general population[31].

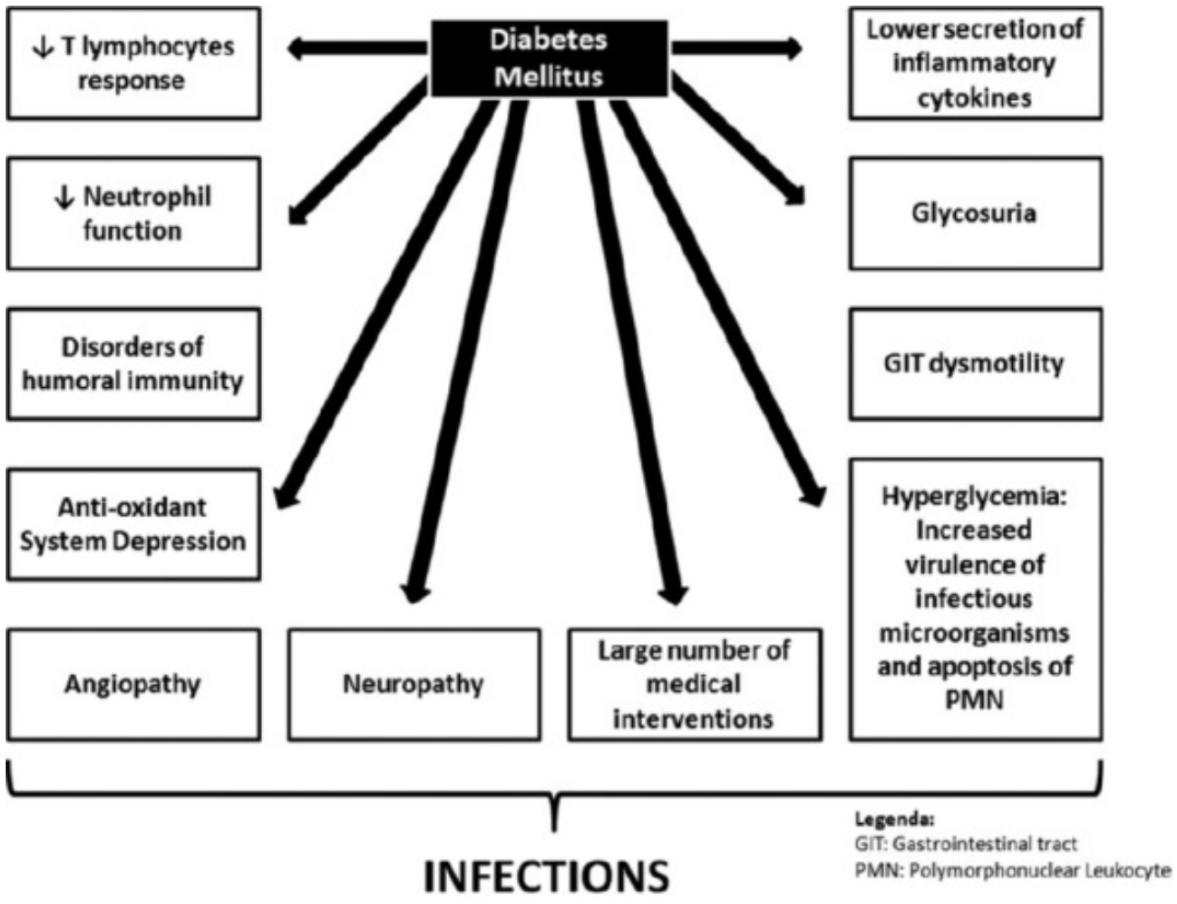

Figure 1.2: Possible mechanisms for immunosuppression seen in diabetic patients. Image obtained from Casqueiro et al., 2012[32]

1.2. Current treatments for type 1 diabetes

1.2.1 Insulin

Insulin, the essential anabolic hormone produced by the pancreas, is the mainstay of T1DM therapy today. It was discovered in 1921 at the University of Toronto and changed T1DM from a fatal to a chronic disease[33,34]. Insulin was initially obtained from animal sources including pigs and cows until the 1980's when modified, synthetic forms of insulin became more available[35]. Today, most patients with T1DM use a combination consisting of both a long acting

(basal) insulin and additional insulin taken at mealtimes (bolus), which simulates the biphasic insulin secretion pathway seen in patients without diabetes[14,36–38].

Exogenous insulin therapy allows for the cellular uptake of glucose, and allows patients with T1DM to avoid many diabetic complications with good glycemic control[30,39]. However, insulin therapy is cumbersome, and requires a significant amount of patient responsibility and education as patients have to test their blood glucose and administer insulin by subcutaneous injection multiple times daily[40]. Over the past 50 years alternate methods of insulin replacement have been investigated, including transplantation of pancreata or islet cells, continuous subcutaneous insulin infusion by insulin pumps, as well as the concept of an artificial pancreas which connects continuous glucose monitoring to an insulin pump allowing for continuous adjustment to blood glucose levels[41,42]. These methods are not currently available to all patients with T1DM due to cost and accessibility.

1.2.2 Immunomodulation & cellular therapy

The concept of immunomodulation in T1DM stems from the idea that intervention early in the phase of autoimmune beta cell death could stabilize the remaining beta cells and prevent the onset of T1DM[43]. Multiple immune mediated pathways appear to play roles in beta cell death in T1DM, and this leads to the need for combination immunomodulatory therapy in order to prevent cell loss[43,44]. Cellular targeted therapy to induce immunomodulatory properties within beta cells specifically for their preservation is another prominent field of research[44]. To this point, despite a variety of trials, there is currently no clinically accepted method which uses immunomodulation to prevent T1DM progression with acceptable levels of immunocompromise[43].

1.2.3 Pancreas transplantation

Pancreas transplantation leading to insulin independence was first achieved in 1966 at the University of Minnesota by Drs. Kelly and Lillhei who transplanted a duct-ligated segmental pancreas alongside a kidney into a 28 year old patient with diabetes whom also had renal failure[45]. The patient's post-operative course was complicated by postoperative pancreatitis and a

pancreatic fistula; however, she developed insulin independence for 6 days. Unfortunately, during her hospital stay, the patient required removal of the transplant graft and died from a pulmonary embolus[45]. Experimental trials with different operative techniques were completed until the mid 1980s before consistent success[45]. Since conception pancreas transplants have often been completed alongside kidney transplantation in a method known as simultaneous kidney pancreas (SKP) transplant[45]. Success of pancreas transplantation is largely based on the length of insulin independence in the recipient. Current graft survival rates are 89% for SKP transplant at one year and 71% at 5 years[45]. Although pancreas transplantation can provide long term insulin independence it is a major, invasive surgical procedure that carries significant morbidity and mortality, and patients require lifelong immunosuppression.

1.2.4 Islet transplantation

Given islet transplantation is the focus of our study, we will discuss it further in **1.3**

1.3 Islet transplantation

1.3.1 History of islet transplantation

The first attempt at islet transplantation was recorded in 1893 where Dr. Watson Williams out of the Bristol Royal Infirmary in the United Kingdom attempted to implant pieces of sheep's pancreas into the subcutaneous tissue of a 13 year old child suffering from diabetic ketoacidosis (DKA)[46,47]. Unfortunately, the patient passed in the following days, but this attempt set the stage for further research. Eventual discovery of a feasible protocol allowing for treatment of diabetes by islet transplant emerged over 100 years later. Outlined in the article by Shapiro et al., 2000, a research group from the University of Alberta in Edmonton, Alberta, Canada achieved reproducible T1DM reversal and insulin independence for over one year in 7 out of 7 human patients[48]. This success was a dramatic change from previous islet transplantation results, in which only 8% of patients were deemed to be insulin free at one year[46]. An international trial using the same protocol demonstrated consistently improved results across a number of centers worldwide, with 44% of patients having insulin independence at 1 year after transplantation[49].

Islet transplantation is currently an approved clinical treatment for patients with T1DM with hypoglycemic unawareness who have failed less invasive therapies[50]. Over 1000 patients with T1DM had received islet transplantations between 1999 and 2015[51]. However, access and necessity of lifelong immunosuppression have limited its widespread use.

1.3.2 Anatomic sites & methods of islet transplantation

The current accepted method for islet transplantation is by infusion through the portal venous system. This allows islets to settle in the liver sinusoids, where they are able to detect changes in glucose homeostasis and release insulin directly into the portal vein[52] **(Figure 1.3)**. This technique is less invasive than solid organ transplant and carries a lower morbidity and mortality[52]. Islet transplantation by portal vein infusion still poses various challenges including procedural complications such as: bleeding, thrombosis, biliary leak and arteriovenous fistula[53]. In addition, clinicians are unable to easily retrieve islet grafts following infusion, and biopsies and graft monitoring is difficult[54]. Multiple other islet transplantation sites have been tried in animal and human models with varying success, including subcutaneous tissue, intramuscular, intraperitoneal, as well as under the kidney, spleen or liver capsule **(Figure 1.4)**[53].

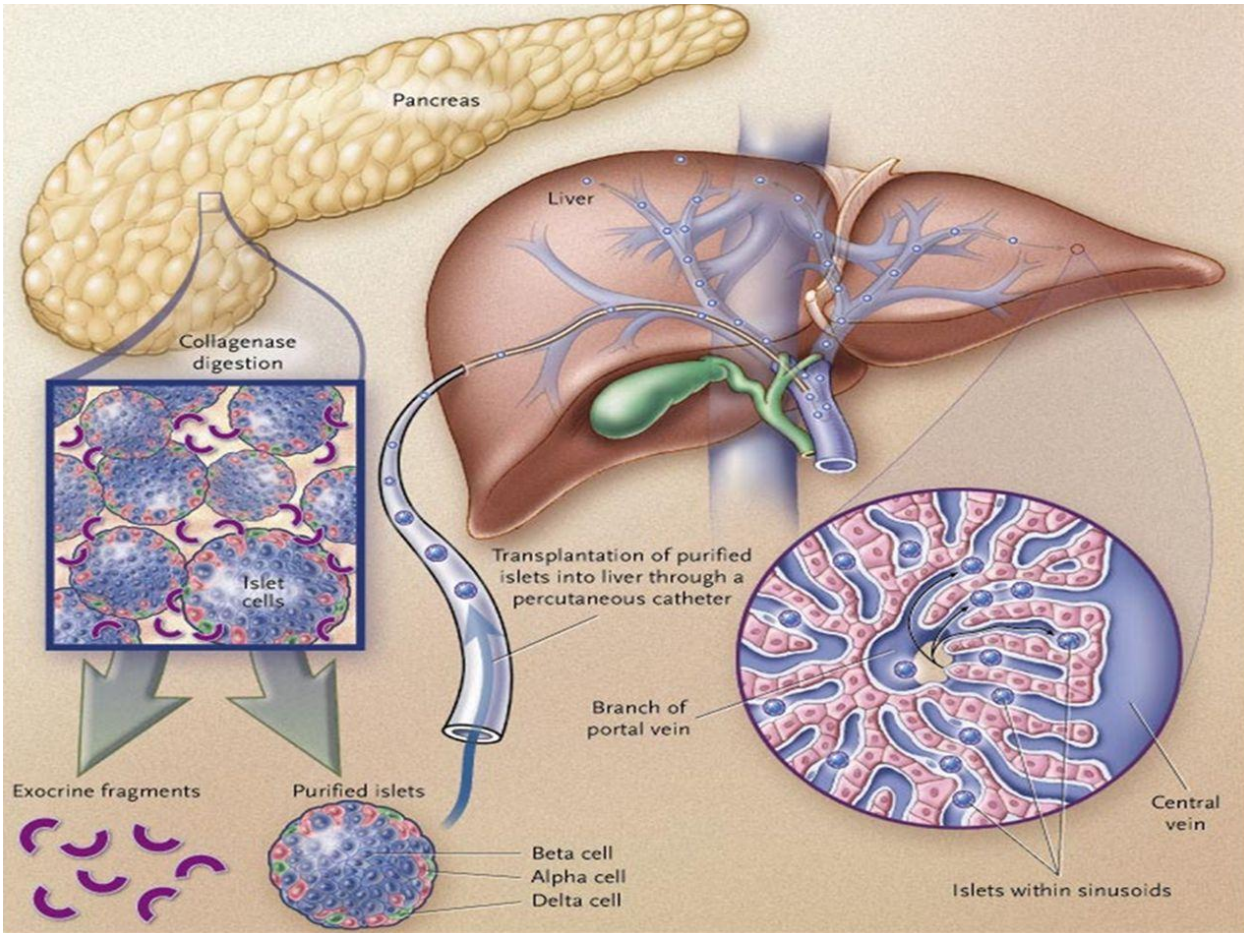

Figure 1.3: Conceptual diagram detailing the method of islet transplantation by infusion into the portal venous system. Image obtained from Robertson, 2004[52]

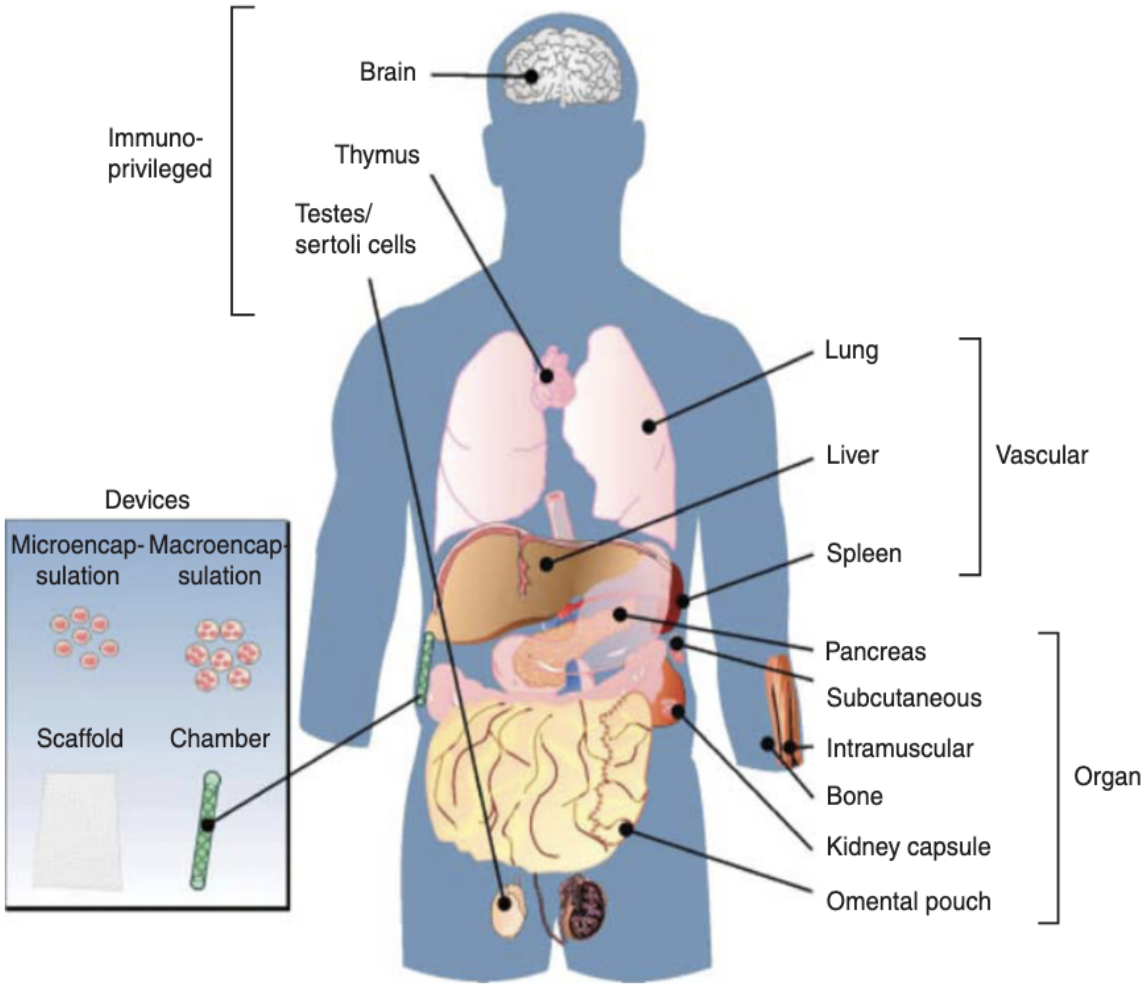

Figure 1.4: Alternative sites considered for islet transplantation. Image obtained from Merani et al., 2008[53]

The renal capsule is the most common transplant site utilized in rodents; however, it is limited in larger animals and humans due to anatomic differences and poor vascular supply[53,55]. Superficial areas utilized for transplant could solve the current difficulties associated with post transplantation biopsy access and facilitate graft retrieval following graft failure[54]. However, these superficial sites are poorly vascularized and lead to the systemic and not physiologic release of insulin. The volume of clinical data in alternative sites lags behind that of infusion through the portal venous system[54,56].

1.3.3 Major barriers to the application of islet transplantation

Current major barriers to clinical islet transplantation include: i) The number of donor pancreata available, which is inadequate to meet the demand for transplantation, ii) The need for lifelong immunosuppression following islet transplantation to try minimize immune rejection and islet graft loss and iii) The monitoring of cellular transplant grafts in vivo is difficult, which limits the ability to follow and understand graft health and islet loss[57–59].

1.3.3.1 Shortage of donor organs

A common problem amongst North American transplantation programs is the lack of donors. According to organdonor.gov, an American governmental tracking system, 39000 organ transplants were performed in the United States in 2019[60]. Despite this large number of transplants, the waiting list is reported at over 100000 individuals[60]. This is further compounded in the field of islet transplantation by the strict criteria for pancreas organ donation, and the need for high numbers of islets which are not usually available from one donor pancreas[48,61]. Additional sources of transplantable tissue would provide great benefit. Two potential sources of tissue being: the utilization of islets from different species, known as xenotransplantation, or the use of stem cells[62]. Xenotransplantation, the focus of the content within this thesis, will be further discussed in section **1.4**.

1.3.3.2 Immunosuppression and immune rejection

Understanding the immune mechanisms which impede the success of islet transplantation is critical for future research; however, this is not the focus of this thesis so will be covered briefly, with a focus on islet xenotransplantation. Common immune mechanisms involved in islet loss include: the innate immune system including the instant blood mediated inflammatory reaction (IBMIR), humoral rejection including both hyperacute rejection and acute humoral xenograft rejection (AHXR) and cell mediated rejection[63].

IBMIR has been well characterized as a significant, early mechanism that leads to significant islet graft loss following transplantation[64]. Xenotransplantation of pig islets into non-human primates leads to the activation of a significant immune response and deployment of factors involved in the clotting cascade[64–66]. IBMIR is not unique to xenotransplantation and also

occurs following human islet allotransplantation, likely due to the presence of immune triggers not normally in contact with the blood, including tissue factor (TF) and collagen[55,65,67]. This leads to significant cell loss immediately upon islet transfusion[55,65,68]. Much research has been done to try ameliorate this response, with recent studies showing that anticoagulants, antibodies against tissue factor (TF) and nicotinamide, a vitamin D derivative which inhibits TF can be used with some success[66,69–71].

Other immune mechanisms behind graft rejection seen in xenotransplantation can be categorized into three primary groups: hyperacute rejection, acute humoral xenograft rejection (AHXR) and cellular rejection[72,73]. Hyperacute xenograft rejection occurs quickly, within minutes to hours following transplantation and is due to natural, preformed antibodies in the recipient. These antibodies bind to epitopes displayed on transplanted xenogeneic endothelial tissues, activating complement, disrupting graft vasculature and leading to graft failure[73–75]. Carbohydrate alpha 1,3-galactosyltransferase, also known as alpha-Gal, is a major known xenoantigen that leads to hyperacute rejection[74]. This carbohydrate is expressed in most mammals including pigs; however, humans lack this enzyme and have preformed antibodies against it[63,73,74]. Different ages of pigs (neonatal vs adult) demonstrate different amounts of alpha-Gal, which may make neonatal pigs more susceptible to hyperacute xenograft rejection than adult pigs[9]. Recent studies have been working on creating genetically modified pigs that do not express alpha-Gal, and organs from these pigs have been tried in non-human primates. These genetically modified organs without alpha-Gal still experience graft rejection, deemed acute humoral xenograft rejection (AHXR), which appears to be a different process than hyperacute rejection and is thought to be related to non-Gal antigens[73,76,77]. Overall, humoral rejection, encompassing hyperacute rejection and AHXR appears to be more of a concern for solid organ transplantation than cellular islet xenotransplantation[78–80].

T-cell mediated rejection appears to be the most important immune response in the rejection of pig islet xenotransplants[63,78,79,81,82]. Understanding the T-cell immune response is critical to attaining what is considered the pinnacle of transplantation medicine, which is being able to transplant engineered tissues without having to put patients on aggressive immunosuppression[83]. Multiple T-cell mediated immune pathways, including the direct and indirect pathways of MHC class II recognition are involved in xenotransplant rejection[84]. Specifically, it appears that CD4+ T-cells play a major role and that in vivo depletion of CD4+

T-cells can prevent proislet xenograft rejection in mice[84]. Overall, the mechanisms behind the T-cell mediated response within xenotransplantation is complex, varies significantly from species to species and are not the primary focus of the projects later outlined in this thesis[83].

1.3.3.3 Monitoring islets after transplantation

To better understand the post transplantation course and rejection processes experienced by islet grafts, we must be able to monitor the transplanted grafts in vivo. Currently, clinical monitoring of islet grafts is primarily done through metabolic parameters including blood glucose, insulin levels and hemoglobin A1C, and abnormalities in these parameters often appear in late stages of graft failure[85,86]. An ideal mechanism for islet graft monitoring would be non-invasive and allow for early detection of graft stress which would help facilitate the rescue of islet grafts before complete graft failure. Many current high resolution imaging modalities pair methods used to label the islet cells such as bioluminescence, fluorescence, radionuclides or magnetic particles with a clinical method of imaging which spans ultrasonography, single-photon emission computerized tomography (SPECT), positron emission tomography (PET) and magnetic resonance imaging[87].

Of specific interest to our research group is labelling of islets using superparamagnetic iron oxide (SPIO) nanoparticles. Iron oxide nanoparticles exhibit a characteristic known as superparamagnetism, which allows for the magnetic field of these particles to randomly flip. This can be used to label cells and improve resolution on MRI, which can be used to monitor islet grafts[88]. This technology has been previously tested in multiple species including rodents, non-human primates and humans[89]. Beyond this, monitoring with SPIO labelled islets and MRI imaging has allowed previous islet graft salvage in rodent models[90]. As will be seen in Chapter 2, we use a novel synthetic polymer, polyvinylpyrrolidone, to coat SPIO nanoparticles which are then used to label neonatal pig islets, enhancing their contrast on MRI imaging[85,91].

1.4 Pig islet xenotransplantation

1.4.1 Pig islet xenotransplantation rationale and history

Pig islet xenotransplantation has long been touted as the potential solution to two of the major problems preventing islet transplantation from clinical application. Firstly, utilizing pigs as islet donors would solve the underlying issue of organ shortages, as pigs would be able to be bred specifically for transplantation purposes[92,93]. Secondly, xenotransplantation allows for more freedom in experimental genetic modification and could eventually allow for transplantation of islets without immunosuppression[92]. Of note, these benefits are not islet transplantation specific and xenotransplantation is being investigated for potential use in many other cellular and whole organ transplants[94].

Pigs are seen as one of the most promising models for islet xenotransplantation. From a species point of view, pigs have an excellent breeding potential, a short time to maturity, a high number of offspring as well as physiologic and anatomic similarities to humans[93] (**Figure 1.5**). Pig insulin has been used successfully to treat diabetes in the past, and was only replaced by exogenous synthetic human insulin in the 1980s[35,95].

	Pig	Baboon
Availability	Unlimited	Limited
Breeding potential	Good	Poor
Period to reproductive maturity	4–8 months	3–5 years
Length of pregnancy	114 ± 2 days	173–193 days
Number of offspring	5–12	1–2
Size of adult organs	Adequate	Inadequate*
Cost of maintenance	Significantly lower	High
Anatomical similarity to humans	Moderately close	Close
Physiological similarity to humans	Moderately close	Close
Experience with genetic engineering	Considerable	None
Risk of transfer of infection	Low	High

Figure 1.5: Comparison between pig and baboon tissue in the setting of xenotransplantation. Image obtained from Cooper et al., 2015[93]

Xenotransplantation would be advantageous for transplant surgeons worldwide as it would provide a markedly improved supply of organs, turn transplant surgery into an elective procedure and allow for the donor organ to be healthy at the time of procurement[93,94]. Challenges to the success of pig islet xenotransplantation stem largely from our inability to overcome the deleterious effects of the host's immune system on the islet grafts[96]. In addition, valid fears exist regarding the potential for the transfer of animal pathogens to humans[96–98].

Previous research in xenotransplantation of islets has made major progress, with animal models showing success in various species[99]. Of specific interest, multiple groups have demonstrated insulin free periods following pig islet transplant in non-human primates[100–102]. Many groups have received islet graft survival of over one year, with some achieving graft survival of longer than two years[100–102]. In humans, there have been 7 recorded trials of pig islet xenotransplantation with heterogeneous results, varying from the inability for islets to decrease insulin requirements to reported successes with authors suggesting the reversal of diabetes and improvement in diabetic complications[63,103,104]. However, it was largely felt that these clinical experiments were premature, and concerns existed with their validity and safety[105]. This led to the WHO regulation of xenotransplantation through a consensus statement released in 2004 followed by a consensus statement by the International Xenotransplantation Association (IXA) in 2009 outlining specific requirements for research groups to meet before participating in islet xenotransplantation trials in human participants[97,106]. Since 2009, the IXA has made regular updates to their guidelines to help direct appropriate research in xenotransplantation[98].

1.4.2 Ideal age of pig islet donors

Although pig islets are well supported as an excellent candidate for future xenotransplantation, there is much debate regarding what age of pig donors should be utilized, with physiologic and practical differences existing between the use of fetal pig islets, neonatal pig islets and adult pig islets[107,108]. Fetal and neonatal pig islets are more robust at the culture stage than adult islets[109]. However, they require a significant amount of time to mature, yield a relatively small number of islets and are not particularly effective in reversing diabetes in animal

models immediately upon transplantation[109]. Neonatal pig islets have a more robust insulin response than fetal pig islets, but still have a poor insulin secretory response to glucose initially and have delayed in vivo functionality when compared to adult pig islets[8,109]. Adult pig islets are able to function well in vitro and in vivo immediately upon isolation[109]. Due to the larger size of an adult pig pancreas, adult pigs lead to higher islet numbers upon isolation however, adult pig islets are delicate in culture and more susceptible to ischemic and hypoxic damage than their fetal and neonatal equivalents[109]. Practically, the housing of a pig from birth do adulthood in a pathogen free environment is costly and would be a barrier to large scale pig islet isolation.

1.4.3 System barriers to pig islet xenotransplantation

As previously mentioned, the International Xenotransplantation Association (IXA) exists to help develop guidelines to safely and ethically direct xenotransplantation related clinical research[97,98]. The IXA committee has attempted to help academic and corporate programs interested in xenotransplantation develop standardized requirements and allow for productive discussion between research groups. The IXA statement, which is updated regularly, provides dialog on multiple system barriers including: the research ethics of xenotransplantation, the requirements for the housing and use of donor tissues to minimize the risk of disease transmission, clinical outcomes required in NHP trials prior to partaking in human clinical trials and guidelines for informed consent[97]. In order to advance to clinical trials researchers must demonstrate robust, reproducible support from NHP models[97,108]. In addition to international guidelines set out by the IXA, there are regulations in each country involved in xenotransplantation at the national level to ensure research is being explored in a safe, ethical manner[77,110].

Given the potential for global catastrophe with trans species disease modification, it is appropriate that concerns are raised around such in xenotransplantation. In pigs, the primary viruses of interest are porcine endogenous retroviruses (PERVs), which are a class of viruses that are integrated in the pig genomic sequence[111] . These have been addressed in the IXA guidelines and the risks associated with such have been the focus of many previous studies, and researchers are able to breed some of the gene sequences associated with PERVs out of certain pig populations, as well as suppress or inactivate other PERV classes through RNA interference and

CRISPR-Cas 9 genetic modification[112–114]. Previous clinical trials have shown no evidence of PERV transmission associated with pig islet xenotransplantation[115,116]. A significant amount of screening and research has been done to try minimize risk from these viruses, and we must continue to remain vigilant due to the potential consequences[117].

1.4.4 Genetically modified pigs

Following some of the first experiments creating genetically modified pigs in 2003 much research has been done on different immunologic targets[76]. The first genetically modified pigs tailored to overcome hyperacute rejection possessed α-1,3-galactosyltransferase (alpha-Gal) knockout properties, and since then, multiple strains of transgenic pigs have surfaced, proving the feasibility of genetic editing[76,77]. Multiple strains of genetically edited pigs are currently commercially available, with various key immunologic molecules removed from their DNA[118].

1.5 Pig islet cellular biology

Despite the novel research related to pig xenotransplantation including gene editing, clinical trials and minimizing the potential risk of PERVs, little research has been done on the basic cellular biology of pig islets. Most academic knowledge behind the cell-cell adhesion and insulin secretion pathways existing in pigs is inferred from previous studies focused on rodents and humans. Although we acknowledge the possibility that these pathways are conserved in pig islets given their relationship on the mammalian phylogenetic tree, we feel that there is still necessary work which must be completed to have an appropriate amount of basic science knowledge to successfully bring pig islet xenotransplantation into the clinical realm. Based on previous study, the degree of phylogenetic disparity of islet grafts dictates the reliance on indirect CD4 T cell antigen recognition for rejection[119]. In other words, the mechanism(s) of cell-mediated immune rejection of an islet graft depends on the donor-recipient combination. Therefore, understanding the basic biology of pig islets not only help us in identifying molecules that are important for their survival and function but also for development of immune-based anti-rejection therapy. Addressing certain aspects of these basic pathways will be the focus of Chapter 3 of this thesis.

1.5.1 Pig islet endocrine cell distribution

Previous studies have demonstrated that islet architecture and function is different across species, raising concerns about the appropriateness of applying findings found in rodent or human models to pig islets[13]. Looking at islet architecture, previous research by Cabrera et al. found differences in the proportion and distribution of beta and non-beta cells in mice, primates and other mammal models[13]. Specifically, looking at the two most well studied models, mouse islets were found to have a higher proportion of insulin containing cells and lower proportion of glucagon containing cells than human islets at 77% vs 55% and 18% vs 38% respectively[13,120]. In terms of gross islet arrangement, rodent beta cells were found to be focused within the core of the islet whereas human beta cells have less of a defined topographic arrangement[13,120–123]. When comparing these findings to those patterns seen in pig islets, we see similarities between pigs and both rodent & human islets (**Figure 1.6**)[13,121]. This reinforces the idea that differences exist in the islet distribution in different mammals, suggesting that pig islets warrant species-specific investigation.

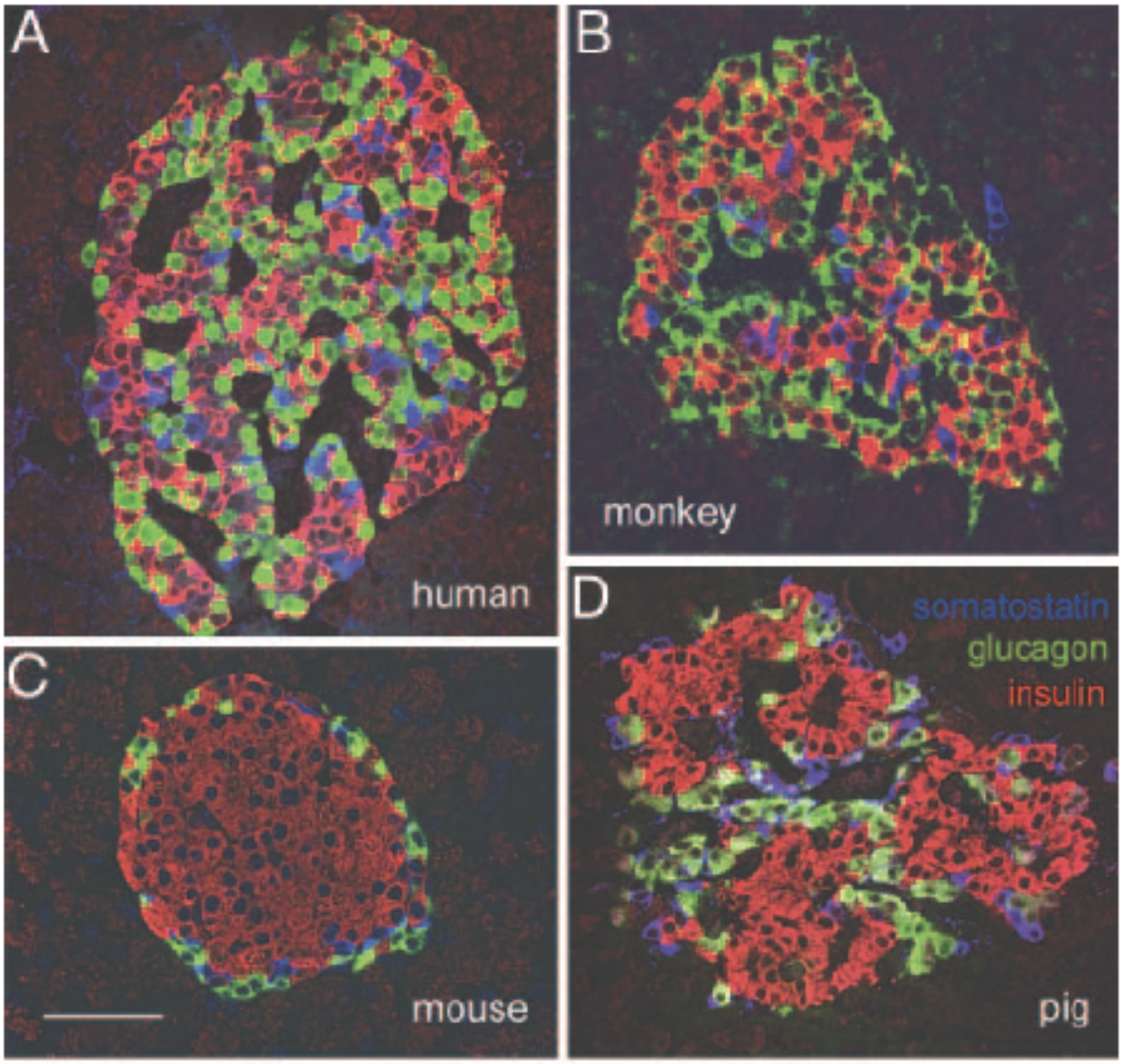

Figure 1.6: Immunofluorescence outlining interspecies differences between islets in different species. A) Human, B) Monkey, C) Mouse, and D) Pig. Red fluorescence demonstrates insulin, green fluorescence demonstrates glucagon, blue fluorescence demonstrates somatostatin. Image obtained from Cabrera et al., 2006[13]

Further exploring the current literature available that describes the endocrine cell distribution in pig islets, a comparative study by Kim et al. demonstrated 6 month old pigs to have a greater proportion of beta cells in their islets compared to humans or monkeys at 89% vs 64% vs 79%, respectively[123]. However, most previous data is descriptive or based on small sample sizes[123,124]. In addition, variation in endocrine cell distribution can likely arise due to the different physiologic and environmental conditions faced by each animal, and differences may be seen within individuals of the same species[13,121,123–125].

We believe that these specific arrangements seen within islets are driven by cell adhesion molecules (CAMs) directing the aggregation and organization of certain endocrine cells[120]. Pancreatic endocrine cells are known to communicate through paracrine signals, and the topographic distribution of the different endocrine cells within the islet is likely driven by such[13]. Of particular interest to our lab is the role of the calcium dependent adhesion molecules, Epithelial (E) and Vascular Endothelial (VE)-cadherin, which will be discussed further in section 1.5.2 and is the primary focus of the experiments outlined in Chapter 3. Outside of the endocrine cells, many other stromal elements are incorporated within the islets including vascular, connective, immune and nerve cells[126,127]. The conserved structure and intricate microenvironment is key to the function of islet cells[128].

1.5.2 Cadherins and their role in calcium dependent cell-cell adhesion

Cadherins are a family of transmembrane glycoproteins with a conserved fundamental motif, which are involved in calcium dependent cell-cell adhesion[129]. Within this family of proteins there are numerous subclasses characterized by their tissue of origin and selective cell-cell adhesion properties[129]. Cadherin proteins span the plasma membrane, possessing a conserved homophilic extracellular domain, and an association with actin bundles on the cytoplasmic side of the plasma membrane (PM)[129]. This allows for their role in cell-cell migration and cell junction formation[129]. E-cadherins in particular have been documented to play key roles in insulin secretion[38,128,130–134]. The intracellular pathway associated with E-cadherin includes numerous molecules including α-actin, β-catenin, γ-catenin, and p120; however, the discussion of their detailed interactions goes beyond the scope of this thesis[120,135–138]. Looking at the role of these molecules in islets, it appears that cadherins mediate adhesion within islets, and islet structure and function can be disturbed by antibodies against E-cadherin, proving its importance in insulin secretion[128,130]. This has however, not been confirmed in pig islets.

1.5.2.1 Epithelial cadherin

E-cadherin, is encoded by the gene *CDH1*, and is of interest in cellular transplantation and the development of islets and beta cells[128,134]. E-cadherin is intricately linked to the rosette shaped islet structure demonstrated in **Figure 1.7**, and appears to regulate the aggregation of

pancreatic beta cells in vivo, as inhibition of such can lead to the inability for beta cells to properly cluster in mouse models[129,133,134]. As is seen in **Figure 1.7**, as was outlined by Geron in 2015, E-cadherin is a key molecule in the maintenance of beta cell edges which allow for contact between beta cells and the surrounding vasculature[128]. Mechanistically, E-cadherin mediated adhesion appears to have an impact on glucose stimulated insulin secretion in mouse MIN6 beta cells and in human beta cells[128,139]. Jacques et al. demonstrated that the inhibition of E-cadherin expression in MIN6 beta cells using small hairpin RNAs (shRNAs) caused the islets to be less able to respond to stimulated insulin secretion, whereas the islets basal insulin secretion rate was not affected[139,140]. This finding was further supported in human islets by Geron et al., who demonstrated that islets were unable to increase the amount of insulin they secreted in response to high glucose conditions when E-cadherin was inhibited through the use of calcium chelator Ethylenediaminetetraacetic acid (EDTA)[128]. In addition, it appears that E-cadherin is also involved in the regulation of beta cell proliferation; with reduced beta cell proliferation at increased E-cadherin expression, suggesting its involvement in several aspects of pancreatic endocrine cell development[141]. No previous studies have been completed on the role of E-cadherin in neonatal pig islet development. Based on the results discussed above, outlining key studies completed in humans and mouse models, we hypothesize that E-cadherin likely plays an important role in early pig islet development and function, and this is further explored in Chapter 3 of this thesis.

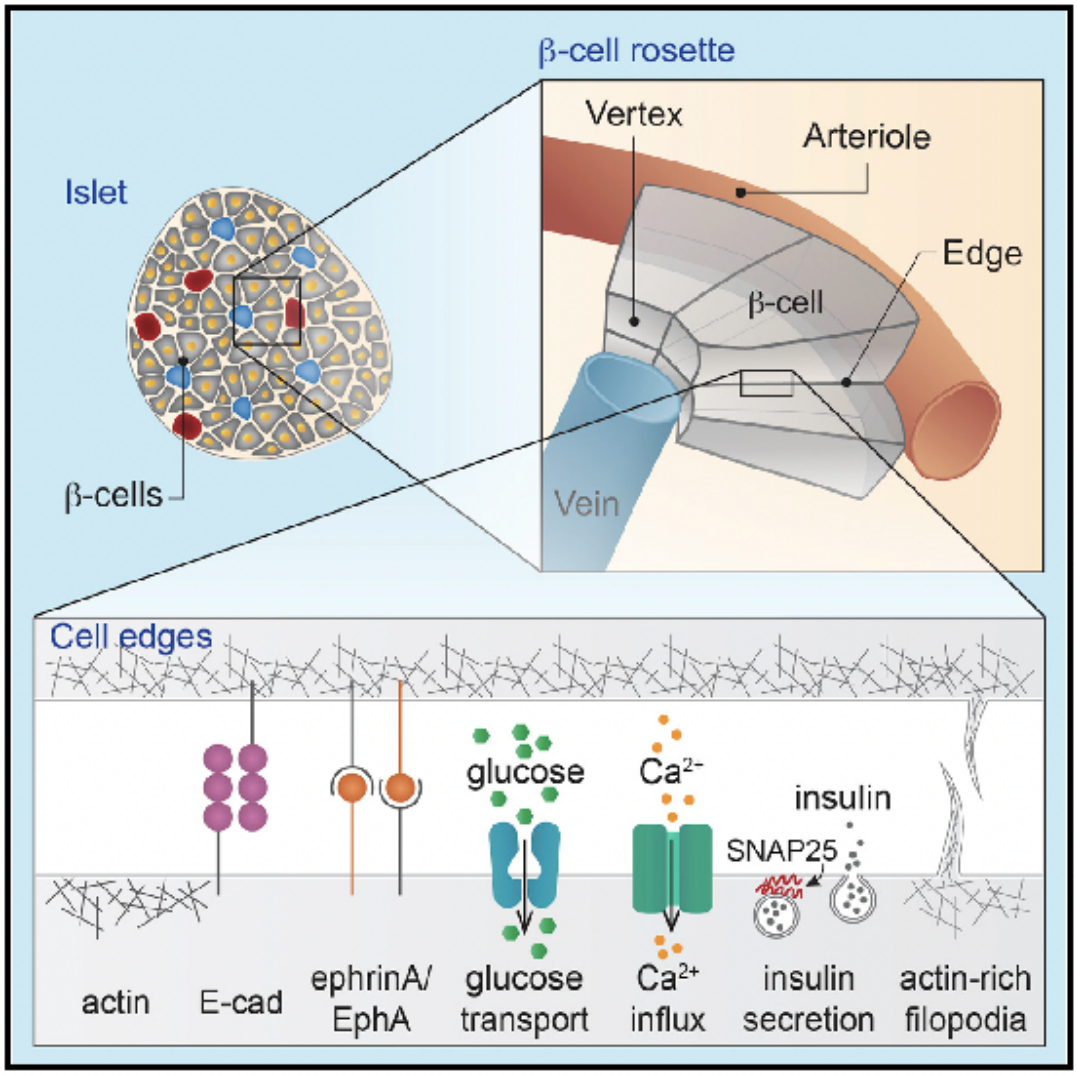

Figure 1.7 A) Schematic diagram outlining the rosette structure and conserved vascular orientation seen in beta cells within human and murine islets. Image obtained from Geron et al., 2015[128]

1.5.2.2 Vascular endothelial cadherin

VE-cadherin, is encoded by the gene *CDH5* and is critical for the formation of endothelial adherens junctions, important in angiogenesis[142]. VE-cadherin gradients appear to be regulated by notch/vascular endothelial growth factor receptor (VEGFR) regulated pathways and drive differential endothelial cell rearrangement allowing for vessel growth[143]. This has been demonstrated in vitro and in vivo in mouse models in which VE-cadherin abnormalities result in abnormal vessel phenotypes[143]. With the intricate vascular arrangements seen in islets and the

importance of vascularization and oxygenation of islets following transplantation, molecules like VE-cadherin are of great interest. In addition to maintaining endothelial adherens junctions, VE-cadherin molecules appear to also play a role in intercellular signaling related to contact inhibition, cell polarity and interactions with surrounding tissues, making them key to the understanding of cell-cell adhesion in islet transplantation[142]. Limited study on VE-cadherin has been completed in islet cells of any species; however, the expression of VE-cadherin appears to be increased in diabetic mice[144]. No previous studies looking at VE-cadherin expression in pig islets have been reported.

1.5.3 Insulin secretion pathway

Appropriate blood glucose regulation is critical for the maintenance of cellular function. The insulin secretion pathway appears to be relatively conserved in rodents and humans; however, few specific studies have been performed in pigs[145]. Briefly explaining the physiologic pathway, insulin is produced by the beta cells in the pancreas, and is secreted in a biphasic manner in response to blood glucose levels, a process which appears to be regulated through movement of ions by ATP regulated potassium channels and voltage-dependent calcium channels[146,147]. In the absence of glucose, potassium channels on the cell membrane of the beta cells allow potassium to flow outwards, leading to a negative membrane potential[147]. In high extracellular glucose conditions, glucose transporters including GLUT2, transport glucose molecules into the cell where it is broken down and transformed into ATP, triggering the closure of the voltage-gated calcium channels leading to a shift in membrane potential. This shift in membrane potential triggers the calcium channels to open, allowing for cytoplasmic Ca^{2+} to rise[146–149]. This influx of calcium triggers a pathway that prompts insulin granules to fuse with the plasma membrane, leading to insulin secretion[147]. The biphasic nature of insulin release appears to be due to two distinct populations of insulin granules, the readily releasable pool, which is immediately adjacent to the PM and the reserve pool, which is further from the PM and therefore less readily accessible[145,147,149]. After initial rapid release (first phase insulin secretion) insulin granules from the reserve pools are mobilized and recruited through ATP dependent processes which appear to involve the actin cytoskeleton[147,149]. The mobilization and release of insulin from these reserve pools, which hold the majority of the insulin granules (>95%) is

known as the second phase of insulin secretion[147]. The second phase is maintained until the stimulus from hyperglycemia is ameliorated[38]. During this biphasic process, numerous proteins play key roles, with many of them triggering structural changes in the actin cytoskeleton leading to insulin release[149]. Our molecules of interest within this pathway are highlighted in **Figure 1.8** and will be discussed further in the paragraphs below.

1.5.3.1 Actin cytoskeleton

The actin cytoskeleton plays a major role in the regulation of the cellular structure and the fusion and release of insulin granules with the PM[150]. It appears to have a two-fold role in insulin secretion, being able act as a barrier in preventing excess insulin granule access to the PM when not stimulated, while also assisting in the mobilization of insulin granules towards the plasma membrane during the second phase of insulin secretion[36,149,151]. This process of interactions between F-actin and insulin granules, is tightly regulated involving a variety of proteins, with two of particular interest to our research being Ras-related C3 botulinum toxin substrate 1 (RAC1) and Synaptosome Associated Protein of 25 kDA (SNAP25) which will be further discussed below[36].

1.5.3.2 GLUT2

GLUT2, also known as solute carrier family 2 (facilitated glucose transporter), member 2 (*SLC2A2*), is a transmembrane carrier protein that belongs to the GLUT family of glucose transporters[152,153]. GLUT2 is the primary glucose transporter in mice, and likely the tertiary transporter in humans[152,154,155]. GLUT2 is one of the best studied glucose transporters; however, has very heterogeneous expression across different mammals, even differing with age or diet within the same species[156–158]. Functionally, GLUT2 is a very efficient carrier for glucose and in mouse islets it has over 10 fold higher expression than the next highest GLUT transporter[152]. In humans *SLC2A1* (GLUT1) and *SLC2A3* (GLUT3) are suggested to be the primary transporters, being expressed at 2.8 and 2.7 fold higher than GLUT2[152]**.** In pigs, limited research has been done on such; immunohistochemistry based studies suggest that GLUT2 stains juvenile pig islet sections less vividly than seen in primates or rodents[159]. In addition, there are differences in the

GLUT2 amino acid sequences across species, with pigs being 87% identical to humans and 79.4% identical to mice[158]. No studies have been reported looking at GLUT2 in neonatal pigs.

1.5.3.3 RAC1

RAC1, also known as Ras-related C3 botulinum toxin substrate 1, is encoded by the *RAC1* gene[160]. It is a small Rho family GTPase, a class of molecule which binds guanosine triphosphate (GTP) and hydrolyzes it to guanosine diphosphate[161,162]. GTPases serve multiple roles in mammals and are common molecular switches for physiologic pathways directing cellular growth, cytoskeleton organization, signal transduction and activation of various types of protein kinases[161,162]. RAC1 is of interest in the research of islet cells due to its role in the mediation of insulin secretion from beta cells through F-actin remodeling[160,163,164]. RAC1 specifically, is expressed heavily in insulin sensitive tissues, and plays a role in insulin release by regulating actin cytoskeleton remodeling by the Cdc42-PAK1-RAC1 signaling pathway[160,163,164]. In vitro studies show that RAC1 is translocated to the plasma membrane in beta cells upon glucose stimulation, leading to the recruitment of secretory granules to the plasma membrane[149,165,166]. The process takes around 15-20 minutes, supporting that its role is related to the second phase of insulin secretion[36]. Furthermore, islets obtained from RAC1 knockout mice have marked impairments in second phase glucose mediated insulin secretion[165]. RAC1 is also known to stabilize adherens junctions and plays a role in endothelial function, indicating its possible involvement with cadherin molecules[142].

In pigs there has been minimal research on RAC1. There are limited studies observing the RAC1 GTPase in reproductive cells in both female and male pigs; however, it appears that no research has been published on the role of RAC1 in the pig insulin secretion pathway[167,168].

1.5.3.4 SNAP25

SNAP25, (Synaptosome Associated Protein of 25 kDA) encoded by the gene *SNAP25* is a presynaptic plasma membrane protein[169–171]. It is classified as a target soluble N-ethylmaleimide-sensitive factor (NSF) attachment protein receptor (t-SNARE)[171,172]. These proteins are key in the role of vesicle fusion to the plasma membrane, and play a role in exocytosis across various cell types[171,173]. In the endocrine pancreas, SNARE proteins allow for

the fusion of insulin granules with the plasma membrane of the beta cell[36]. SNAP25 is abundant in normal islets[174]. The docking of insulin containing granules occurs near areas of the PM that have high actin content, which suggest the interaction of the actin cytoskeleton with SNAP25[149]. There are no previous studies on SNAP25 in pig models related to insulin secretion or diabetes.

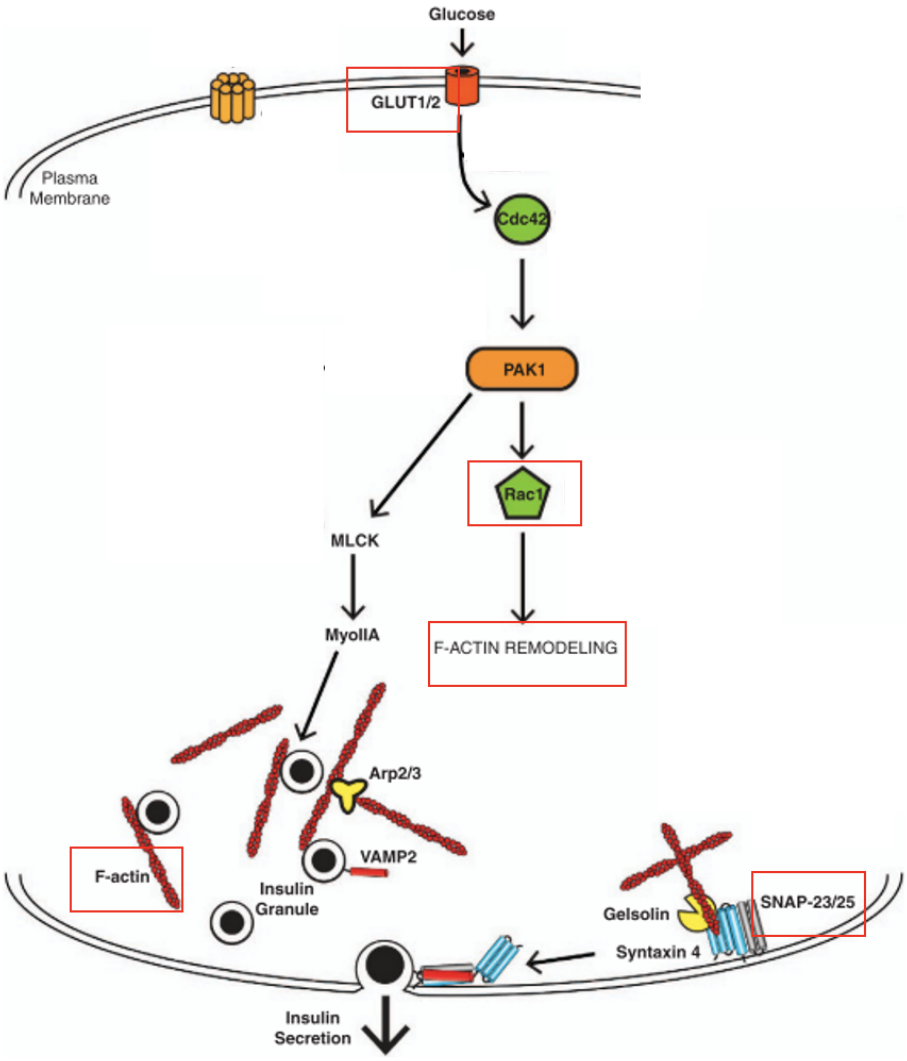

Figure 1.8: Insulin secretion pathway in human and mouse beta cells. Red boxes indicate proteins of interest. Image modified from Kalwat et al., 2013[149]

1.6 Objectives and outline

As previously mentioned, a variety of barriers currently limit the use of islet transplantation in the clinical setting. These include: the shortage of donor organs, challenges with immune rejection and long term immunosuppression and methods by which to monitor the

islets and their status following transplantation. Our lab focuses on research in the field of pig islet xenotransplantation, which could potentially provide a near unlimited tissue source for research and clinical islet transplantation.

The research outlined in this thesis focuses on two main topics. In our first series of experiments, we explore methods for non-invasive in vivo monitoring of islets following transplantation. Secondly, we explore early pig biology and development and try to characterize the role of cadherin cell-cell-adhesion molecules and their impact on the insulin secretion pathway in neonatal pigs.

Specifically, in Chapter 2, we perform in vivo experiments which validate the use of polymer coated SPIO nanoparticles for the labelling of neonatal pig islets to improve contrast on post-transplant MRI imaging. Our objective for this set of experiments was to demonstrate that the polymer polyvinylpyrrolidone (PVP) can be used to coat SPIO nanoparticles to enhance their resolution on MRI while not impacting the ability for the neonatal pig islets (NPI) to reverse diabetes in the diabetic mouse models used. Based on previous findings with SPIO molecules in human and rodent models, we hypothesized that PVP-SPIO labelling of NPI would improve the resolution on MRI while not impacting islet viability. In our manuscript, which has been published in the journal Xenotransplantation, we show that PVP-SPIO is a promising method by which to visualize NPI following transplantation.

Motivated by the lack of literature on pig specific physiologic pathways, we subsequently perform a series of experiments to explore pig islet cell-cell adhesion and signaling pathways, which may differ from the mechanisms seen in rodents and humans. In Chapter 3 we have identified specific molecules of interest spanning the cell adhesion and the insulin secretion pathways including: calcium dependent adhesion molecules, E and VE-cadherin, glucose transporter GLUT2, GTPase RAC1, which is involved in F-actin remodeling in islet cells, and SNAP25, a protein involved in insulin granule exocytosis. A better understanding of the changes in gene and protein expression of these molecules in NPI during in vitro culture and a correlation to differences seen in islet insulin secretory capabilities will potentially help us recognize methods by which we can improve the success of pig islet xenotransplantation.

Specific objectives targeted in Chapter 3 include: 1) The determination of gene and protein expression of E-cadherin, VE-cadherin, GLUT2, RAC1 and SNAP25 by neonatal islets during in vitro culture, 2) The determination of the insulin secretory capacity of islets obtained

from 1,3 and 7-day-old neonatal pigs on 7 days of culture and 3) Characterizing the impact of E-cadherin inhibition on the insulin secretory capacity seen in neonatal pig islets. We hypothesize that as neonatal pig islets develop in culture they will increase the expression of these key molecules which are known to be involved in the promotion of islet cell aggregation and function in species other than pigs[128,134,175]. We will correlate increases in expression of these molecules with changes in islet function across different ages of neonatal pigs, with the hope that these experiments shed light on which molecules should be targeted in genetic manipulation of pig islets to optimize them for transplantation.

Overall, the chapters of this thesis address two major challenges that are encountered in the field of pig islet xenotransplantation. A deeper understanding of the tissue that we intend to use for transplantation and methods by which to follow its progress in vivo following transplantation is fundamental for the translation of pig islet transplantation to the clinical realm.

Chapter 2 MRI monitoring of transplanted neonatal porcine islets labelled with polyvinylpyrrolidone-coated superparamagnetic iron oxide nanoparticles in a mouse model

Adapted from:

Purich, K, Cai, H, Yang, B, et al. MRI monitoring of transplanted neonatal porcine islets labeled with polyvinylpyrrolidone-coated superparamagnetic iron oxide nanoparticles in a mouse model, *Xenotransplantation*. 2022; 29:e12720. https://doi.org/10.1111/xen.12720

Abstract

Islet transplantation is a potential treatment option for certain patients with type 1 diabetes; however, it still faces barriers to widespread use, including the lack of tools to monitor islet grafts post-transplantation. This study investigates whether labelling neonatal porcine islets (NPI) with polyvinylpyrrolidone coated superparamagnetic iron oxide nanoparticles (PVP-SPIO) affects their function, and whether this nanoparticle can be utilized to monitor NPI xenografts with magnetic resonance imaging (MRI) in a mouse model. In vitro, PVP-SPIO labelled NPI in an agarose gel was visualized clearly by MRI. PVP-SPIO labelled islets were then transplanted under the kidney capsules of immunodeficient non-diabetic and diabetic mice. All diabetic mice that received transplantation of PVP-SPIO labelled islets reached normoglycemia. Grafts appeared as hypo-intense areas on MRI and were distinguishable from the surrounding tissues. Following injection of spleen cells from immunocompetent mice, normoglycemic recipient mice became diabetic and islet grafts showed an increase in volume, accompanied by a mixed signal on MRI. Overall, this study demonstrates that PVP-SPIO did not affect the function of NPI, that PVP-SPIO labelled islets were easily seen on MRI, and changes in MRI signals following rejection suggest a potential use of PVP-SPIO labelled islets to monitor graft viability.

1. Introduction

Islet transplantation is a promising therapeutic approach for type 1 diabetes mellitus (DM)[49,57,176]. However, barriers limiting the applicability of islet transplantation exist, including: the loss of islets post-transplantation, the shortage of islets from human donors, the need for lifelong immunosuppression, and the limited ability to monitor islet graft function in vivo[57,177]. Islet mass is lost at various stages of the transplantation process, including during isolation and purification from hypoxia and inflammation, and following transplantation due to poor revascularization, autoimmunity, instant blood mediated inflammatory reaction (IBMIR) and immunosuppressive drug toxicity. These insults cause decreased islet numbers, leading to eventual treatment failure[178–180].

In order to understand the mechanisms leading to islet cell loss after transplantation we require improvements in our ability to monitor and follow the condition of the transplanted islets. The ideal modality would be a non-invasive monitoring technique that would allow clinicians to adjust treatment regimens and rescue islets prior to cell death[177,181]. Current metabolic parameters routinely monitored include blood glucose, insulin, C-peptide levels, hemoglobin A1C and arginine stimulation tests. Changes in these markers appear at late stages of graft dysfunction, and do not reveal any insight to the mechanism of islet loss[86,90].

Several imaging methods have been proposed to monitor the islet graft following transplantation, including: positron emission tomography, optical imaging, magnetic resonance imaging (MRI) and ultrasonography. MRI following ex vivo islet labelling is advantageous as it avoids exposure to ionizing radiation and allows for high spatial resolution[181,182]. Yet, islets remain too small and similar in relaxivity properties to many endogenous tissues for direct visualization even with MRI. Therefore, previous research has tested various agents to label the islets to increase conspicuity for MRI visualization[59,183].

Superparamagnetic iron oxide (SPIO) nanoparticles are a commonly researched susceptibility effect-based MRI contrast agent used in molecular and cellular imaging, which confer dramatic sensitivity gains that allow imaging of small labelled cell populations that would ordinarily be inconspicuous and below the spatial resolution of MRI[184]. Multiple compounds with high stability, biocompatibility, and low toxicity have been developed based on SPIO, such as SPIO coated with dextran, 1-hydroxyethylidene-1.1-bisphosphonic acid (HEDP), and heparin[185–187]. SPIO nanoparticles have previously been used successfully for islet visualization on MRI in

both human and animal models[90,188,189]. Our group previously utilized a synthetic polymer, polyvinylpyrrolidone, to coat SPIO (PVP-SPIO) and demonstrated that mouse islets transplanted under the mouse kidney capsule can be visualized by 3T MR scan[91]. PVP-SPIO has excellent uptake and biocompatibility with islet cells, and when compared to Feridex, a FDA approved, commercially available SPIO contrast agent, PVP-SPIO demonstrated a better superparamagnetic effect while not affecting the long-term viability or function of the islet grafts[59,91,183]. There is limited previous research on this specific SPIO polymer.

Research related to the use of modified SPIO nanoparticles for the monitoring of transplanted islet grafts by MRI is ongoing. In vitro, isolated islets cultured in a medium containing SPIO enhanced contrast have allowed for islets to be detected by MRI[190]. In regard to in vivo studies, islets from various donor species have been labelled and imaged successfully with various SPIO contrast agents[59,181,191–195]. In humans, this technology has been proven, including in the study by Saudek et al. in which type 2 diabetic patients received ferucarbotran labelled islets by portal vein transplantation[196]. The islets were able to be visualized as hypo-intense spots in the liver that were able to be followed up with MRI for at least 24 weeks. Other recent studies demonstrate that the number of hypo-intense spots decreased with time, which appeared to be related to islet loss, providing support for the use of this technology in a quantitative manner[191,196,197].

Beyond the current obstacle of monitoring islet grafts post-transplantation, there is also difficulty obtaining adequate islet numbers for transplantation[198,199]. Xenotransplantation is an attractive option, which could serve as a limitless source of islets. Neonatal porcine islets (NPI) have many favorable characteristics for xenotransplantation[200]. Compared to adult porcine islets, NPI are less fragile after isolation, and have the capacity to resist inflammatory and hypoxia-induced apoptosis seen in early post-transplantation[201,202]. There is a paucity of studies utilizing SPIO agents to label NPI, and no previous studies utilizing PVP-SPIO to label porcine islets[193,203]. The aims of this study were to reveal how PVP-SPIO affects function of NPI in vivo, whether PVP-SPIO could be used with MRI to monitor NPI xenografts in the kidney capsule transplant site in vivo, and whether PVP-SPIO labelled islets would show quantifiable changes on MRI upon rejection.

2. Materials and methods

This research was approved by the University of Alberta's Research Ethics Board. The University of Alberta Animal Care and Use Committee approved all animal procedures.

2.1 Synthesis of PVP-SPIO

PVP-SPIO particles were synthesized by high temperature hydrolysis of chelate metal alkoxide complexes in liquid polyol as described previously[91].

2.2 Animals

Three-day-old Duroc/Landrace Large White F1-cross neonatal pigs (Swine Research Centre, University of Alberta, Edmonton, Alberta, Canada) were used as islet donors. Three-month-old male B6 *rag1 -/-* (C57BL/6-rag1$^{tm1/mom}$ [B6 rag1-/-], H-2^{b}) and male NOD.SCID-Gamma (NOD.Cg-*Prkdc*^{scid} *Il2rg*^{tm1Wjl}/SzJ) mice (Jackson Laboratory, Bar Harbor, ME, USA) were used as transplant recipients, in which some were rendered diabetic by a single intraperitoneal injection of streptozotocin (180mg/kg body weight; Sigma-Aldrich, St. Louis, MO, USA) 3 to 5 days before islet transplantation. Blood samples were obtained at least once a week by poking the tail vein with a 27G hypodermic needle to monitor blood glucose levels using a Life Scan One Touch Ultra Mini Meter (Life Scan, Burnaby, British Columbia, Canada). In this study, all diabetic mice before transplantation had two consecutive non-fasting blood glucose levels of more than 18mmol/l, which is our definition of hyperglycemia. Blood glucose levels less than 10mmol/l indicated successful islet engraftment and our definition of normoglycemia. Mice were fed standard laboratory food and cared for according to the guidelines established by the University of Alberta's Animal Care and Use Committee and the Canadian Council on Animal Care.

2.3 Neonatal porcine islet isolation and transplantation

Neonatal porcine islets were isolated as previously described[202,204]. In short, the pancreas from neonatal pigs was procured, placed in Hanks' Balanced Salt Solution (HBSS, Sigma-Aldrich), cut into small pieces, and digested with 1mg/ml collagenase XI (Sigma-Aldrich). Digested tissue was filtered through a 500-μm nylon screen then cultured for 7 days in Ham's F-10 Nutrient Mixture (Sigma-Aldrich) at 37°C, 5% CO_2 and 95% air. On the 7th day, islets were counted and labelled with PVP-SPIO for 24 hours. Islets appeared healthy and viable at the time of transplantation. 2000 IEQ of non-labelled or PVP-SPIO labelled NPI were transplanted under

the right and/or left kidney capsule of non-diabetic or diabetic mice as previously described[202,205,206]. This number of islets has been previously determined to be able to reverse diabetes in 100% of various mouse strains and has been previously used in our lab[119,204–206]. For diabetic recipients, islet engraftment was considered successful when blood glucose levels of these mice reached <10 mmol/l post-transplantation. Rejection of NPI xenograft in mice was defined as the first of two consecutive days of hyperglycemia (>10 mmol/l) and was confirmed by histological analysis of the graft.

2.4 Spleen cell isolation for adoptive transfer studies

Spleen from non-diabetic B6 and NOD mice (Jackson Laboratory, Bar Harbor, ME, USA) were procured and spleen cells were isolated by dissociation of spleen tissue using mechanical disruption between the rough ends of two glass slides and Lympholyte®-Mammal Cell Separation Media (CEDARLANE, Burlington, Ontario, Canada) following our standard protocol[119,206]. Approximately $25x10^6$ spleen cells were injected into the peritoneum of recipient mice once they established stable normoglycemia. Blood glucose levels of these mice were monitored until they became diabetic.

2.5 MR imaging

MRI experiments were performed with a 9.4T/21.5 cm horizontal bore magnet (Magnex Scientific, Oxford, UK). The magnet was interfaced to an NRC TMX console (National Research Council of Canada Institute for Biodiagnostics West, Calgary, Alberta, Canada). MR excitation and data acquisition were performed with a transmit/receive birdcage radiofrequency (RF) coil. Dead mice were placed in 50ml conical tube filled with formaldehyde solution. Live mice were anesthetized by isoflurane and vital signs were monitored when under scan. T2-weighted anatomic images were acquired using a spin echo (SE) acquisition technique with the field of view (FOV) = 27mm × 27mm, matrix size = 128 × 128, slice thickness = 0.5mm, TR = 3 s, and TE = 35 ms. The entire area of the graft, in some cases consisting of homogenous and heterogeneous components, was calculated manually by the radiology team, who contoured graft volumes of each MRI slice, using the raw unfiltered anatomical images multiplying the results by 1.1 to account for gaps in between slices and the resulting areas added together (example demonstrated in Supplementary Fig. 1).

MRI of islet phantom model

In a six well non-tissue culture plate, 1000 islet equivalents (IEQ) of NPI with varying concentrations (10, 30, and 50μg/ml) of PVP-SPIO solution were cultured overnight in physiological conditions. Unlabelled 1000 IEQ of NPI were also cultured in Ham's F-10 medium. An agarose (Sigma-Aldrich) phantom gel was created by setting 30ml of 3% agarose into a 50ml conical tube to provide a stable underlayer for a circular gel created in a 50ml conical tube cap. This circular gel, containing wells with the conditions of interest was lifted and placed within the 50ml conical tube, on top of the 30ml of agarose gel. Aliquots of non-labelled and labelled islets with various concentrations of PVP-SPIO, Ham's F-10 medium and PVP-SPIO (50μg/ml) only were transferred into the agarose gel containing wells. The tube was then filled with melted 3% agarose and allow to set for at least 15 minutes for MR imaging. In our case, with the 9.4T small animal magnet, the tiny size of the bore (a few cm) necessitated using a small 50ml conical tube, rather than some other approaches using beakers.

Imaging of PVP-SPIO labelled NPI in a mouse model

Aliquots of 2000 IEQ of non-labelled or PVP-SPIO-labelled islets were transplanted under the kidney capsule of mouse recipients. Initially, six non-diabetic B6 *rag -/-* mice were transplanted with PVP-SPIO (10, 30 and 50μg/ml) labelled islets under the right kidney capsule and unlabelled islets under the left kidney capsule. These mice were euthanized and imaged by MRI at 1 and 8 days post-transplantation to test the feasibility of visualization of NPI grafts in mouse recipients. To determine whether PVP-SPIO labelled islets can also be visualized in live mice, three non-diabetic B6 *rag -/-* mice were transplanted with PVP-SPIO (10, 30 and 50μg/ml) labelled islets under the left kidney capsule and unlabelled islets under the right kidney capsule. These mice were imaged by MRI at 2 and 9 days post-transplantation.

2.6 In vivo function of PVP-SPIO labelled NPI

To determine whether we can monitor the function of PVP-SPIO labelled islets and correlate this with the MR images of the islet grafts, four diabetic B6 *rag -/-* mice were transplanted with 2000 IEQ of 30μg/ml PVP-SPIO labelled NPI under the left kidney capsule, three of whom died due to complications of diabetes. Blood glucose levels of these mice were monitored at least

once a week. Once stable normoglycemia was achieved, cell reconstitution was performed and intermittent MRI scans followed until the islet graft was rejected by the reconstituted spleen cells. Subsequently, five diabetic NOD.SCID-Gamma mice were transplanted with 2000 IEQ of 30μg/ml PVP-SPIO labelled islets under the left kidney capsule. Their blood glucose levels were monitored weekly. After achieving stable normoglycemia, the mice were reconstituted with spleen cells from non-diabetic NOD mice. Their blood glucose levels were monitored at least once a week until the graft was rejected. Mice that were not reconstituted with spleen cells underwent MRI at 100 days post-transplantation followed by a survival nephrectomy. All mice returned to the diabetic state following either spleen cell reconstitution or nephrectomy and were euthanized.

2.7 Immunohistochemistry

Kidneys that contained the islet graft were procured at the end of the study and examined following our published protocol[204]. Paraffin-embedded kidney tissue sections were stained with guinea pig anti-porcine insulin antibody (1:1000 dilution; Dako Laboratories, Mississauga, Ontario, Canada), guinea pig anti-porcine glucagon antibody (1:5000 dilution; Dako Laboratories or Sigma-Aldrich), and mouse anti-human cytokeratin-7 (CK-7) antibody, a marker for pancreatic ductal cells (1:200 dilution, Dako Laboratories) for 30 minutes, followed by the addition of biotinylated goat anti-guinea pig IgG (1:200 dilution, Vector Laboratories, Burlingame, CA, USA) or biotinylated goat anti-mouse IgG secondary antibody (1:200 dilution, Jackson ImmunoResearch Laboratories, West Grove, PA, USA). Heat-mediated antigen-retrieval was utilized for CK-7 staining using a domestic microwave. Iron particles were identified by incubating the tissue sections with Perls Prussian blue solution (2% potassium ferrocyanide/4% hydrochloric acid: 1/1) for 30 min and tissue sections were counterstained with either Harris' hematoxylin and eosin or nuclear fast red (Pan Path B.V., Budel, The Netherlands)[91]. Cryopreserved tissue sections were stained with rat anti-mouse CD4 antibody (1:500; BD Pharmingen, San Diego, CA, USA) and rat anti-mouse CD11b antibody (1:300; BD Pharmingen) followed by biotinylated rabbit anti-rat IgG secondary antibody (1:200; Vector Laboratories). Cryopreserved tissue sections were counterstained with Harris' hematoxylin only. Avidin-biotin complex/horseradish peroxidase (Vector Laboratories) and 3, 3-diaminobenzidinetetrahydrochloride (BioGenex, San Ramon, CA, USA) were used to detect positive-stained cells (brown color).

2.8 Statistical analysis

Graft volumes were recorded as mean ± standard error of the mean (SEM). Due to the small sample size, we could not assume normality and therefore used the non-parametric Wilcoxon signed rank test. Statistical significance was assigned if the probability value (p) was less than 0.05 (two-tailed). Analyses were done utilizing GraphPad Prism Version 8.0.0.

3. Results

3.1 PVP-SPIO labelled islets in a phantom gel was detected by MRI

Since this was our first experience with imaging PVP-SPIO labelled porcine islets using MRI, we first determined whether we could visualize PVP-SPIO and PVP-SPIO labelled NPI in a phantom gel. PVP-SPIO and PVP-SPIO labelled islets appeared as hypo-intense regions on MRI of the phantom (Fig. 1A). While media or non-labelled islets did not show a hypo-intense signal. The size of hypo-intensity appeared to be concentration-dependent, with a greater proportion of the area appearing hypo-intense in the 50μg/ml PVP-SPIO labelled islets.

3.2 PVP-SPIO labelled NPI grafts under the kidney capsule could be visualized by MRI in euthanized B6 *rag -/-* mice

Having positive results from the phantom gel experiment we next determined whether MRI could visualize PVP-SPIO labelled NPI grafts under the kidney capsule of mouse recipients. Non-diabetic B6 *rag -/-* mice were transplanted with 2000 IEQ of PVP-SPIO labelled NPI under the right kidney capsule and 2000 IEQ of non-labelled NPI under the left kidney capsule. The mice were then euthanized and PVP-SPIO labelled islet grafts could be visualized as hypo-intense foci in both axial (Fig. 1B-1D) and coronal (Figure. 1E-2G) sections by MRI at both 1 (Fig.1) and 8 (Supplementary Fig.2) days post-transplantation. There was no obvious visible difference of MR hypo-intensity related to the concentration of SPIO at 30μg/ml compared to 50μg/ml. Non-labelled islet grafts under the left kidney capsule could not be differentiated from kidney tissue on MRI.

3.3 PVP-SPIO labelled NPI grafts under the kidney capsule could be visualized by MRI in live B6 *rag -/-* mice

We then determined whether NPI grafts labelled with various concentrations (10, 30, and 50µg/ml) of PVP-SPIO could be visualized by MRI in live B6 *rag-/-* mice at various time points post-transplantation. Non-diabetic B6 *rag-/-* mice (n=3) transplanted with PVP-SPIO labelled NPI and unlabelled NPI under the left and right kidney capsule, respectively were exposed to MRI on days 2 and 9 post-transplantation. MR imaging could visualize PVP-SPIO labelled islet grafts as hypo-intense foci in both axial (Fig. 2A-2E) and coronal (Fig. 2F-2J) cross sections. As previously observed in MRI scans of islet grafts in euthanized mice, there was no obvious visible difference of MR hypo-intensity related to the concentration of SPIO at 30µg/ml compared to 50µg/ml in live mice. Non-labelled islet grafts under the right kidney capsule could not be differentiated from the kidney tissue on MRI. The mice that received 30µg/ml and 50µg/ml PVP-SPIO labelled islets died post-imaging (at 2- and 9-days post-transplantation, respectively. The mouse that received 10µg/ml PVP-SPIO labelled islets survived the MRI procedures on both days (Fig. 2A, 2D, 2F, 2I).

3.4 PVP-SPIO labelled NPI grafts under the kidney capsule pre- and post-cell reconstitution in B6 *rag -/-* mice

Since the ultimate goal of this study was to monitor graft rejection of PVP-SPIO labelled NPI using MRI, we performed a proof of concept experiment where four diabetic immunodeficient B6 *rag -/-* mice were transplanted with 2000 IEQ of PVP-SPIO (30µg/ml) labelled NPI under their left kidney capsule and spleen cell reconstitution of these mice once stable normoglycemia was established. We first selected B6 *rag-/-* mouse in this experiment since we have previously used this mouse strain as recipients of NPI to confirm the function of the islets and spleen cell reconstitution to study the mouse immune response to NPI xenografts. Our intention was to monitor graft function and rejection by blood glucose measurements and MR imaging of the islet graft in recipient mice at several time points post-transplantation and cell reconstitution. Three B6 *rag -/-* mice became sick due to complications of diabetes and had to be euthanized within 9 days post-transplantation. The remaining mouse survived until the end point of the experiment and achieved normoglycemia at 84 days post-transplantation (Fig.3A). The first MR imaging was performed on day 29 post-transplantation when the mouse was still diabetic. At 100 days post-transplantation, the mouse maintained normoglycemia and the second set of MR imaging was performed. The following day, this mouse was injected with $25x10^6$ spleen cells from naïve B6

mice and blood glucose levels were monitored at least once a week. The mouse remained normoglycemic at 4 days post-cell reconstitution and the blood glucose levels began to rise thereafter, from 15.8 mmol/l to 25.3 mmol/l when the mouse was euthanized (Fig. 3A).

Serial axial (Fig. 3B-3F) and coronal (Fig. 3G-3K) MRI scans demonstrate the hypo-enhancing area signifying the islet graft. The size of the islet graft appeared relatively stable on MRI throughout the first 100 days following transplant and at 6 days post-cell reconstitution. However, we observed the appearance of somewhat enlarged grafts by days 13 and 27 post-cell reconstitution, which correspond to 114- and 128-days post-transplant, respectively (Fig. 3L). This correlated with the upward trend in blood glucose measured after spleen cell injection (Fig. 3A). Histological staining of the islet grafts from the reconstituted mice demonstrated very few insulin, glucagon, or CK-7-positive stained cells present (Fig. 4A-4L). However, Prussian blue was present at the graft site, indicating the presence of iron from PVP-SPIO label used (Fig.4G-4L). There were also significant numbers of $CD4^+$ T cells and $CD11b^+$ monocytes identified in the islet graft (Fig.4M-4P). In contrast, abundant insulin and glucagon but not CK-7-positive stained cells were detected in non-reconstituted B6 *rag -/-* mouse recipients of non-labelled NPI, which indicate that the islets have fully matured and were not rejected since there were no adaptive immune cells in the recipient mouse (Supplementary Fig. 3A-3L). Prussian blue was not detected in the islet graft of this mouse (Supplementary Fig. 3G-3L).

3.5 PVP-SPIO labelled NPI grafts under the kidney capsule pre- and post-cell reconstitution in NOD.SCID-Gamma mice

We were encouraged by the previous MRI results obtained in B6 *rag-/-* mice; however, due to the difficulties with mouse mortality following diabetes induction, we decided to attempt the same experiment with NOD.SCID-Gamma mice and reduce the time points for MR imaging. We have also used NOD.SCID-Gamma mice for immune cell reconstitution to study the immune response to NPI in a mouse model with autoimmune background. Five diabetic NOD.SCID-Gamma mice were transplanted with 2000 IEQ of PVP-SPIO (30µg/ml) labelled NPI under their left kidney capsule. Given we had determined that the graft volume remained relatively similar prior to reconstitution based on the previous results in B6 *rag-/-* mouse experiment, we decided to perform MR imaging at the time points of interest, this being once the mice achieved stable normoglycemia and within 4 weeks after spleen cell reconstitution. This time, all mice (n=5) survived until the end

of the experiment and achieved normoglycemia between 6- and 12-weeks post-transplantation (Fig. 5A). At 13 weeks post-transplant, three mice underwent MRI and were injected with $26x10^6$ spleen cells from non-diabetic NOD mice 5 days post-MRI. These mice became diabetic at 17 weeks post-transplant (23 days post-cell reconstitution) with blood glucose levels at 22.6mmol/l, 26.9mmol/l and 23.6mmol/l. Two mice were not reconstituted with spleen cells to serve as controls and underwent MR imaging at 14 weeks post-transplantation. Subsequent survival nephrectomy was performed one week post-MRI and these control mice reverted to their diabetic state with blood glucose levels at 24.5 mmol/l and 36 mmol/l, 5 days post-nephrectomy (Fig. 5A).

Serial axial (Fig. 5B-5F) and coronal (Fig. 5G-5K) MRI scans obtained prior to spleen cell reconstitution demonstrate the hypo-enhancing area signifying the islet graft. Subsequent enlargement of size of the islet graft post-spleen cell reconstitution is clearly demonstrated in the MRI scans shown in Fig. 6A-6F. Qualitatively, it can be seen that the islet graft became heterogeneous after injection with spleen cells and the islet graft grew in size post-cell reconstitution. Although this did not reach statistical significance, it was probably because the sample size was only 3 ($p=0.250$, Fig.6G).

Immunohistochemistry demonstrated very few stained-cells positive for insulin, glucagon and CK-7 in the cell reconstituted mice (Fig. 7A-7L, Supplementary Fig. 4A-4L and Supplementary Fig. 5A-5L) but were abundant in the non-reconstituted control mice (Fig.8, Supplementary Fig. 6, and Supplementary Fig. 7). As previously observed in B6 *rag-/-* mice, Prussian blue was present at the transplant site of PVP-SPIO labelled islets (Fig. 7G-7L and Fig. 8), but not non-labelled islets (Supplementary Fig. 7) indicating the presence of iron from PVP-SPIO used to label the islets. Majority of Prussian blue was identified in the vicinity of the islet graft of mice reconstituted with spleen cells. While double stained cells for Prussian blue and insulin or glucagon but not CK-7 were detected in islet graft of non-reconstituted control mice (Fig. 8). $CD4^+$ T cells and $CD11b^+$ monocytes were present in the islet grafts of cell reconstituted mice (Fig. 7M-7P, Supplementary Fig. 4M-4P and Supplementary Fig. 5M-5P), suggesting rejection and loss of function of the islet graft, which was supported by the blood glucose levels (Fig.5A).

4. Discussion

Real time monitoring of islet graft function following transplantation has been an ongoing clinical challenge. An ideal monitoring technique would be non-invasive and detect early changes in the islet graft. Our group has previously demonstrated that PVP-SPIO labelling provides excellent resolution on MRI, that it does not compromise the viability or function of mouse islet cells in vitro, and that it demonstrated a better superparamagnetic effect than the FDA approved label Feridex[91,207]. In our study, we demonstrate the ability for PVP-SPIO to be used with NPI, while not affecting their ability to reverse hyperglycemia in diabetic mice following kidney subcapsular islet transplantation.

Our in vivo models demonstrated clear 9.4T MRI visualization of PVP-SPIO labelled NPI transplanted under the kidney capsule, and the signal persisted throughout the study period, confirming stability of the label. The kidney capsule site was chosen specifically as it is advantageous as the transplanted islets are not exposed to the blood, IBMIR is decreased and there is less of an acute loss of beta cells upon transplantation, which is often seen in xenotransplantation[208]. Our study is the first to demonstrate the biocompatibility of this compound with functioning NPI. All diabetic NOD.SCID-Gamma mice attained normoglycemia between 6 to 12 weeks following transplantation. The delay in the reversal of the diabetes was attributed to NPI being immature at the time of transplantation, requiring subsequent differentiation in vivo prior to the reversal of diabetes[202]. Although the monitoring of beta cell mass would be an excellent addition to our study, the maturation of precursor cells leads to an increase in beta cell mass, which is ongoing at the same time as beta cell loss from immune response in mice reconstituted with spleen cells. This makes it difficult to quantify such, and will require a separate study. Nevertheless, our study clearly demonstrated that insulin and glucagon-positive stained cells were scarce in cell-reconstituted mice and abundant in non-reconstituted mice. From our results, it could be concluded that NPI functioned adequately when labelled with PVP-SPIO prior to transplantation. A previous study using PVP-SPIO demonstrates co-localization of Prussian blue staining for iron alongside staining for insulin in mouse islet cells[91]. In our study, we showed co-localization of Prussian blue staining with both insulin and glucagon. It is interesting to note that staining for CK-7 precursor cells did not co-localize with Prussian blue. Further study will have to be completed to identify more details regarding the staining patterns seen with NPI as they mature post-transplantation.

MRI scans revealed that PVP-SPIO remained localized at the site of islet grafts, with the size and signal of the graft staying constant prior to reconstitution and graft rejection (Fig. 3 and Fig. 5). Non-labelled NPI under the opposite kidney capsule did not demonstrate appreciable signal on MRI (Fig. 1 and Fig. 2). These results were consistent with our previous study and others' published reports[59,91,186,194]. We also investigated quantitative changes to the islet graft on MRI following reconstitution and graft rejection. The clinical applicability for PVP-SPIO remains in question, and there have been differing results across studies on whether or not visible changes in the signal on MRI using SPIO labelled islet grafts are indicative of graft status and function. This discrepancy may be due to the use of different SPIO nanoparticles, islets from different donor species and variation within the transplant models. Zacharovova et al. who performed experiments on syngeneic and allogeneic rat islets did not observe any difference between MRI signals of functioning islets and rejected islets in the kidney capsule transplant location[209]. This was explained by suggesting the SPIO nanoparticles move out of the islets into surrounding cells such as macrophages, limiting the potential for SPIO labelled nanoparticles to be used to monitor graft function[209]. These findings are not congruent with our results, as outlined in Fig. 3 and 5 which demonstrate an increase in graft size seen following islet graft rejection, as well as our group's previous and current findings that PVP-SPIO could be localized in insulin and glucagon-producing cells within the islet graft, respectively[91]. This is likely explained by Zacharovova et al. selecting much higher sensitivity T2*-weighted MRI sequences for imaging, which can detect even miniscule concentrations of residual SPIO, but at the cost of much greater susceptibility artifact and associated signal loss[209]. In contrast, we used T2-weighted imaging, which, despite lower sensitivity, had more than adequate sensitivity to detect our islet grafts at even the lowest labelling concentrations. With our T2-weighted imaging technique, we could more readily image pathologic processes leading to coexistent, superimposed T2 hyper-intensity in the same voxel volumes, such as edema in the setting of graft rejection associated inflammation. Our findings are more in keeping with data from Wang et al., who used a 6T MRI machine, T2-weighted imaging and calculated T2 relaxation times, to demonstrate quantitative detection of islets transplanted under the kidney capsule[191]. The differences seen amongst studies is likely at least partially due to different field strengths of MRI used for imaging, and it should be noted that clinical medicine does not routinely use some of these ultra-high field strength MRI systems due to possible health risks[210]. The ability to quantitatively detect islets in the subcapsular kidney transplant site is of

particular interest with recent arguments suggesting the site could be advantageous in clinical porcine islet xenotransplantation[208].

It should be noted that MRI monitoring of SPIO labelled islets transplanted in the liver demonstrate a different picture. SPIO labelled islets situated in the liver consistently demonstrated attenuated signals following rejection, and the decreasing number of islet-related hypo-attenuated MRI signals more clearly correlated with clearance of rejected islets[90,188,209]. SPIO particles released from rejected islets in the liver site do not persist long-term in the transplant area and cannot be detected by the MRI once rejection is complete, giving support to the use of SPIO labelling to monitor for graft rejection in portal vein islet transplant[191,209]. This difference in SPIO labelled islet metabolism in the liver may be due to increased exposure to blood supply and immune cells including Kupffer cells, which have previously been documented to uptake SPIO particles, as well as greater capacity for hepatic parenchymal turnover and regeneration, with presumably associated clearance[211].

Previous studies have observed and documented the process of rejection of NPI grafts under kidney capsule; however, imaging utilizing MRI, and the apparent expansion of graft volume has never been previously mentioned[206]. In our study, grafts enlarged in size post-reconstitution with associated development of heterogeneous T2 hyper-intensity, a common finding with edema (Fig. 3 and Fig. 5). Our findings on immunohistochemistry suggests that the mechanism behind this expansion in size is an influx of immune cells. We specifically looked at $CD4^+$ T cells and $CD11b^+$ monocytes/macrophages due to their importance in porcine islet xenograft rejection[206,212] We suspect that the death of islet cells by immune mediated rejection could also lead to edema and enlargement of the islet graft. The findings of our project differ from those of previous similar studies in a number of ways. We utilized 2000 IEQ, a larger amount than many previous studies, in addition, upon reconstitution our grafts experienced an immune response reacting to a xenogeneic graft. This potentially could result in a greater immune response in the host than would be encountered with an allogeneic islet graft, which may account for the visible increase in graft size upon rejection. Alternatively, the response of an enlarging islet graft on MRI following immune rejection may be a unique characteristic of NPI grafts. As previously mentioned, an ideal imaging modality for islet grafts would demonstrate changes prior to metabolic parameter changes, well before rejection and the return of hyperglycemia. Success with islet graft salvage following findings on MRI has been recently documented with other SPIO

agents in rat models[90]. These MRI findings could complement many technologies currently being explored for monitoring of immune rejection in islet grafts, including utilizing reporter genes with fluorescent proteins to label islets, and utilizing cDNA and miRNA levels for a biochemical complement to imaging findings[213–215].

Concerning the limitations of our study, we do not have current evidence on the safety of PVP-SPIO, and the death of five of seven B6 *rag-/-* mice is enough to cause concern; however, this appeared to be due to early diabetic complications post-streptozotocin injection. Larger sample sizes would allow further assessment of graft evolution, and a greater ability for statistical quantification of our results. In addition, we do not have further MR images to see the chronological timing and increase in size of the islet graft after reconstitution. Our figures document an increase in graft size beginning at 13 days post-reconstitution, following increases in blood glucose levels, potentially limiting its use in clinical intervention. Further study with PVP-SPIO needs to be focused on the timing of the image change and its ability to monitor functional beta cell volume to determine if MRI can predict rejection prior to the loss of graft function.

Overall, we demonstrated that our self-synthesized PVP-SPIO did not affect the function of NPI and labelled NPI could be reliably visualized and differentiated from non-labelled islets by MRI after transplantation under the kidney capsule of mice. Following induced graft rejection, the area of the islet graft expanded with mixed signal intensity, which has not been demonstrated previously. These results indicate that PVP-SPIO is a viable MR imaging contrast for monitoring NPI grafts, and further research is needed.

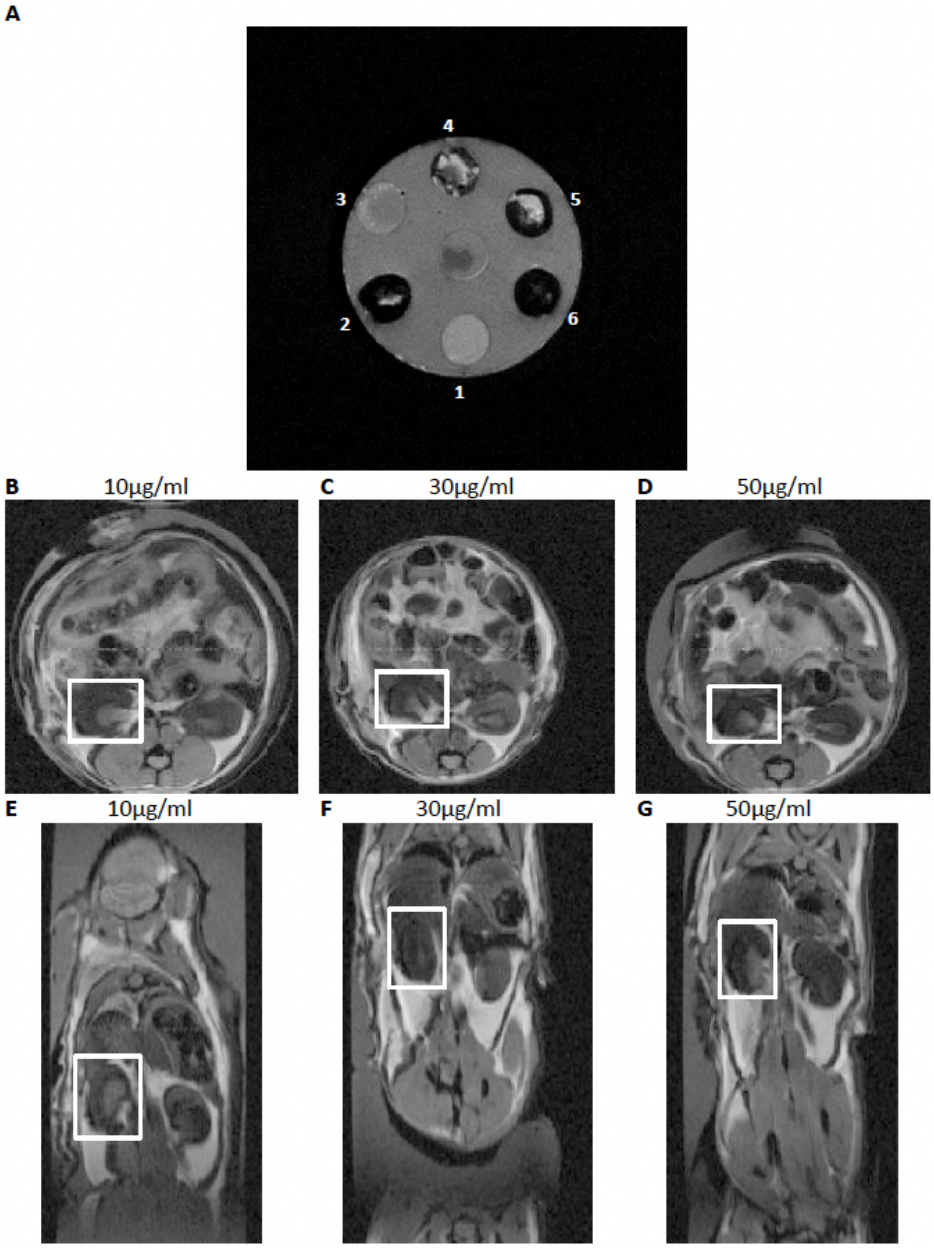

Figure 2.1: MR images of PVP-SPIO labelled islets and islet xenografts. (A) Images demonstrating PVP-SPIO islet labelling on phantom gel. Intermediate background signal (light grey) corresponds to agarose gel utilized for stabilization. (1) HAMs F10 medium only (2) PVP-SPIO only 50µg/ml (3) non-labelled islets (4) 10 µg/ml PVP-SPIO labelled islets (5) 30µg/ml PVP-SPIO labelled islets (6) 50µg/ml PVP-SPIO labelled islets. Axial (B-D) and coronal (E-G) cross sections of mice with NPI labelled PVP-SPIO at differing concentrations, transplanted under the right kidney capsule. MRI was performed 1 day post-transplant. Mice were euthanized prior to MRI. White squares indicate location of PVP-SPIO labelled islet graft in the right kidney while the left kidney contained the unlabelled porcine islet graft and could not be detected by MRI. (B, E) Mouse with islet graft labelled with PVP-SPIO at 10µg/ml, (C, F) mouse with islet graft labelled with PVP-SPIO at 30µg/ml, and (D, G) mouse with islet graft labelled with PVP-SPIO at 50µg/ml.

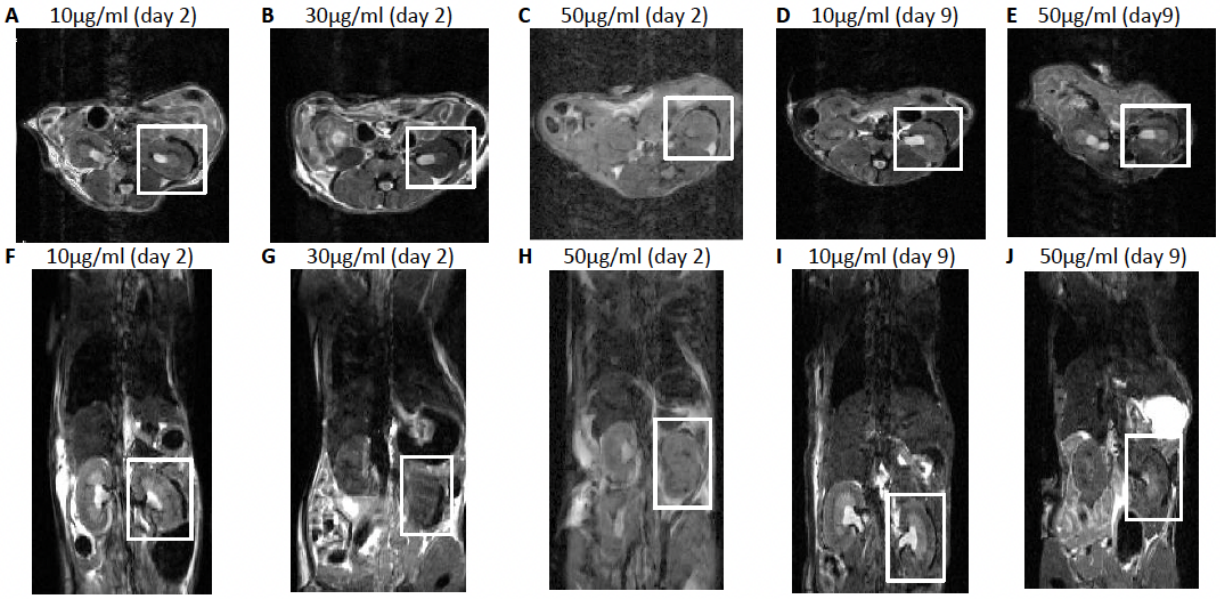

Figure 2.2: MR images of live non-diabetic B6 *rag-/-* mouse recipients of NPI labelled PVP-SPIO. Axial (A-E) and coronal (F-J) cross sections of mice with PVP-SPIO labelled NPI transplanted under the left kidney capsule at 2 (A, B, C and F, G, H) and 9 days (D, E and I, J) post-transplant. White squares show the location of PVP-SPIO labelled islet graft in the left kidney while the right kidney contains the unlabelled islet graft, which could not be detected by MRI. (A, F and D, I) Islet graft labelled with 10µg/ml PVP-SPIO at 2 and 9 days post-transplant, respectively. This mouse was euthanized at 11 days post-transplant. (B, G) islet graft labelled with 30µg/ml PVP-SPIO at 2 days post-transplant. This mouse died post-MRI at 2 days post-transplant. (C, H and E, J) islet graft labelled with 50µg/ml PVP-SPIO at 2 and 9 days post-transplant, respectively. This mouse died post-MRI at 9 days post-transplant.

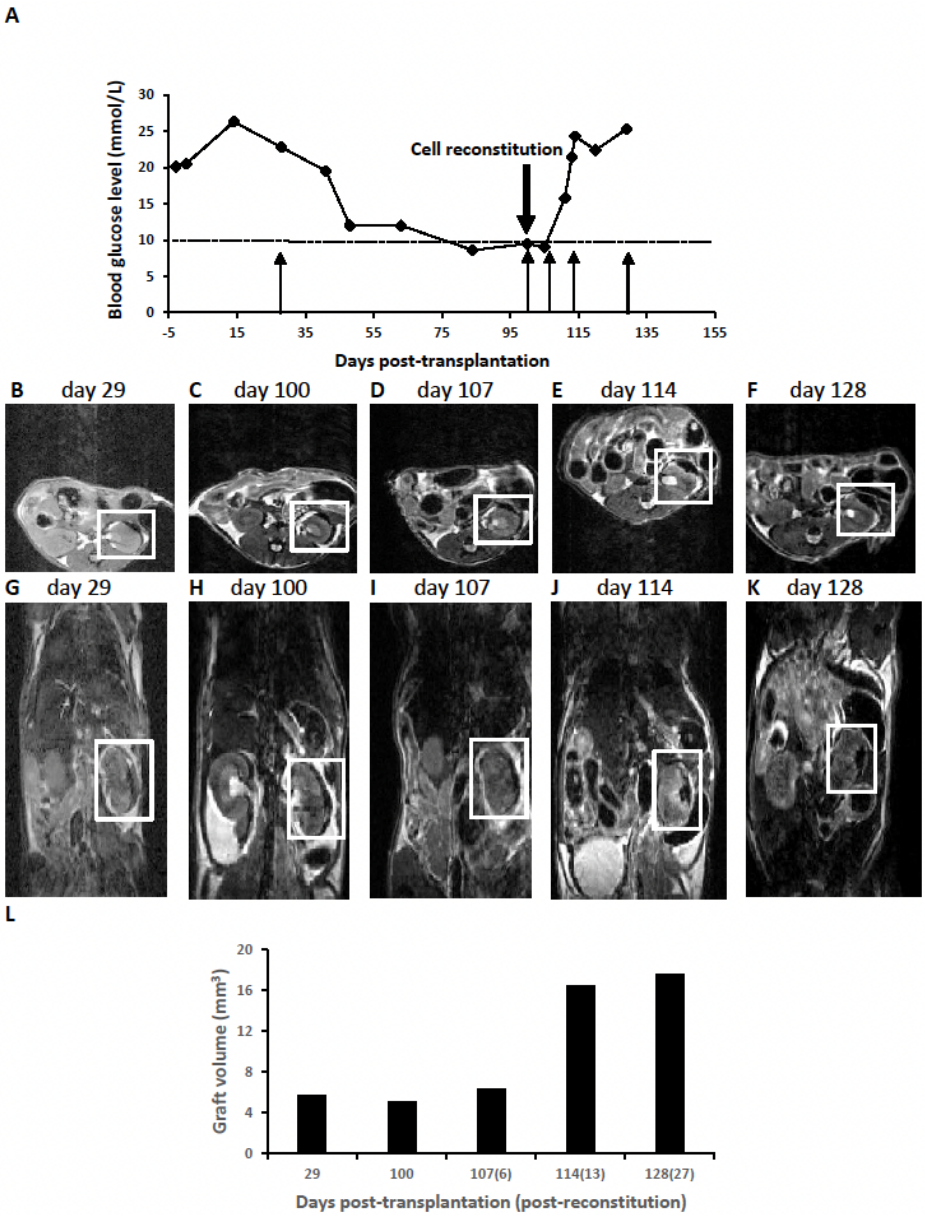

Figure 2.3: Blood glucose measurements and MRI results in a live diabetic B6 rag -/- mouse transplanted with 30µg/ml PVP-SPIO labelled NPI. (A) Blood glucose measurements pre- and post-islet transplantation, upward arrows indicate day of MRI. Axial (B-F) and coronal (G-K) cross sections of the mouse showing left kidney with PVP-SPIO labelled NPI graft at various time points post-transplant. MR images of PVP-SPIO labelled islet grafts under the left kidney capsule before spleen cell reconstitution at 29 days post-transplant (B, G) and 100 days post-transplant (C, H). MR images of PVP-SPIO labelled islet graft at 107 days post-transplant (day 6 post-cell reconstitution; D, I), 114 days post-transplant (day 13 post-cell reconstitution, (E, F) and 128 days post-transplant (day 27 post-cell reconstitution, F, K). White squares show the kidney with PVP-SPIO labelled islet graft. (L) Quantification of islet graft volume at the time of each MRI scan.

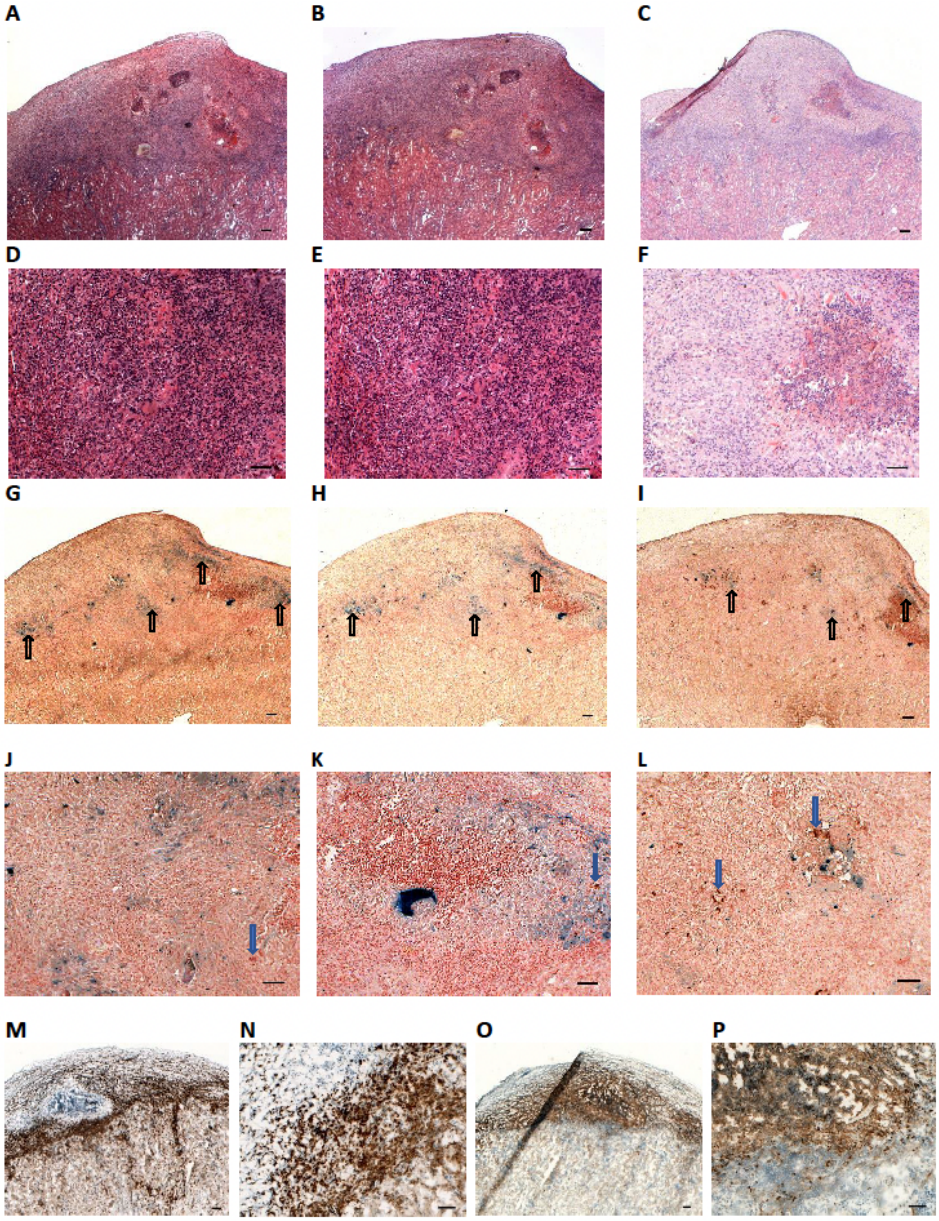

Figure 2.4: Histology of PVP-SPIO labelled islet graft recovered day 28 post cell-reconstitution from a diabetic B6 *rag -/-* mouse (day 129 post-transplant). Immunostained sections for insulin (A, D), glucagon (B, E), and CK-7 (C, F) were counterstained with Harris' hematoxylin and eosin. Histology of PVP-SPIO labelled islet graft sections stained for insulin (G, J), glucagon (H, K) and CK-7 (I, L). These tissue sections were also stained with Prussian blue as shown as upward open black arrows (G, H, I) to identify the PVP-SPIO nanoparticles in the graft and counterstained with nuclear fast red to identify the nuclei. The remaining insulin-, glucagon- and CK-7-positive cells in the rejected graft are shown as blue downward arrows (J, K, L). Tissue sections immunostained for $CD4^+$ T cells (M, N) and $CD11b^+$ monocytes (O, P) are shown as brown stained cells. A-C, G-I, M and O are images taken at 2.5x and D-F, J-L, N and P are images taken at 10x magnification. Scale bars represent 100µm for 2.5x magnification and 50µm for 10x magnification.

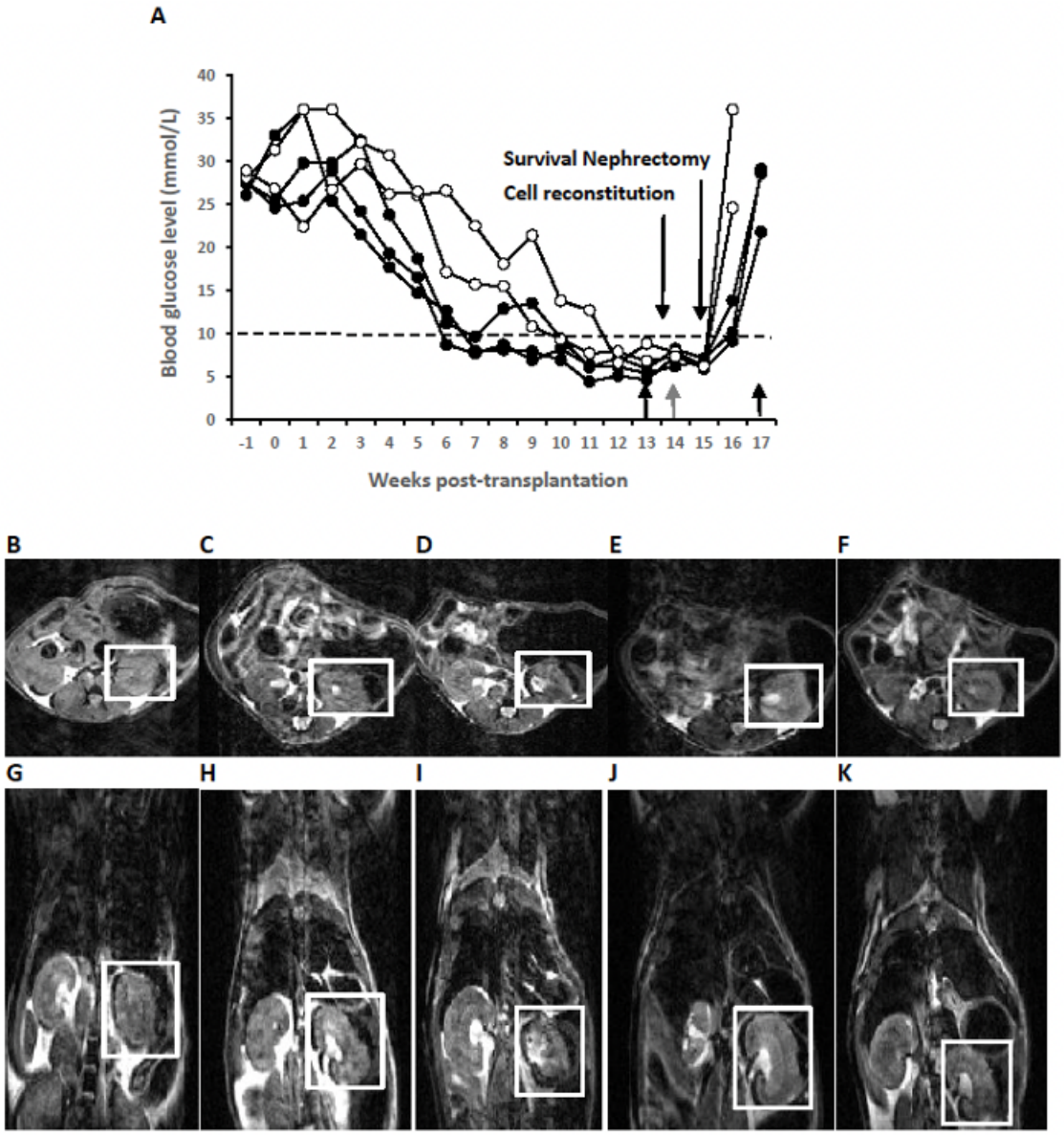

Figure 2.5: Blood glucose measurements compared to graft appearance on MRI in live diabetic NOD.SCID-Gamma mice transplanted with 30µg/ml PVP-SPIO labelled NPI. (A) Weekly blood glucose levels of mice. Black upward arrows indicate day of MR imaging for cell-reconstituted mice, gray upward arrow indicates day of MR imaging for non-reconstituted control mice, in which survival nephrectomy was performed. Axial (B-F) and coronal (G-K) cross sections of each mouse showing left kidney with PVP-SPIO labelled NPI graft. Non-reconstituted mice (n=2) MR scans are shown in B, C and G, H at 14 weeks post-transplant. Blood glucose levels of these mice were 7.8 and 7.3 mmol/l. These mice remained normoglycemic (6.3 and 6.2 mmol/l) at 15 weeks post-transplant and became diabetic (24.6 and 36 mmol/l) 5 days after the kidney that contained the islet graft was procured. MR scans of mice (n=3) prior to reconstitution with spleen cells from NOD mice at 13 weeks post-transplant (D-F and I-K). Blood glucose levels of these mice were 4.6 mmol/l, 5.9mmol/l, and 5.4mmol/l. White squares show the kidney with PVP-SPIO labelled islet grafts.

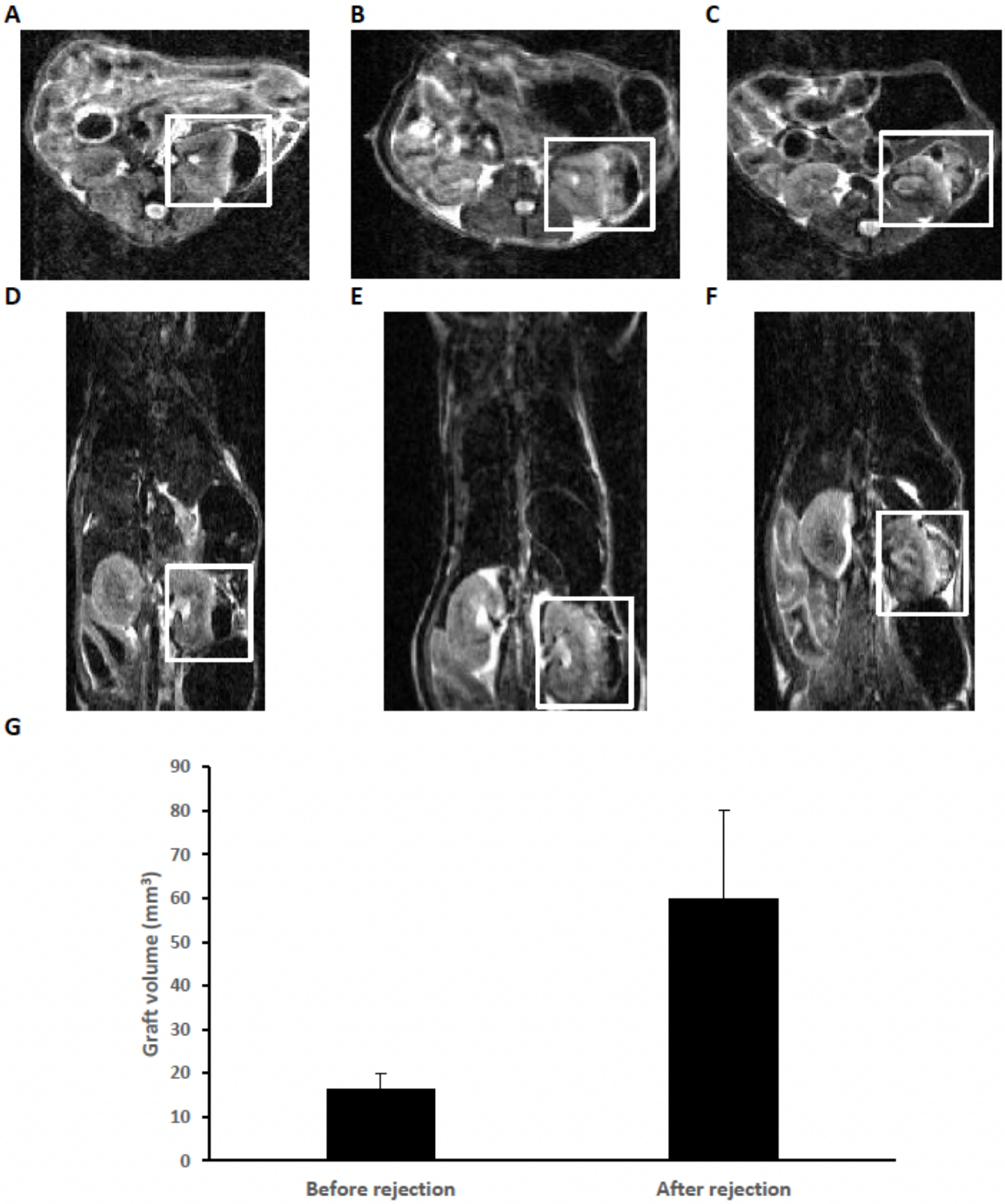

Figure 2.6: MR images of islet grafts under the left kidney capsule of NOD.SCID-Gamma mice at 23 days post-cell reconstitution. Axial images on superior panels (A-C) and coronal images on inferior panels (D-F) from three cell reconstituted NOD.SCID-Gamma mice are shown. The blood glucose levels of these mice were 22.6mmol/l, 26.9mmol/l, and 23.6mmol/l. White squares indicate the PVP-SPIO labelled islet grafts. (G) Quantification of graft volume pre- and post-rejection (n = 3, p = 0.2500).

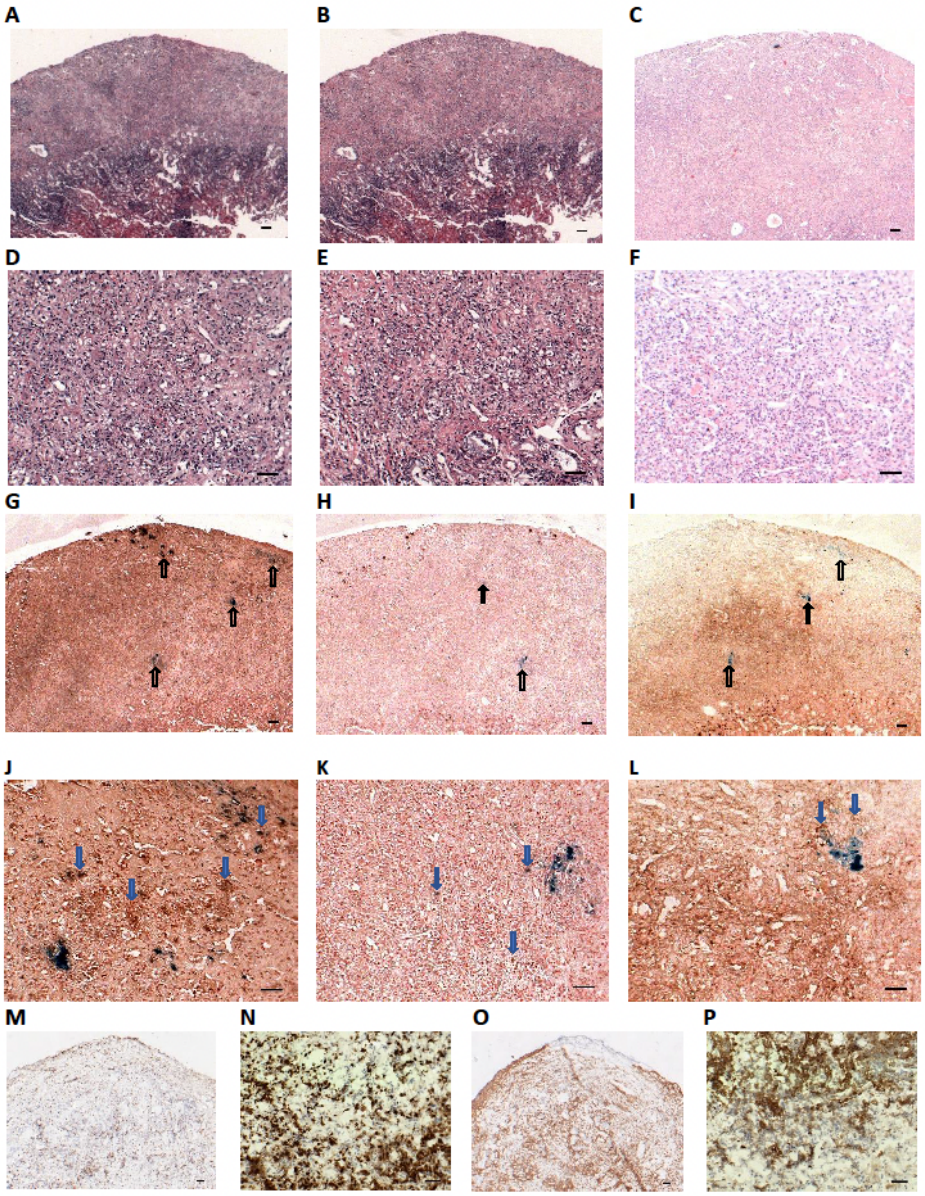

Figure 2.7: Histology of PVP-SPIO labelled islet grafts recovered on day 25 post cell-reconstitution (day 122 post-transplant) from one of the three cell reconstituted NOD.SCID-Gamma mice. Images of the islet grafts from the remaining two mice are shown in Supplementary Fig. 4 and Supplementary Fig. 5. Tissue sections stained for insulin (A, D, G, J), glucagon (B, E, H, K), and CK-7 (C, F, I, L) were counterstained with Harris' hematoxylin and eosin (A-F) or nuclear fast red (G-L). These latter tissue sections (G-L) were also stained with Prussian blue as shown as upward open black arrows (G, H, I). The remaining insulin-, glucagon- and CK-7-positive cells in the rejected graft are shown as blue downward arrows (J, K, L). $CD4^+$ T cells (M, N) and $CD11b^+$ monocytes (O, P) are shown as brown-stained cells and they make up the majority of immune cells detected in the graft. A-C, G-I, M and O are images taken at 2.5x magnification and D-F, J-L, N and P are images taken at 10x magnification. Scale bars represent 100µm for 2.5x magnification and 50µm for 10x magnification.

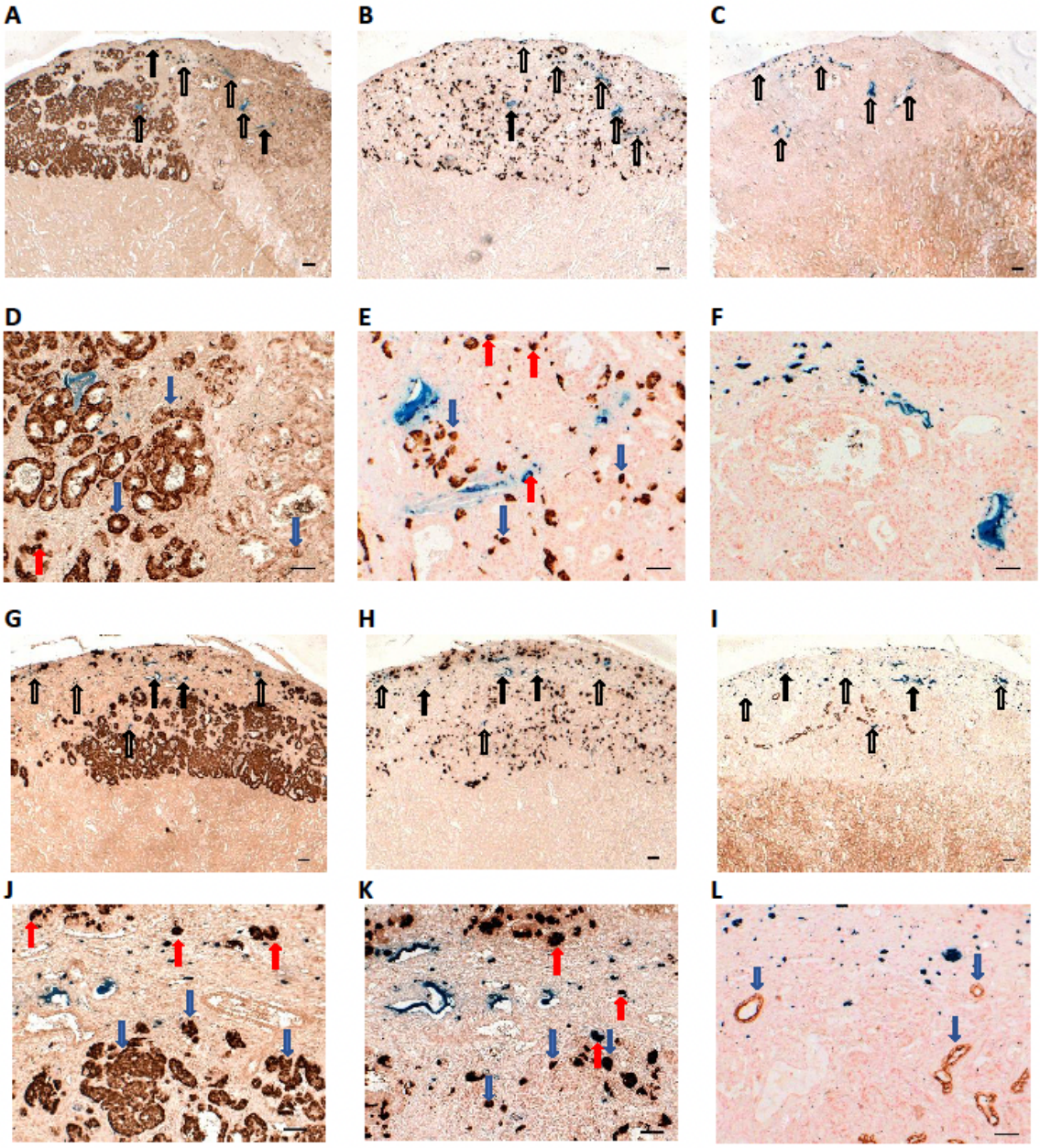

Figure 2.8: Histology of PVP-SPIO labelled islet grafts recovered from non-reconstituted control NOD.SCID-Gamma mice (day 106 post-transplant). Tissue sections from two control mice were stained for insulin (A, D, G, J), glucagon (B, E, H, K), and CK-7 (C, F, I, L). These tissue sections were stained with Prussian blue as shown as upward open black arrows (A-C and G-I) and counterstained with nuclear fast red. Insulin, glucagon and CK-7-stained cells are shown as brown structures in the islet graft and indicated by the blue downward arrows (D-F and J-L). Co-localization of Prussian blue with insulin and glucagon are shown as red arrows in J and K, respectively. Images A-C, G-I were taken at 2.5x magnification and images D-F and J-L were taken at 10x magnification. Scale bars represent 100µm in images taken at 2.5x and 50µm in images taken at 10x magnification.

A

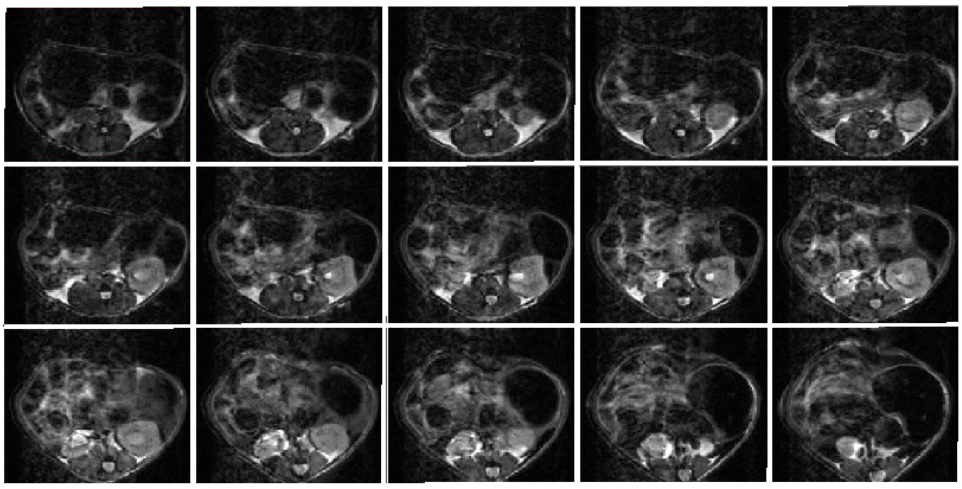

B

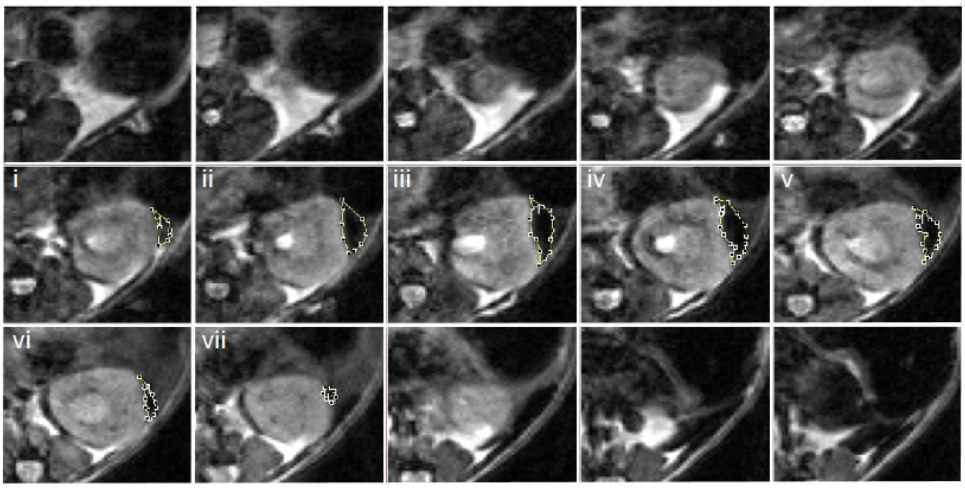

C

Areas (mm^2):	Areas multiplied by 1.1 to include gaps between slices:	Volume (mm^3) (sum of Areas):
i. 1.51	i. 1.66	21.35
ii. 3.85	ii. 4.24	
iii. 4.30	iii. 4.73	
iv. 4.71	iv. 5.18	
v. 3.16	v. 3.48	
vi. 1.24	vi. 1.36	
vii. 0.64	vii. 0.70	

Supplementary Figure 2.9:.Example of volume segmentation for PVP-SPIO labeled graft in NOD.SCID-Gamma mouse. (A) Raw images obtained from MRI scan. (B) Magnified images demonstrating manual measurements of islet graft. Panels of interest numbered i-vii. (C) Area measurements for panels i-vii, and overall calculated volume of islet graft.

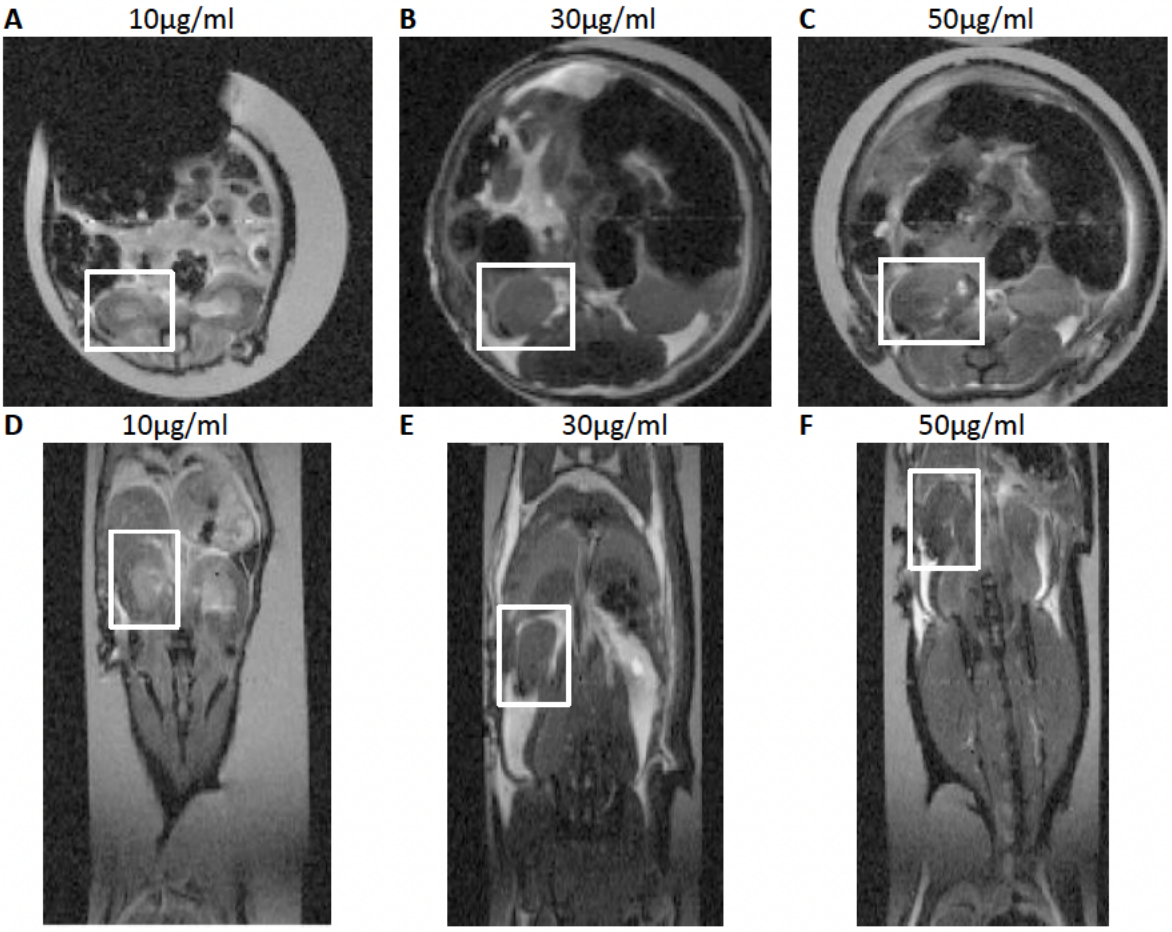

Supplementary Figure 2.10: Axial (A-C) and coronal (D-F) cross sections of mice transplanted with differing concentrations of PVP-SPIO labelled islets under the right kidney capsule, 8 days post-transplant. White squares indicate location of PVP-SPIO labelled islet graft in the right kidney while the left kidney contained the non-labelled porcine islet graft and could not be detected by MRI. Islets labelled with PVP-SPIO at 10µg/ml (A, D), islets labelled with PVP-SPIO at 30µg/ml (B, E), islets labelled with PVP-SPIO at 50µg/ml (C, F) are shown.

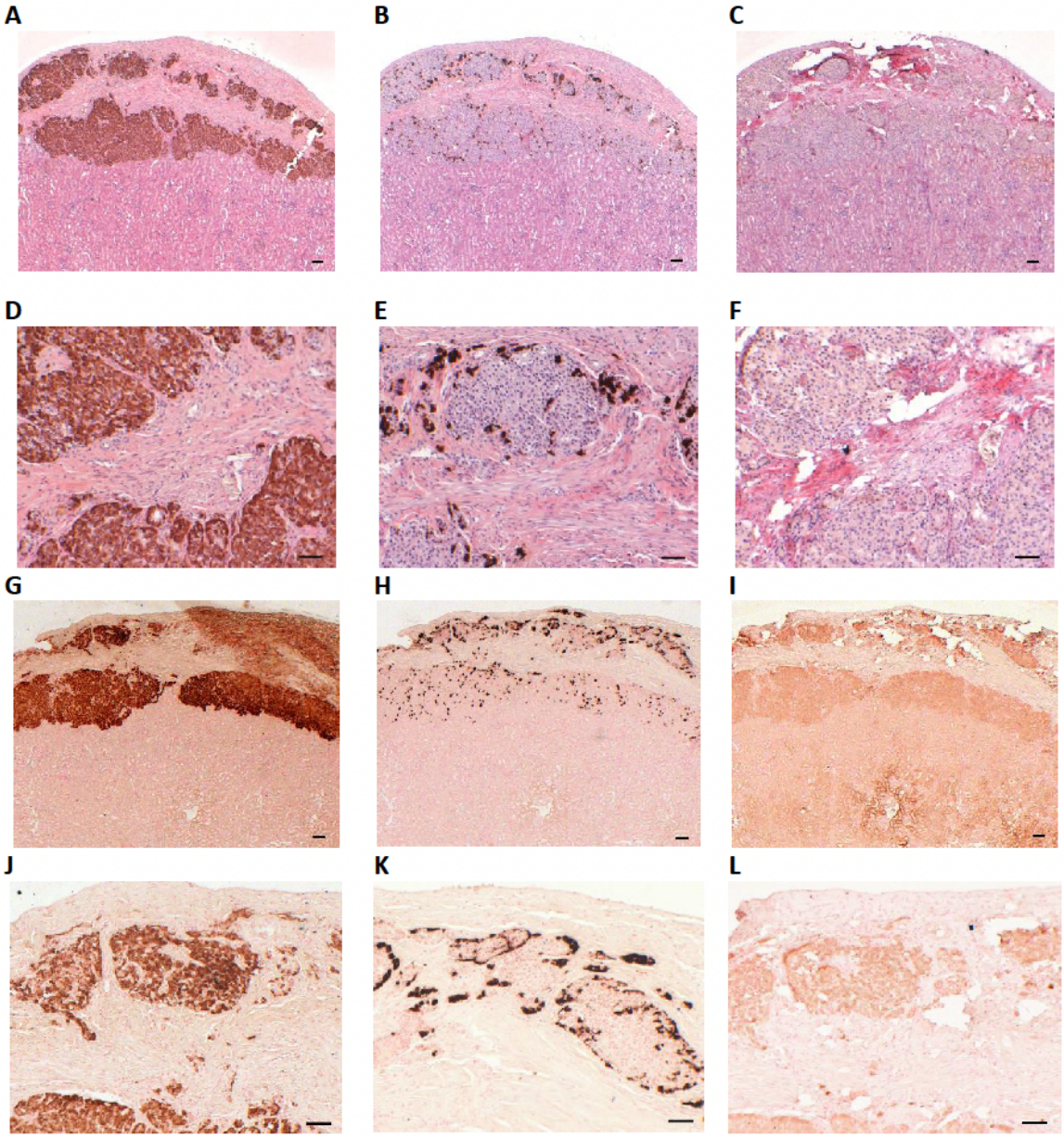

Supplementary Figure 2.11: Histology of non-labelled NPI graft obtained from a non-reconstituted B6 *rag-/-* mouse. Tissue sections were stained for insulin (A, D, G, J), glucagon (B, E, H, K), and CK-7 (C, F, I, L). These tissue sections were counterstained with Harris' hematoxylin and eosin (A-F) or stained with Prussian blue and counterstained with nuclear fast red (G-L). The positive blue stain detected in PVP-SPIO labelled islet grafts is absent. Insulin, glucagon, and CK7-stained cells are shown as brown structures in the islet graft. Images A-C and G-I were taken at 2.5x magnification and images D-F and J-L were taken at 10x magnification. Scale bars represent 100µm in images taken at 2.5x and 50µm in images taken at 10x magnification.

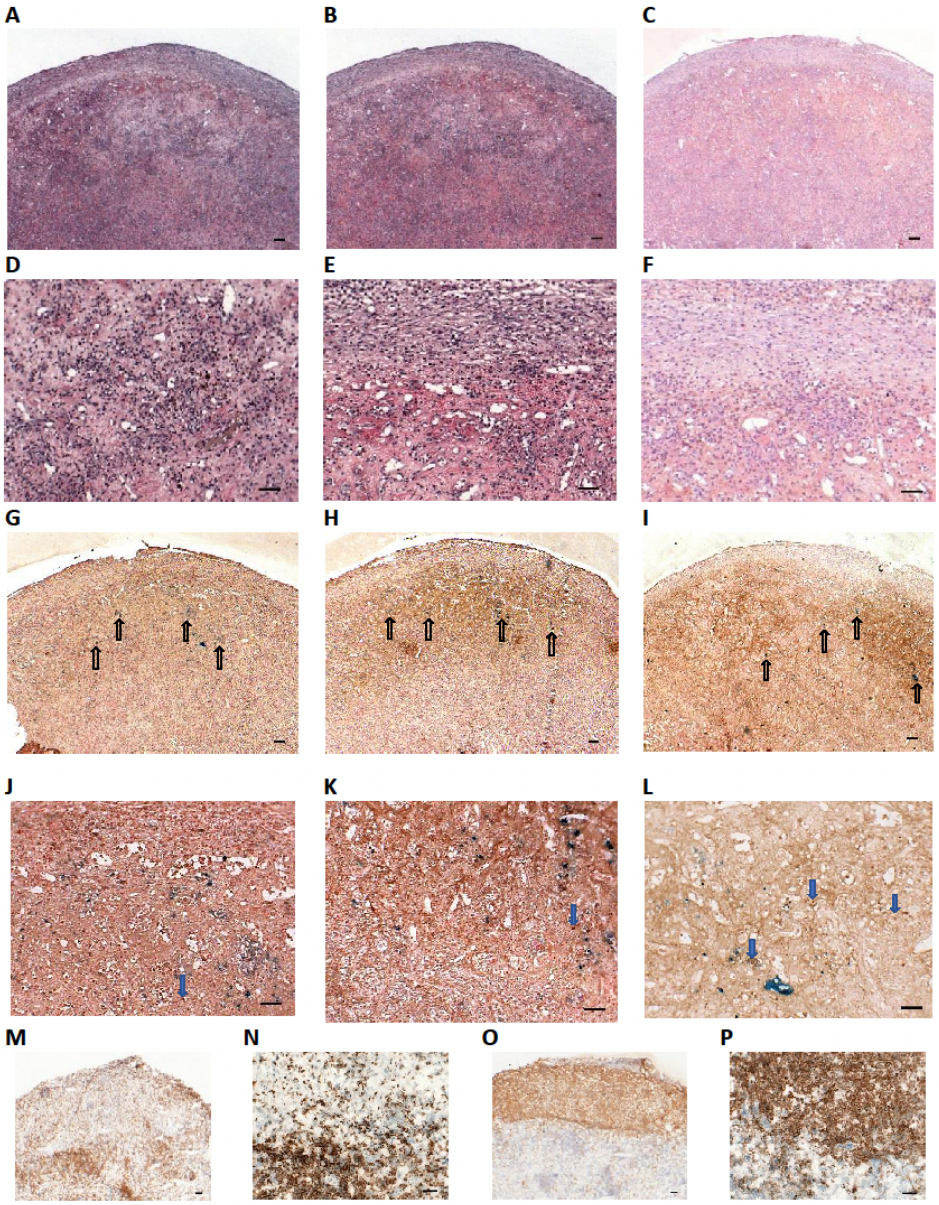

Supplementary Figure 2.12: Histology of PVP-SPIO labelled islet graft obtained from the second cell reconstituted NOD.SCID-Gamma mouse. Tissue sections stained for insulin (A, D, G, J), glucagon (B, E, H, K), and CK-7 (C, F, I, L) were counterstained with Harris' hematoxylin and eosin (A-F) or stained with Prussian blue as shown as upward open black arrows (G, H, I) and counterstained with nuclear fast red (G-L). The remaining insulin-, glucagon- and CK-7-positive cells in the rejected graft are shown as blue downward arrows (J, K, L). CD4+ T cells (M, N) and CD11b+ monocytes (O, P) are shown as brown stained cells and they make up the majority of immune cells detected in the graft. A-C, G-I, M and O are images taken at 2.5x magnification and D-F, J-L, N and P are images taken at 10x magnification. Scale bars represent 100µm for 2.5x magnification and 50µm for 10x magnification.

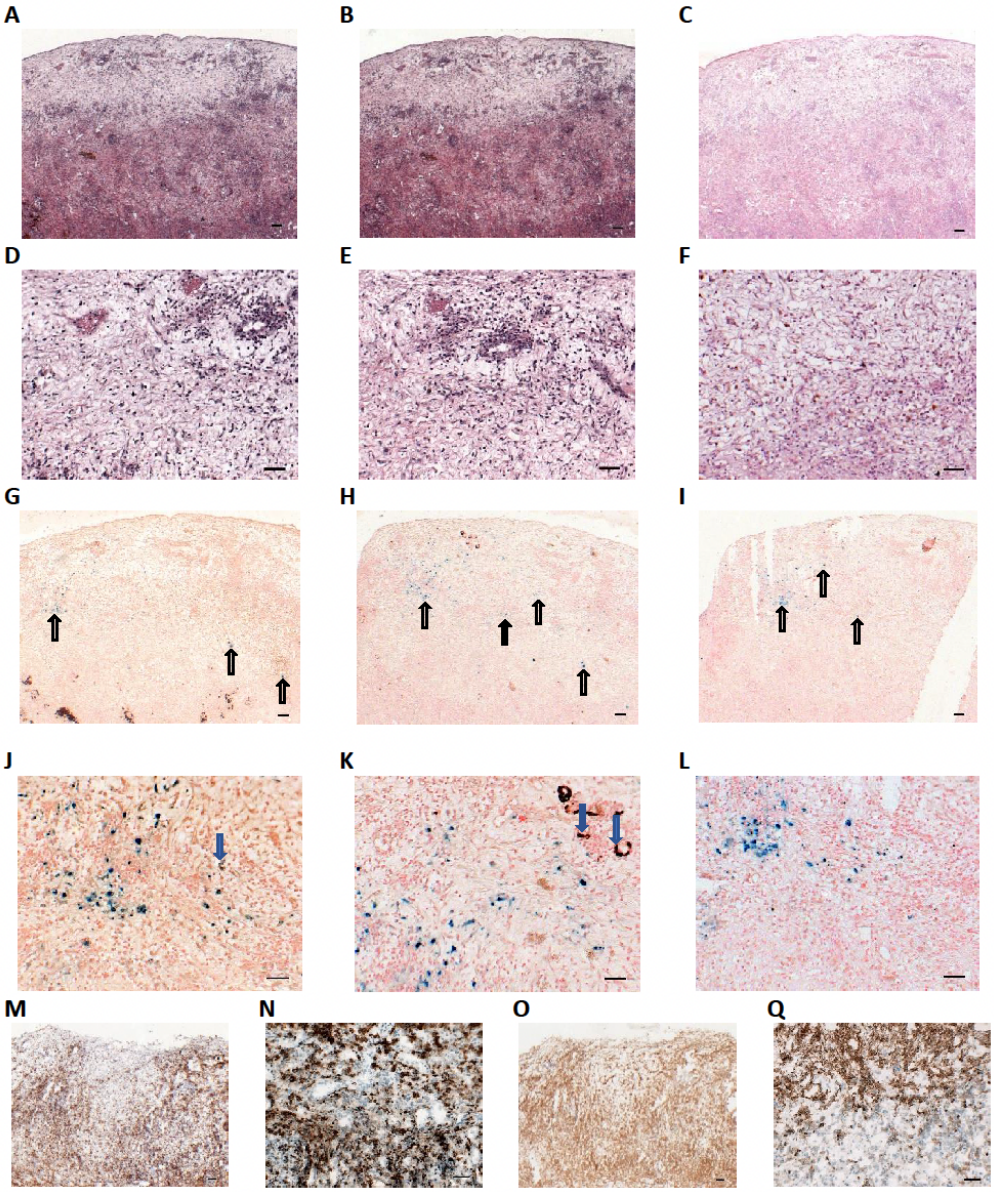

Supplementary Figure 2.13: Histology of PVP-SPIO labelled islet graft obtained from the third cell reconstituted NOD.SCID-Gamma mouse. Tissue sections stained for insulin (A, D, G, J), glucagon (B, E, H, K), and CK-7 (C, F, I, L) were counterstained with Harris' hematoxylin and eosin (A-F) or stained with Prussian blue as shown as upward open black arrows (G, H, I) and counterstained with nuclear fast red (G-L). The remaining insulin-, glucagon- and CK-7-positive cells in the rejected graft are shown as blue downward arrows (J, K, L). CD4+ T cells (M, N) and CD11b+ monocytes (O, P) are shown as brown stained cells and they make up the majority of immune cells detected in the graft. A-C, G-I, M and O are images taken at 2.5x magnification and D-F, J-L, N and P are images taken at 10x magnification. Scale bars represent 100µm for 2.5x magnification and 50µm for 10x magnification.

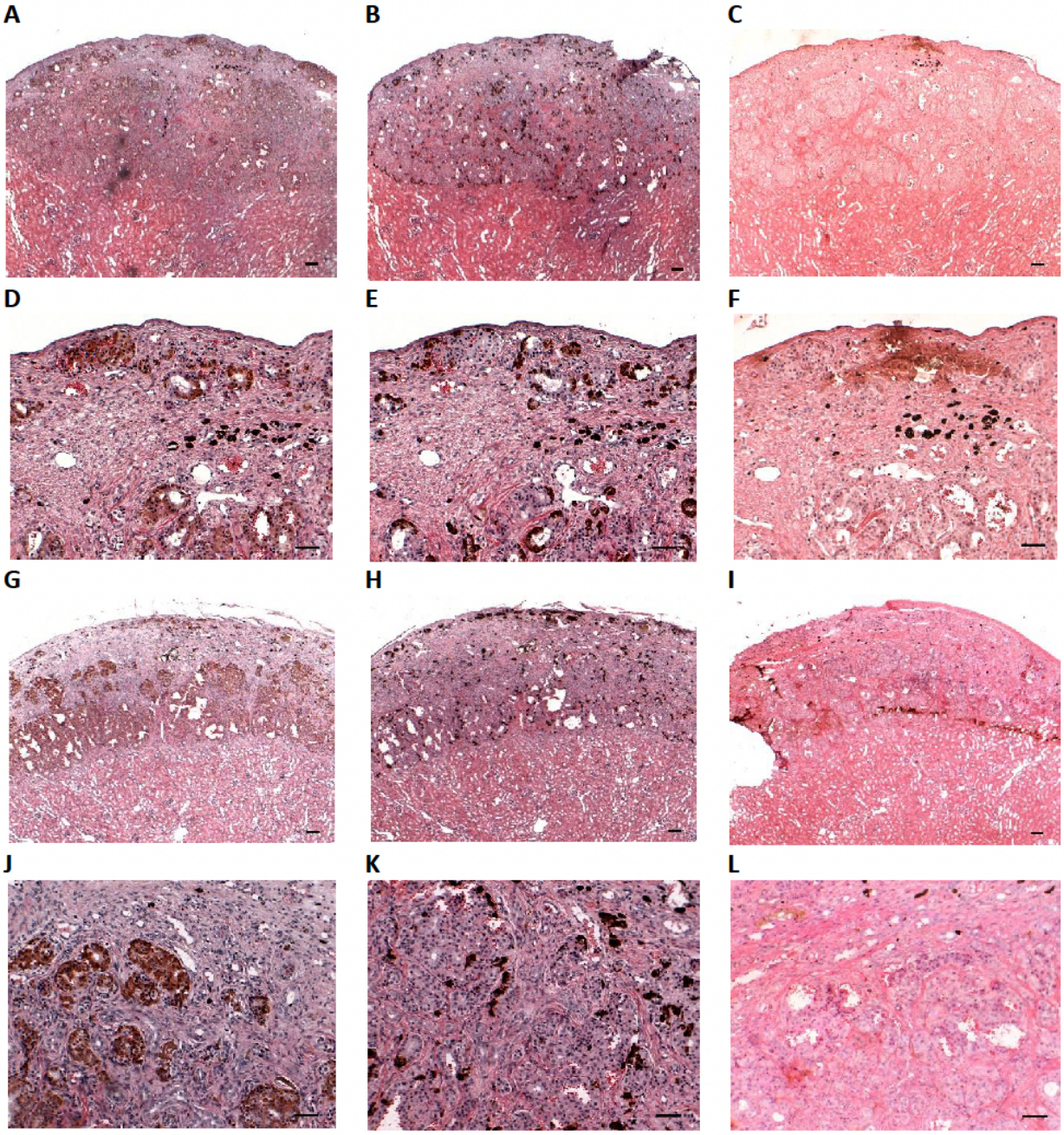

Supplementary Figure 2.14: Histology of PVP-SPIO labelled islet graft obtained from two non-reconstituted NOD.SCID-Gamma mice. Tissue sections were stained for insulin (A, D, G, J), glucagon (B, E, H, K), or CK-7 (C, F, I, L), shown as brown-stained cells and counterstained with Harris' hematoxylin and eosin. A-C and G-I are images taken at 2.5x magnification and D-F and J-L are images taken at 10x magnification. Scale bars represent 100µm for 2.5x magnification and 50µm for 10x magnification.

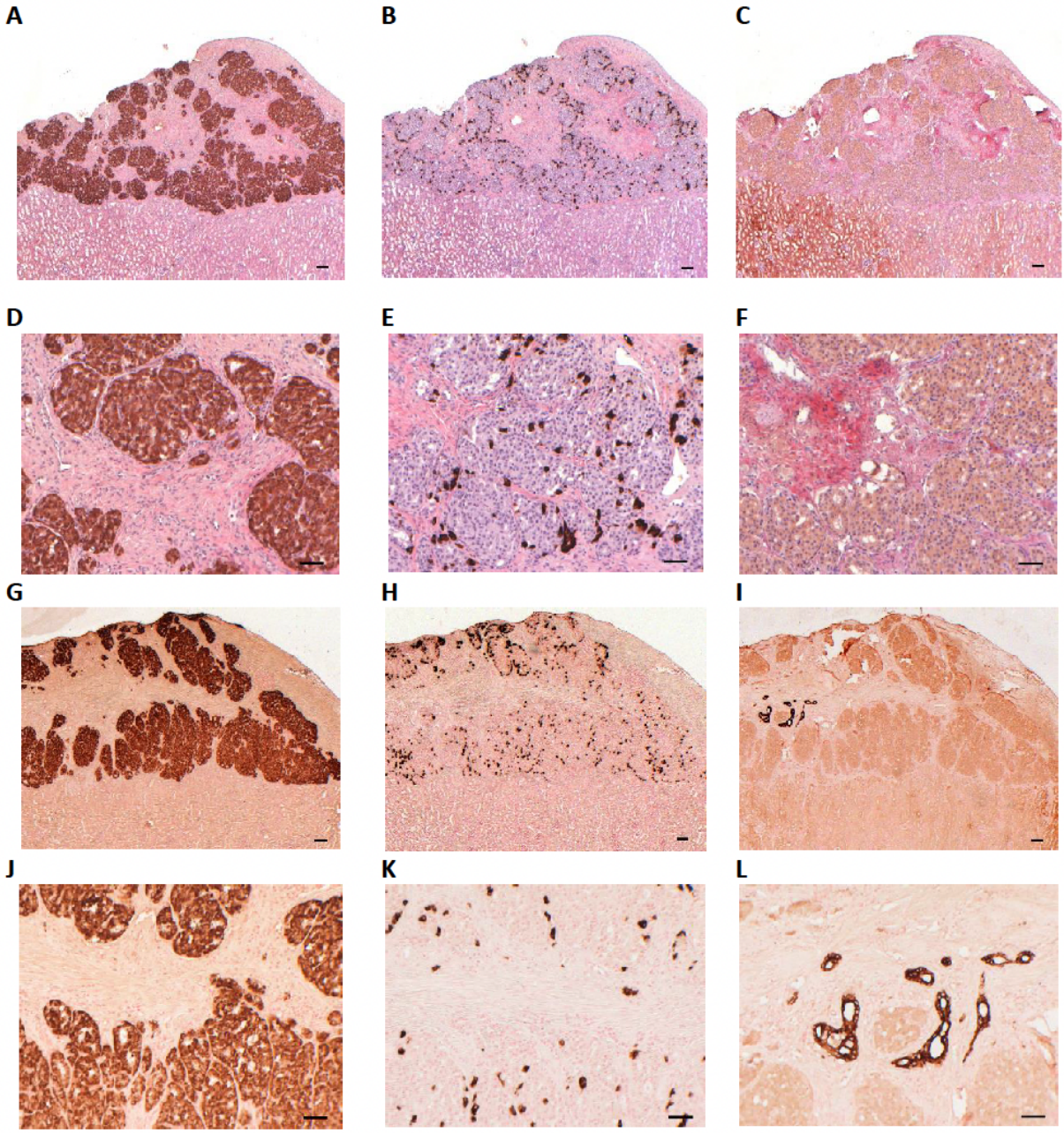

Supplementary Figure 2.15: Histology of non-labelled islet graft obtained from non-reconstituted NOD.SCID-Gamma mice. Tissue sections stained for insulin (A, D, G, J), glucagon (B, E, H, K), and CK-7 (C, F, I, L) were counterstained with Harris' hematoxylin and eosin (A-F) or Prussian blue (G-L). The positive blue stain detected in PVP-SPIO labelled islet grafts is absent. Insulin, glucagon, and CK7-stained cells are shown as brown structures in the islet graft. Images A-C and G-I were taken at 2.5x magnification and images D-F and J-L were taken at 10x magnification. Scale bars represent 100µm in images taken at 2.5x and 50µm in images taken at 10x magnification.

Chapter 3 Exploring the postnatal development of pig islets: an in vitro model

This chapter is in preparation to submit for publication

Authors: Kieran Purich[a], Josue R. Silva[a], Wenlong Huang[b], Jim Wickware[a], Thomas Williams[a], Adnan Black[a], David Bigam[a], Daniel Schiller[a], Gina R. Rayat[a]

Affiliations:

[a]Department of Surgery, Ray Rajotte Surgical-Medical Research Institute, Alberta Diabetes Institute, Faculty of Medicine and Dentistry, University of Alberta, Edmonton, Alberta, Canada

[b]General Surgery, First Affiliated Hospital of Shantou University Medical College, Shantou, China

Abstract

Pig islet xenotransplantation has the potential to address the limited supply of human organs available for islet transplantation however, multiple barriers remain including difficulties in preventing the rejection of pig donor tissue by transplant recipients. Limitations in the knowledge of pig islet biology have hampered the translation of pig islet xenotransplantation to the clinical realm. This exploratory study attempts to discern changes in gene and protein expression during early neonatal pig islet development. Specifically, we explore the cell-cell adhesion molecules E and VE-cadherin, and their impact on the function of islets, as well as specific molecules involved in the insulin secretion pathway, with the primary goal of identifying which age of neonatal pig islet are most suitable for transplantation.

Through a combination of methods including RT-qPCR, automated western blot, in vitro and in vivo assessment of islet function, we explore the expression of E and VE-cadherin in early neonatal pig islet development and its correlation with various molecules of interest from the insulin secretion pathway including GTPase RAC1 and membrane fusion protein, SNAP25. Major findings of our study include an apparent trend towards improved islet function in vitro and in vivo in islets from 3 and 7-day-old pigs compared to 1-day-old pigs, and experimental validation demonstrating that E-cadherin is linked to glucose stimulated insulin secretion, which has not been previously demonstrated in pig islets.

Overall, this study serves as a starting point to understanding the interconnections between the insulin secretion pathway and cadherin mediated cell-cell adhesion during the postnatal development of pig islets.

KEYWORDS

Islet xenotransplantation, neonatal pig islets, E-cadherin, VE-cadherin, type 1 diabetes mellitus, glucose stimulated insulin secretion

Introduction

Pig islet xenotransplantation is a method that could help address the limited number of human organs available for islet transplantation[93]. Pig islets have been used successfully towards the reversal of diabetes in animal models including non-human primates; however few human studies have been performed[104,216–218]. Many recent studies in the field of xenotransplantation have focused on the creation of genetically modified pigs in an attempt to prevent immune rejection upon transplantation, with less focus placed upon pig islet biology and development[218].

Significant physiologic differences exist within the endocrine pancreas across species, making it important to study physiologic pathways in pigs as they likely differ from that seen in rodents and humans[13,123,219,220]. Similar to others, our research group believes that based on practical and biological advantages, neonatal pig islets (NPI) are the most promising source for xenotransplantation tissue[202,220,221]. To better be able to successfully transplant this tissue, we need a better understanding of how neonatal pig islets develop over time and the molecules involved during this process.

The primary cellular pathway in which we are interested spans members within the conserved family of transmembrane adhesion molecules, known as cadherins[129]. In particular endothelial (E) and vascular endothelial (VE) cadherins are known to play a role in endocrine pancreas development in humans and rodents but these findings have not been previously explored in pigs[134].

E-cadherin, encoded by gene *CDH1*, is a transmembrane protein which plays a role in actin linked cellular signalling pathways, and is involved in the aggregation of the islet beta cells[134,141,175,222]. The mechanism by which E-cadherin impacts islet function is still currently under investigation, but is felt to be through its association with gap junction protein CX-36[128,131,134,139,141,223]. To correlate E-cadherin expression with expression of molecules involved in the insulin secretion pathway, we chose proteins of interest at different stages of the insulin secretion pathway within the beta cell. These molecules were: glucose transporter, GLUT2, also known as solute carrier family 2 member 2 (*SLC2A2*)[149,159], Ras-related C3 botulinum toxin substrate 1 (GTPase RAC1) which plays a key role in actin cytoskeletal remodeling during

glucose mediated insulin secretion[160,165], and Synaptosome Associated Protein of 25 kDA (SNAP25) which allows for the fusion of insulin granules on the plasma membrane[149].

The second cadherin of interest is VE-cadherin, encoded by the gene *CDH5*, is key in the development of junctions between endothelial cells and is crucial for directing vessel growth, which is of significant interest in the field of islet transplantation[143,224]. During islet isolation, the vascular connection of islets within the surrounding exocrine tissue is destroyed and during transplantation, much difficulty surrounds ensuring appropriate neovascularization of islet grafts. To date, little is known about the fate of VE-cadherins during in vitro postnatal development of pig islets and this is a significant gap in the field. Islets are known to be prone to oxidative stress during islet isolation and transplantation, which may be partly due to the exposure of islets to hypoxic conditions at early time points post-transplantation. Understanding the role of VE-cadherins in neovascularization post-transplantation may help us develop new strategies to enhance the survival of islets post-transplantation.

The objectives of this study were 1) to characterize the changes seen in E-cadherin gene and protein expression during early neonatal pig islet development in vitro and correlate such with the expression of key molecules involved in insulin secretion as well as with the function of islets through glucose stimulated insulin secretion assay and transplantation into diabetic mice; 2) to characterize the expression of VE-cadherin during early neonatal pig islet development in vitro.

Materials and methods

All research detailed in this manuscript was approved by the University of Alberta's Animal Care and Use Committee following the guidelines by the Canadian Council on Animal Care for all animal related procedures.

Neonatal pig islet isolation and culture

Neonatal Duroc/Landrace Large White F1-cross neonatal pigs of 1, 3 and 7-days-old were obtained and transported to the University of Alberta's Ray Rajotte Surgical Medical Research Institute (RRSMRI). Pancreata were procured and placed in cooled Hanks Balanced

Salt Solution (HBSS, H6136, Sigma-Aldrich, St. Louis, MO, USA). Pancreata were then digested using 1mg/mL of collagenase XI (C7657, Sigma-Aldrich) for 8-15 minutes at 37°C and filtered through a 500µm nylon screen following our standard protocols[85,202]. Following isolation, islets were placed in Ham's F-10 Nutrient Mixture (N6635, Sigma-Aldrich) and kept at 37°C, 5% CO_2 and 95% air. On days 1, 3, 5 and 7 culture media was changed, and samples were taken for analysis by microscopy, viability assessment by Trypan Blue dye exclusion test, RT-qPCR and protein analysis[225]. On the 7th day of culture, islets were counted, and glucose stimulated insulin secretion (GSIS) assay or transplantation into streptozotocin-induced diabetic B6 *Rag -/-* mice was performed.

Light microscopy

Images were taken on each day of culture using a Leica DMIL microscope with a Zeiss AxioCam HRc camera and analyzed with AxioVision version 4.7.2.

Gene expression determined by quantitative reverse transcription PCR (RT-qPCR)

Our RT-qPCR protocol was guided by the Minimum Information for Publication of Quantitative Real-Time PCR Experiments (MIQE) Guidelines[226]. At time of sample collection, approximately 200 islet equivalents (IEQ) were introduced to 500µL Trizol (15596018, Ambion Inc., Austin, Texas, USA), vortexed for 30 seconds and immediately placed in a -80°C freezer. For RNA extraction, samples were thawed, and processed through a series of steps involving glycogen (AM9510, Ambion), chloroform, isopropanol and multiple washing steps with 70% ethanol. RNA was suspended in 40µL of RNAse free water supplemented with Superase In RNAse inhibitor (AM2696, Invitrogen, Waltham, MA, USA).

Sample concentration was determined using a Nanodrop spectrophotometer (NanoDrop 1000, Thermo Scientific, Waltham, MA, USA) to ensure 260/280 and 260/230 absorbance ratios of approximately 2. RNA was then treated with a Turbo-DNAse kit (AM2238, Invitrogen). Following DNAse treatment, sample concentration was determined again on Nanodrop and diluted to 100ng/µL. RNA quality was tested using two separate methods: RNA integrity (Agilent 2100 Bioanalyzer, Agilent Technologies Inc., Santa Clara, CA, USA) and by

RNAIQ Assay (Qubit spectrophotometer, ThermoFisher, Waltham, MA, USA). RNA samples with unacceptable quality were not used.

RNA was transformed into cDNA using 600ng of total RNA using the Applied Biosystems High Capacity RNA-to-cDNA kit (43874056, Applied Biosystems, Waltham, MA, USA). All RNA samples had negative RT controls completed. Samples were run on a BioRad T100 thermal cycler (Life Science, Mississauga, ON, Canada) for one hour at 37^{o}C followed by 5 minutes at 95^{o}C. cDNA samples were stored at -20^{o}C.

For RT-qPCR assays, TaqMan primers were used. Commercially available sequences were used when available, whereas for SNAP25, a Custom TaqMan primer was designed using gene sequences obtained from the National Center for Biotechnology Information (NCBI). Gene variants were aligned using the Basic Local Alignment Search Tool (BLAST) database to ensure that all transcript variants would be detected and the resulting primer/probe set was ordered through the custom assay design tool available from ThermoFisher. Details on the primer ID's and sequences are available in **Supplementary Tables 3.1 and 3.2.**

All primers were validated in two reproducible analyses across 5 fold concentrations with efficiencies between 83.8% and 100.9%. PCR amplification assays were completed using Applied Biosystems TaqMan Fast Advanced Master Mix (4444557, Applied Biosystems), had a 10µL total reaction volume, were manually pipetted and run for 40 cycles on an StepOnePlus real time PCR system (Applied Biosystems). All samples were run in triplicate, and samples were manually reviewed for outliers (>0.5 CT value difference between triplicates), and averages were taken. Three reference genes (Beta Actin, GAPDH and HPRT1) which spanned different physiologic pathways were run alongside the samples. Relative gene expression was determined using multiple gene analysis, which was completed manually using Microsoft Excel version 16.58[227].

Protein expression quantified by ProteinSimple's Western immunoassay

Protein from 2000 IEQ was extracted using RIPA buffer (20-188, MilliporeSigma, Burlington, MA, USA) with 0.1% protease inhibitor (P8340, Sigma) following standard protocols. A Pierce BCA protein kit (23227, ThermoFisher) was used to quantify total protein

concentration. Specific protein quantification was performed using ProteinSimple's WES machine (San Jose, California, USA) following standard protocols. Lysate and antibody concentrations were optimized as follows: E-cadherin (lysate 200µg/mL, 4A2C7 antibody concentration 1:50, Invitrogen), VE-cadherin (lysate 750µg/mL, ab33168, antibody concentration 1:50, Abcam, Cambridge, United Kingdom), GLUT2 (lysate 1000µg/mL, LS-C40343 antibody concentration 1:50, LSBio, Seattle, Washington, USA), RAC1 (lysate 1000µg/mL, LS-C464102 antibody concentration 1:50, LSBio), SNAP25 (lysate 1000µg/mL, ab11102 antibody concentration 1:50, Abcam). The intensity of binding was visualized by chemiluminescence. All samples were run in duplicate, and the averages of both samples taken. Data was analyzed using ProteinSimple's Compass software. Detected standards and peaks were fitted manually to get the best estimates of areas under the curve.

In vitro islet function assessment by glucose stimulated insulin secretion assay

For each pig, duplicates of 200 IEQ were placed in Ham's F10 medium within Eppendorf tubes at 37°C for 1 hour. KRBH solutions (**Supplementary Table 3.3**) were made with 2.8mM of glucose, 20mM of glucose and 20mM of glucose with 30mM of KCl (an independent non-nutrient insulin secretagogue) and pre warmed to 37°C. Following a 1 hour incubation at 37°C, tubes were removed from the incubator, spun down at 1000 RPM and all supernatant removed without disturbing the pellet. Islets were rinsed with 1.5mL of 2.8mM KRBH solution and replaced in the incubator for 2 hours. This process was repeated twice. Afterwards, Eppendorfs containing the islets were removed from the incubator, spun down, and supernatant was removed. Then, 750µL of 2.8mM of KRBH was added, incubated for 1 hour, and 500µL of the solution collected for analysis. This was repeated with the 20mM glucose solution and the 20mM glucose solution with KCl. After collecting all the samples for the experimental conditions, 750µL of Azol buffer (obtained from a solution made from 400mL of Milli-Q water and 57mL of glacial acetic acid with 1.25g BSA) was added to liberate all the insulin from the islets in the sample. Samples were vortexed for 5 seconds and then placed in the -20°C freezer until analysis.

Additional in vitro insulin secretion assays were completed on day 8 of culture for 3-day-old pig islets exposing them to the various experimental conditions after exposure to anti E-cadherin monoclonal antibody at a concentration of 5µg/µL. Specifically, for each pig, 1000 IEQ were placed in Eppendorf tubes and were rinsed multiple times with KRBH supplemented with 2.8mM of glucose and then placed in 500µL of KRBH supplemented with 2.8mM of glucose at 37^{o}C to equilibrate for 1 hour. Anti-E-cadherin monoclonal antibody was then added and incubated at 37^{o}C for approximately 90 minutes. Islets were then rinsed with KRBH supplemented with 2.8mM of glucose multiple times then divided into separate Eppendorf tubes each containing approximately 200 IEQ and taken through the KRBH supplemented with 2.8mM and KRBH supplemented with 20mM of glucose conditions in a similar fashion as is detailed in the paragraph above. 200 IEQ were taken for light microscopy to assess differences between islets treated with anti E-cadherin monoclonal antibody compared to those that were not.

Insulin concentrations were analyzed using Porcine Insulin ELISA kit (10-1200-01, Mercodia, Uppsala, Sweden). Samples were run in duplicate, with averages taken and results were read at 450nm (Multiskan Sky, Thermoscientific spectrophotometer).

In vivo islet function assessment by NPI transplantation

On the 7th day of culture, 2000 IEQ were transplanted under the kidney capsule of male 8 week old male B6 *rag1 -/-* (C57BL/6-rag1$^{tm1/mom}$ [B6 rag1-/-], H-2^{b}) mice (Jackson Laboratories), which had been rendered diabetic by intraperitoneal streptozotocin injection (S0130, dose:180mg/kg, MilliporeSigma). Diabetes was defined as blood glucose levels >10 mmol/L. Following transplantation, mice were monitored daily, and blood glucose levels measured weekly. Mice were fed a regular diet and water was provided *ad libitum*. Blood glucose levels were measured by poking the vein at the tip of the tail using 27G sterile needle and a ONETOUCH UltraMini glucose meter (LifeScan Europe GmbH, Zug, Switzerland). Islet engraftment was considered successful when blood glucose levels of the mice dropped below 10mmol/L post transplantation. Following diabetes reversal islet grafts were recovered, with mice undergoing survival nephrectomy to demonstrate the return to their diabetic state.

Statistical analysis

Statistical analysis was completed using Prism, (GraphPad Software, Version 8, San Diego, CA, USA). Differences between groups were identified using Kruskal-Wallis testing with Dunn's post hoc multiple comparisons test. P values ≤0.05 between the groups compared were considered statistically significant.

Results

Islets from various ages of neonatal pigs appeared similar in culture

On light microscopy, NPI from different ages of pigs appeared similar in culture across days 1, 3, 5 and 7. The number of contaminating acinar cells decreased from day 0 to day 7 in culture. The formation of a visible membrane encapsulating the multiple cells of the islet, forming the "micro-organ" structure that has been previously discussed is visualized starting at day 3[228–230] (**Figure 3.1A**). All islets had similar viability in culture, with no significant differences in viability for each age of pig across the 7 days of culture (1-day-old p=0.696, n=4, 3-day-old p=0.063, n=6, 7-day-old p=0.613, n=3) or between the different ages of neonatal pigs at each day of culture (day 0 p=0.711, day 1 p=0.548, day 3 p =0.147, day 5 p=0.517, day 7 p=0.567) **(Figure 3.1B**).

Significant discrepancies in RNA quality using RIN assessment and RNAIQ assay

Reverse transcription negative controls demonstrated no contaminating genomic DNA after DNAse treatment of extracted RNA. Primers were found to have efficiencies between 83.8% and 100.9%. Multigene analysis was initially performed with Beta Actin, GAPDH and HPRT1, and it was determined that for our experiments the optimal normalization factor was achieved when using only two of these genes, Beta Actin and GAPDH as reference genes. RNA Integrity Number (RIN) assessment by the Agilent 2100 Bioanalyzer demonstrated high levels of RNA degradation at days 0 and 1 of culture (RIN = 2.2 +/- 1.0 and 3.2 +/- 2.9 respectively). Therefore, we decided to focus on analyzing gene expression on days 3, 5 and 7 of culture **(Supplementary Table 3.4)**. Interestingly, the values obtained by RNAIQ assay did not correlate

with RIN values across all samples, with significant discrepancies occurring at low RIN values, and these discrepancies were correlated with the inability to amplify and quantify RNA with qRT-PCR (**Supplementary Figure 3.9**). Following this finding, RIN values were used over RNAIQ values for all subsequent samples.

Variable changes in the gene and protein expression of E and VE-cadherin during in vitro postnatal development

E-cadherin gene expression increased in islets isolated from 1- and 7-day old pigs from D3 to D7 of culture (**Figure 3.2A and C** respectively). We did not see this trend in islets from 3-day old pigs even with increased sample size (**Figure 3.2B**). This trend reached significance in islets from 1-day-old pigs (p=0.040) and in 7-day-old pigs (p=0.007), with specific differences identified in islets from 7-day-old pigs between D5 and D7 (p=0.023).

Contradictory to what we expected, VE-cadherin gene expression decreased from D3 to D7 of culture (**Figure 3.2 D, E, F**), with this relationship reaching significance in islets from 1- and 3-day-old pigs, but not in 7-day-old pigs (p=0.002, p=0.009 and p=0.353 respectively). Specific differences in VE-cadherin expression were identified between D3 and D7 for 1-day old pigs and 3-day-old pigs (p=0.011 and 0.013 respectively, **Figure 3.2 D and E**).

In terms of evaluation of the protein expression, our results demonstrate that E-cadherin may have an increasing trend between day 3 and day 5 of culture and moving from day 5 to day 7 it appears to remain stable (**Figure 3.3 A, B, C**). This trend only reached statistical significance in 1-day-old pigs between D3 and D5 of culture (p=0.019, Dunn's multiple comparisons test p= 0.033).

VE cadherin protein expression demonstrated no significant differences or clear trends from D3 to D7 in any age of neonatal pig (**Figure 3.3 D, E, F**).

Variable changes in the gene and protein expression of GLUT2, RAC1 and SNAP25; molecules involved in the insulin secretion pathway

Our results demonstrated that GLUT2 is expressed in low abundance in NPIs, leading to prohibitively high CT values on RT-qPCR. Due to such we were unable to confidently quantify

differences between samples and have not reported them in this manuscript. RAC1 gene expression appeared to be stable across day 3, day 5 and day 7 of culture with no statistically significant values being detected between such days in any age of neonatal pig (**Figure 3.4 A, B, C**). SNAP25 gene expression in our samples appeared to increase from D3 to D7 of culture, and this was found to be statistically significant in 1-day-old (p=0.016) and 3-day-old pigs (p=0.001), with a similar, but not significant trend being seen in 7-day-old pigs (p=0.332, **Figure 3.4, D, E, F**). Specific differences were identified between days 5 and 7 on the 1-day-old pigs (p=0.024) and between days 3 and 7 on the 3-day-old pigs (p=0.002).

In terms of protein expression, RAC1 protein expression appears to be similar to gene expression and was stable in 3-day-old and 7-day-old pigs. However, our data demonstrated a statistically significant decrease in 1-day-old pigs after D3 of culture (p=0.006), which persisted after completing this experiment in a greater number of pigs (n=8), with statistically significant differences existing between D3 and D5 (p=0.008) and D5 and D7 (p=0.049, **Figure 3.5 A, B,C**). For SNAP25 protein expression, there appeared to be a decrease in protein expression which was apparent in trends across all ages of pigs, which contradicted the SNAP25 gene expression (**Figure 3.5, D, E, F**). This decrease in SNAP25 protein expression reached significance in 1-day-old pigs (p=0.003), with post hoc differences being identified between D3 and D7 (p=0.013). Of note, when moving from Day 3 to Day 7 of culture, additional bands at various lengths appeared on western immunoassay, suggesting that although there was less free SNAP25 protein, as determined by the area under the curve at the appropriate molecular weight for SNAP25, that the anti-SNAP25 monoclonal antibody was detecting proteins of alternate molecular weights which possessed the SNAP25 epitope, which could be explained by post translational modification of the protein.

In vitro and in vivo insulin secretory capacity of islets obtained from 1, 3 and 7-day-old neonatal pigs

Figure 3.6 shows results from the glucose stimulated insulin secretion (GSIS) assay quantifying the insulin secretory capacity of islets from 1, 3 and 7-day-old pigs at seven days of culture. Specifically, islets from 1-day-old pigs appear to have a greater proportion of insulin

secreted under high glucose conditions compared to 3-day-old and 7-day old pigs. Interestingly, the 1-day-old islets' insulin % secretion values when exposed to high glucose and KCl was similar to what was observed in high glucose condition without KCl. In contrast, islets obtained from 3-day-old and 7-day-old pigs demonstrated progressively higher proportions of insulin secreted moving from the low glucose to high glucose to high glucose supplemented with KCl conditions.

A greater proportion of mouse recipients of islets from 3-day-old and 7-day-old pigs achieved normoglycemia post-transplantation compared to recipients of islets from 1-day-old pigs

The ability of islets from 1-day-old, 3-day-old and 7-day-old pigs to reverse the diabetic state of immune-deficient B6 *Rag -/-* mouse models was also determined. We found that 75% (3/4) of the mice transplanted with islets from 1-day-old pigs, 100% (4/4) of the mice transplanted with islets from 3-day-old pigs and 100% (6/6) of mice transplanted with islets from the 7-day-old pigs reversed their diabetic state. Time to diabetic reversal across all cohorts varied from mouse to mouse, ranging from 11 to 17 weeks post-transplantation for recipients of islets from 1-day-old pigs, 8 to 22 weeks post-transplantation for recipients of islets from 3-day-old pigs, and 8 to 21 weeks post-transplantation for recipients of islets from 7-day-old pigs (**Figure 3.7).**

Treatment of islets with anti E-cadherin resulted in reduced in vitro insulin secretory capacity

To demonstrate the importance of E-cadherin and cell-cell adhesion in maintaining early NPI structure and function, we treated NPIs with anti E-cadherin monoclonal antibody, subsequently testing their function in vitro. Following treatment with the anti E-cadherin antibody, islets showed qualitative changes, having a less well defined external border as is shown in **Figure 3.8 A and C**. Functionally, these islets were not able to increase the proportion of insulin that they secreted under high glucose conditions, demonstrating an insulin stimulation index of 1.2x compared to the 2.8x seen in the control group (**Figure 3.8 B and D**).

Discussion

Over the past three decades, significant research has been completed on developing genetically modified pigs to combat the immune mechanisms hampering the success of xenotransplantation. During this time, investigation into the basic biology and physiology of pig tissue has been neglected, presumably following the assumption that pig physiologic and developmental pathways are similar to those of humans and mice. Our work explores qualitative and quantitative aspects of early NPI biology, with special interest in cell-cell adhesion and the insulin secretion pathway, ultimately demonstrating the importance of E-cadherin in the insulin secretion pathway. Other key findings in our study include that VE-cadherin appears to decrease across seven days of in vitro culture and that neonatal pig islets obtained from 1-day-old pigs may be less effective in the reversal of diabetes compared to those of 3- and 7- day-old pigs.

Few previous studies have explored the genetic expression in the early neonatal phase of pig islet development. Recently, a study by Kim et al. explored broad gene expression trends with RNA-Seq libraries obtained from pig islets across fetal and select neonatal time periods[220]. We feel our study compliments their data, with our manuscript looking at additional timepoints in the early neonatal phase to identify trends in the expression of our molecules of interest over the first few days in culture. We feel that changes in gene expression experienced during this developmental period are important to identify, as in many xenotransplantation models, NPIs are transplanted following an arbitrary number of days in culture. If we had a better appreciation of the changes in gene and protein expression occurring in these pig islets, we may be better able to predict the best time which to transplant pig islets from culture into recipients.

Other key articles related to cadherin cell-cell adhesion molecules and their impact on islet function in models outside of pigs include an article published by Roullier et al. in 1991, which found that uvomorulin (now more commonly known as E-cadherin), when inhibited by monoclonal antibodies, led to the inability for rat islets to aggregate in culture, suggesting that E-cadherin was a major determinant of cell-cell adhesion within the islet, with cell-cell adhesion and communication being known to be critical for islet function[38,175,231]. In 1996, Dahl et al. explored the role of E-cadherin on islet organization in vivo using a transgenic prenatal mouse

model, demonstrating the inability for pancreatic endocrine cells to cluster when E-cadherin protein was truncated[134]. Beyond promoting cell-cell adhesion and cell clustering, E-cadherin also appears to play a role in pancreatic beta cell proliferation, and over expression of E-cadherin has been shown to limit proliferation of pancreatic beta cells lines [131,141,232]. Further research in rodent models demonstrated multiple types of cell adhesion molecules directing differential cell segregation within islets; however, studies have not been previously completed in pigs[175,233,234]. Specifically, the role of E-cadherin in the development in pig islets has not been previously investigated, spurring the motivation for our study.

Working linearly through our results, we first demonstrate excellent viability of our islets in culture, around 90%, which is comparable to that previously cited for NPI, supporting the quality of our culture methods[221]. Admittedly, when working with pancreatic tissue, a common source of RNAses, we encountered difficulties with RNA degradation[235–237]. Following our experience, we highly recommend routine RNA integrity assessments when working with samples extracted from pancreatic tissue. Our manuscript also highlights discrepancies we encountered between RIN vs RNAIQ, which are touted as two credible assays for RNA assessment[236,238–240]. In our hands, we found that the RNAIQ assay did not always correlate with the RIN values, which is commonly treated as the gold standard for RNA degradation assessment[236]. Differences in quality assessments occurred primarily at times of high RNA degradation, resulting in higher than expected CT values on RT-qPCR, which could be a confounding factor in RT-qPCR results if solely the RNAIQ assay was used. We encourage all groups interested in using the RNAIQ Assay and Qubit spectrophotometer to assess RNA quality to ensure their assay is validated and compared across a variety of RNA levels of degradation before use.

Explaining our variety of gene expression results, starting with E-cadherin, we find the gene expression trends towards an increase during culture. Interestingly, we found the increase in protein expression to stabilize following day 5 in culture, which may be related to a highly regulated balance of E-cadherin expression balancing the cell-cell adhesion properties of high E-cadherin expression with its potential for high expression to decrease beta cell proliferation. Interestingly, Wakae-Takada et al. found a two-fold increase in E-cadherin in beta cells in a

mouse model between birth and 22 days post-natally at which time expression gene expression became constant, demonstrating a somewhat similar trend to our results[131].

Other expression results which deserve discussion include the finding that GLUT2 was not highly expressed in neonatal pigs islets, which is supported by previous studies[159]. SNAP25 appeared to increase in gene expression from day 3 to day 7 of culture, which logically makes sense, given the increase in insulin secretory capacity in older pig islets[219,221]; however, the protein expression did not follow a similar pattern. SNAP25 is a protein commonly involved in synaptic vesicle targeting fusion and exocytosis and undergoes a variety of protein-protein interactions forming numerous multimeric protein complexes, which have potential to confound western blot results[241,242]. This was demonstrated in our results as at later timepoints in culture, our western immunoassay demonstrated a variety of bands, likely due to post translational modifications[241,242]. Without performing immunoprecipitation and separating the free SNAP25 epitope from the attached proteins it is difficult to properly quantify protein expression for this molecule.

We found the gene expression of VE-cadherin to decrease from days 3-7 in culture, which we found surprising as during in vitro culture pig islets do not have a functional blood supply, and we expected them to be producing proteins associated with the formation of endothelial cells, including VE-cadherin. To explain this requires further investigation and our lab plans to investigate different molecules which act as vascular mediators and look at VE-cadherin in an in vivo model.

In terms of neonatal pig islet function, previous study demonstrated a difference in insulin secretory capacity between islets which had spent different amounts of time in culture, with pig islets demonstrating the greatest level of insulin secretion at 7 days of culture compared to 3 and 5 days. This finding led to us performing our in vivo and in vitro testing following 7 days of culture, with the intent to identify differences in function from islets obtained from different ages of neonatal pigs[221]. Looking at the results from Figures 6 and 7 combined, we see that islets from 1-day-old pigs do not seem to follow the expected in vitro secretion pattern and reversed diabetes in 3 of the 4 experimental mice. Normally, we would expect 2000 NPI to reverse diabetes in 100% of diabetic recipient mice, suggesting that 1-day-

old pig islets may not be favorable for transplantation[202]. Previous research has gone beyond our tested time points and observed the in vitro function of fetal neonatal pig islets[220]. Kim et al. showed that the basal and stimulated rate of insulin secretion decreases with time when comparing late fetal pig islets to islets obtained from 22-day-old pigs[220]. Differences seen in our experiment between islets from 1-day-old pigs compared to 7-day-old pigs also demonstrated a decreasing proportion of insulin secreted under high glucose conditions as islets were obtained from older pigs. These findings taken together suggest the possibility for dysregulated insulin secretion under high glucose conditions in islets obtained from fetal or 1-day-old neonatal pigs[220].

Finally, previous studies evaluating the impact of E-cadherin on insulin secretion in cell lines suggest that E-cadherin alterations impact stimulated insulin secretion, likely through its effect on the actin cytoskeleton[139]. To link E-cadherin and neonatal pig islet function we inhibited the interactions of E-cadherins using monoclonal antibodies, subsequently assessing NPI appearance and function. Like the results seen previously in MIN6 cells, we saw the islet clusters become more loosely aggregated, and have a decreased ability to increase insulin secretion under high glucose conditions[140,234,243]. We are the first to demonstrate such in pig islets, which is more applicable to the field of xenotransplantation than previous studies as it is known that clonal cell lines forming pseudoislet structures in vitro do not always follow similar physiologic pathways as native islets[244]. This physiologic alteration and decreased ability for islets inhibited by E-cadherin monoclonal antibodies to respond to high glucose conditions may be related to loss of gap junction communication, as was suggested in MIN6 beta cells, but requires further study[243].

Limitations

During our study, the scope of molecules which we were able to test was limited as pig specific monoclonal antibodies and RNA primers were not available for all our molecules of interest. In the future we plan to investigate the gene and protein expression of additional molecules: beta catenin, ephrinA5 and VAMP2 as they are known to be associated with cadherins and the actin cytoskeleton[134,149,232,241,242,245,246]. In addition, in retrospect, it would

have been interesting to initially perform a broader scope of gene expression analysis through next generation sequencing techniques like RNA-Seq to guide the selection of our molecules of interest. We also encountered difficulties with the downregulation of cadherin molecules through siRNA transfection and were unable to obtain a siRNA sequence that could downregulate pig cadherin mRNA. We eventually overcame this by using monoclonal antibodies targeting E-cadherin to inhibit its function. Future directions to investigate cadherin molecules in pigs could parallel those done in mice by Dahl et al., in which a truncated E-cadherin protein was expressed in beta cells, allowing the study of its loss of function[134]. Lastly, we did not separate our preparation by islet cell type. This was done as our islet products were felt to be more representative of the islet preparations which are transplanted into animal models, but we do acknowledge this makes it difficult to interpret overall gene expression as there is heterogeneity with varying levels of endocrine cells throughout different days of culture.

Conclusions and implications

We demonstrate novel findings in gene expression patterns across specific molecules of interest in early neonatal pig islet development. Specifically, we outline that: E-cadherin gene expression appears to be upregulated across seven days of in vitro culture, whereas VE-cadherin is downregulated, and that E-cadherin mediated cell-cell adhesion appears to be important for NPI insulin secretion under high glucose conditions. Further understanding of pig islet biology is important for the advancement of pig islet xenotransplantation to the clinical setting.

Acknowledgements

This work was supported by grants from the Clinician Investigator Program, a NSERC Discovery Grant, CIHR Canadian Graduate Masters Scholarship (CGS-M), University of Alberta's Masters Entrance Scholarship and the Alberta Graduate Excellence Scholarship (AGES). We would also like to thank Dr. Kunimasa Suzuki of the Alberta Diabetes Institute for his assistance in designing the custom TaqMan primers.

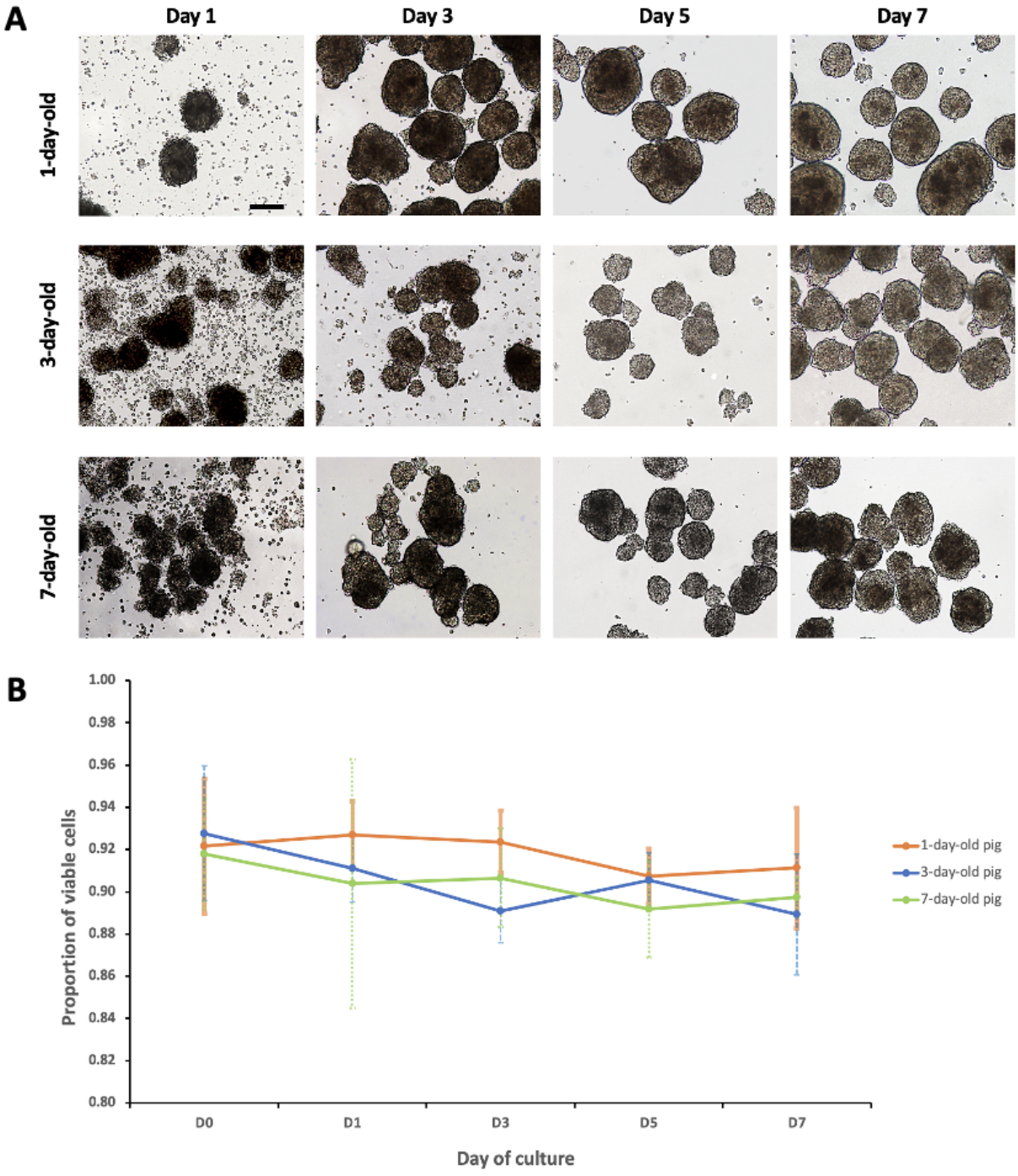

Figure 3.1: Morphology and viability of neonatal pig islets. (A) Light microscopy of neonatal pig islets from different ages of pigs (1, 3 and 7-day-old), taken at different days of in vitro culture (Day 1, 3, 5 and 7). Images taken at 10x objective magnification. Scale bar = 100µm. (B) In vitro viability of islets from different ages of neonatal pigs across 7 days of culture, as measured by Trypan Blue exclusion dye test. Error bars indicate 1 standard deviation.

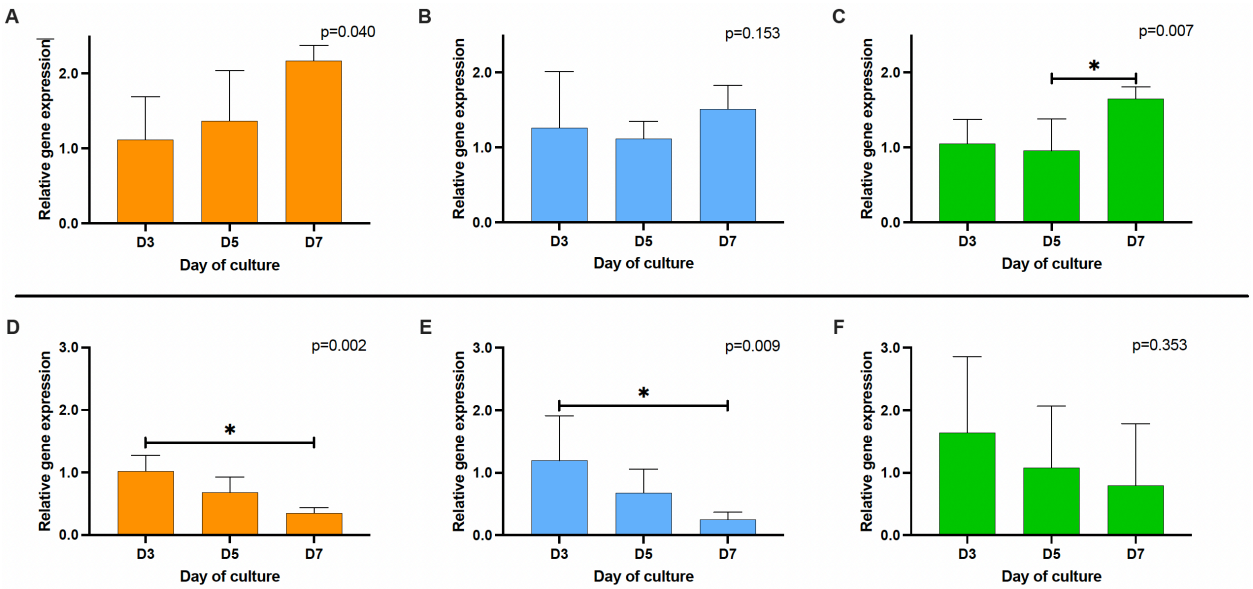

Figure 3.2: Quantification of *CDH1* (E-cadherin) and *CDH5* (VE-cadherin) gene expression by islets obtained from different ages of neonatal pigs (1, 3 and 7-day-old), taken at different days of in vitro culture (Day 3, 5 and 7), as determined by quantitative reverse transcription polymerase chain reaction (RT-qPCR). (A) CDH1 gene expression from 1-day-old pig islets (n=4). (B) CDH1 gene expression from 3-day-old pig islets (n=6). (C) CDH1 gene expression from 7-day-old pig islets (n=5). (D) CDH5 gene expression from 1-day-old pig islets (n=4). (E) CDH5 gene expression from 3-day-old pig islets (n=6). (F) CDH5 gene expression from 7-day-old pig islets (n=5). Error bars indicate standard deviations; numerical reported p-values determined by Kruskal-Wallis testing; asterisks indicate results of Dunn's multiple comparisons post hoc testing; *p<0.05.

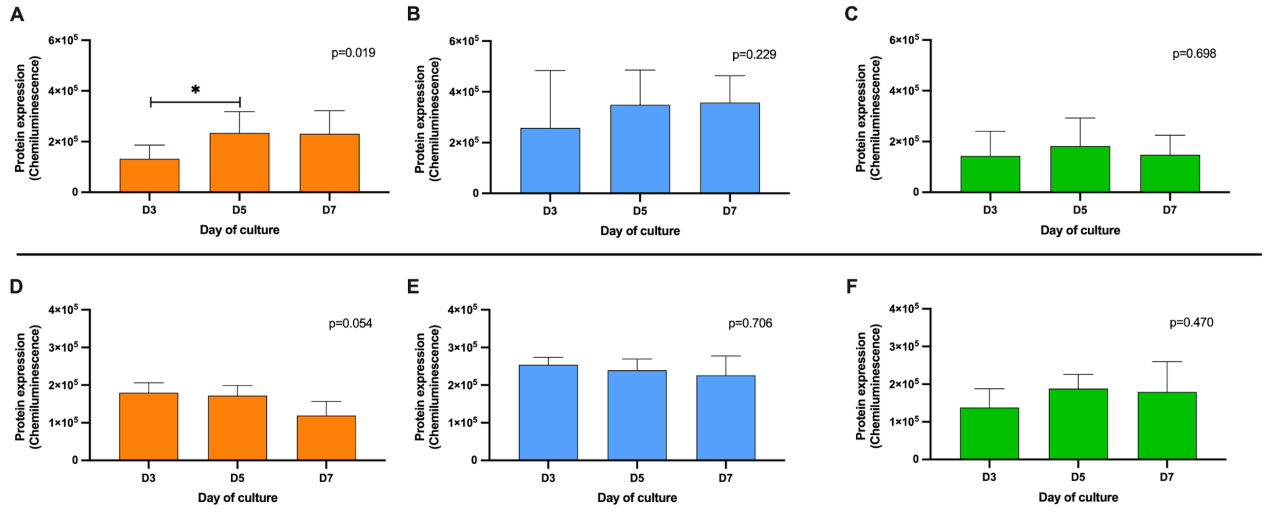

Figure 3.3: Quantification of E-cadherin and VE-cadherin protein expression from different ages of neonatal pigs (1, 3 and 7-day-old), at different days of in vitro culture (Day 3, 5 and 7), as determined by automated western blot. (A) E-cadherin protein expression from 1-day-old pig islets (n=8). (B) E-cadherin protein expression from 3-day-old pig islets (n=8). (C) E-cadherin protein expression from 7-day-old pig islets (n=8). (D) VE-cadherin protein expression from 1-day-old pig islets (n=4). (E) VE-cadherin protein expression from 3-day-old pig islets (n=4). (F) VE-cadherin protein expression from 7-day-old pig islets (n=4). Error bars indicate standard deviations; numerical reported p-values determined by Kruskal-Wallis testing; asterisks indicate results of Dunn's multiple comparisons post hoc testing; *p<0.05.

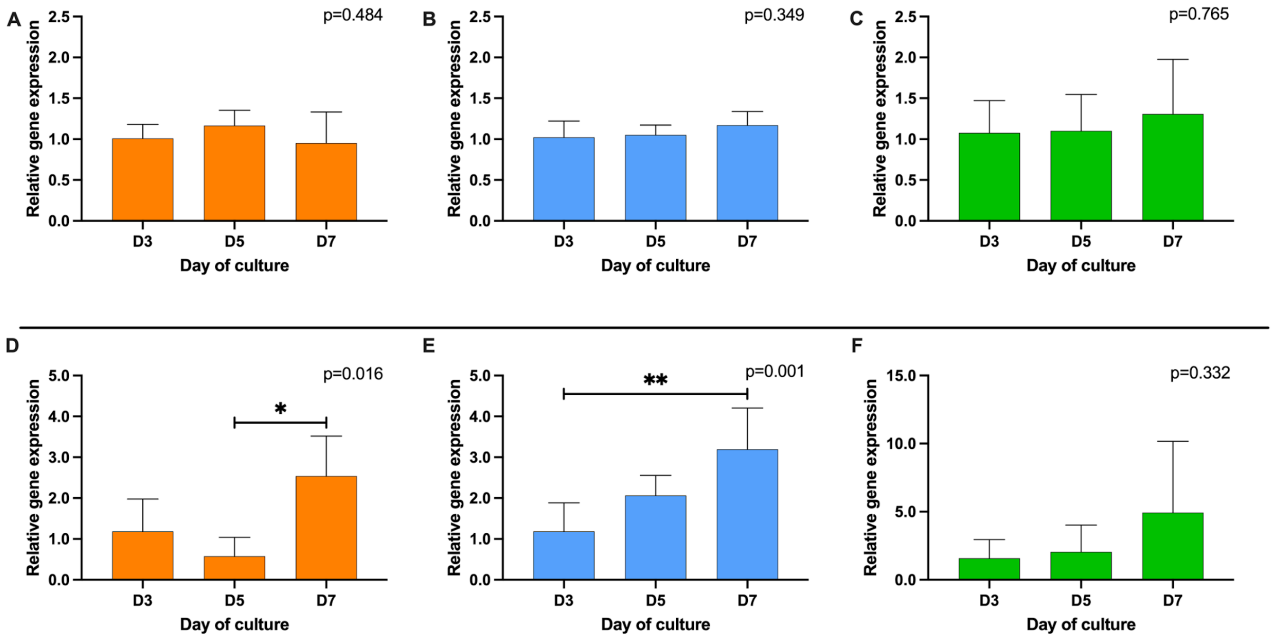

Figure 3.4: Quantification of *RAC1* and *SNAP25* gene expression by islets obtained from different ages of neonatal pigs (1, 3 and 7-day-old), taken at different days of in vitro culture (Day 3, 5 and 7), as determined by quantitative reverse transcription polymerase chain reaction (RT-qPCR). (A) RAC1 gene expression from 1-day-old pig islets (n=4). (B) RAC1 gene expression from 3-day-old pig islets (n=6). (C) RAC1 gene expression from 7-day-old pig islets (n=5). (D) SNAP25 gene expression from 1-day-old pig islets (n=4). (E) SNAP25 gene expression from 3-day-old pig islets (n=6). (F) SNAP25 gene expression from 7-day-old pig islets (n=5). Error bars indicate standard deviations; numerical reported p-values determined by Kruskal-Wallis testing; asterisks indicate results of Dunn's multiple comparisons post hoc testing; *p<0.05, ** p<0.01.

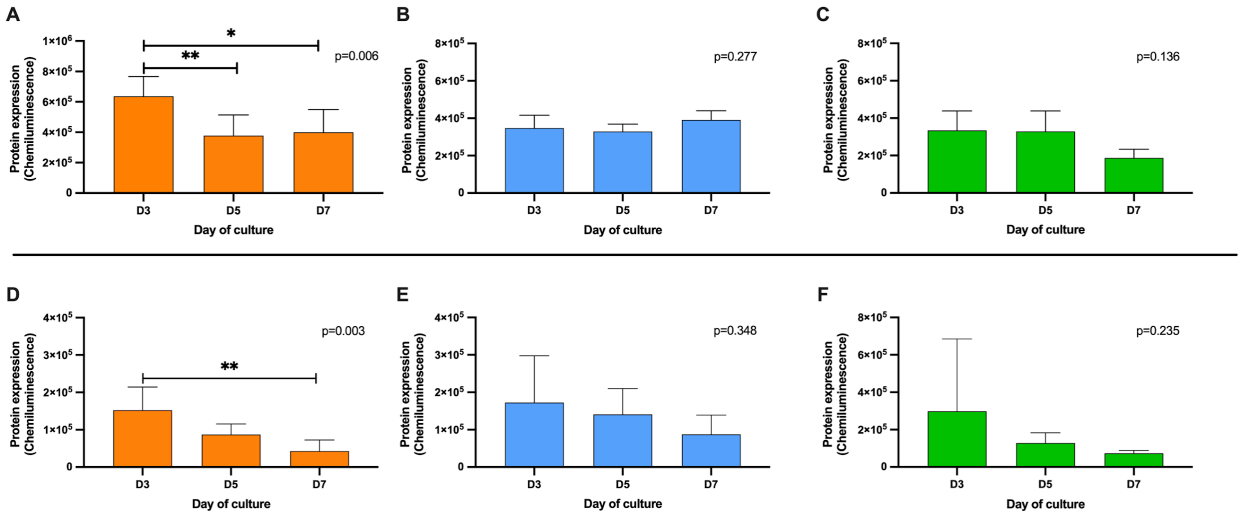

Figure 3.5: Quantification of RAC1 and SNAP25 protein expression by islets obtained from different ages of neonatal pigs (1, 3 and 7-day-old), at different days of in vitro culture (Day 3, 5 and 7), as determined by automated western blot. (A) RAC1 protein expression from 1-day-old pig islets (n=8). (B) RAC1 protein expression from 3-day-old pig islets (n=4). (C) RAC1 protein expression from 7-day-old pig islets (n=4). (D) SNAP25 protein expression from 1-day-old pig islets (n=4). (E) SNAP25 protein expression from 3-day-old pig islets (n=4). (F) SNAP25 protein expression from 7-day-old pig islets (n=4). Error bars indicate standard deviations; numerical reported p-values determined by Kruskal-Wallis testing; asterisks indicate results of Dunn's multiple comparisons post hoc testing; *$p<0.05$, **$p<0.01$.

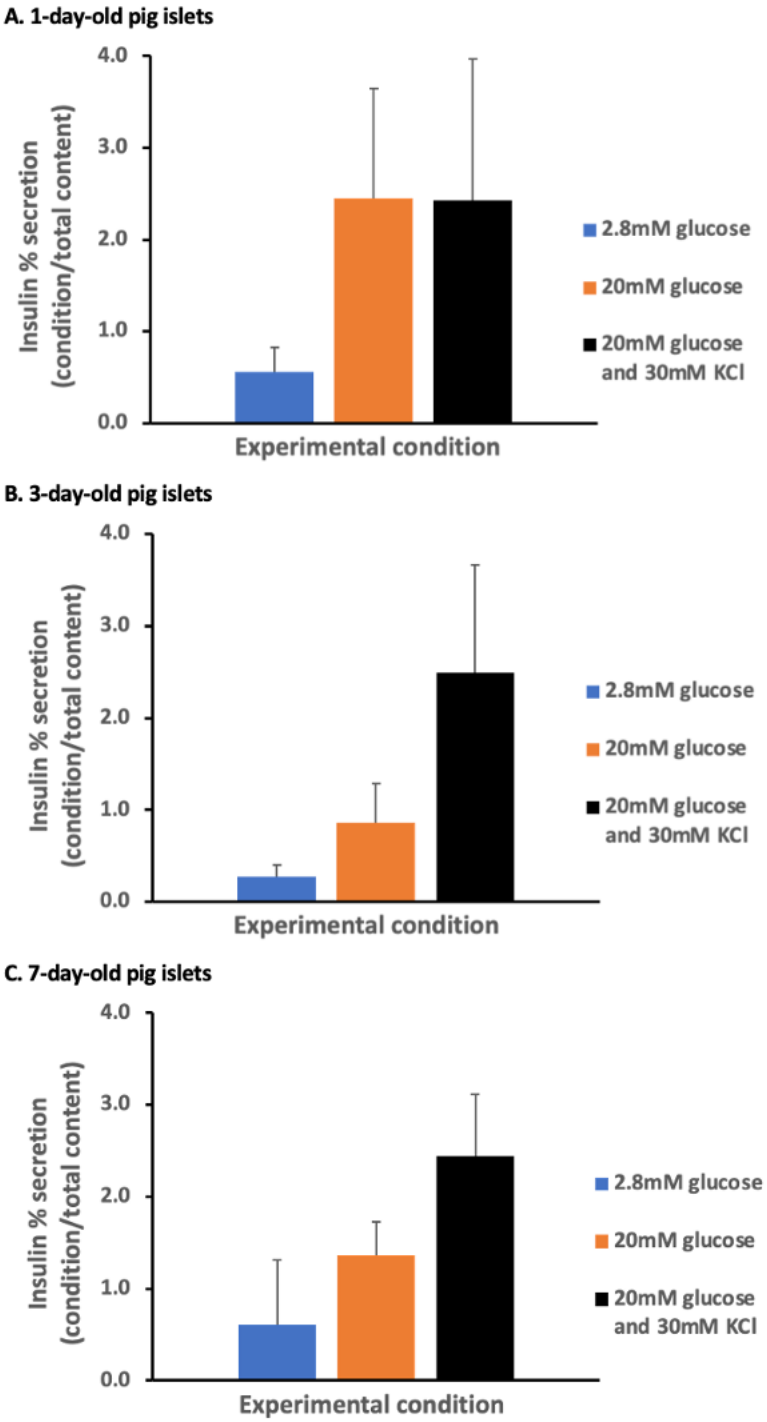

Figure 3.6: In vitro insulin secretory capacity for 200 IEQ of islets obtained from different ages of neonatal pigs, tested at 7 days of culture. (A) 1-day-old pig islets (n=4), (B) 3-day-old pig islets (n=3), and (C) 7-day-old pig islets (n=4). Islets were exposed to 2.8mM of glucose to quantify basal insulin secretion and later exposed to 20mM of glucose and 20mM of glucose with 30mM KCl conditions to quantify stimulated insulin secretion. Error bars indicate standard deviation.

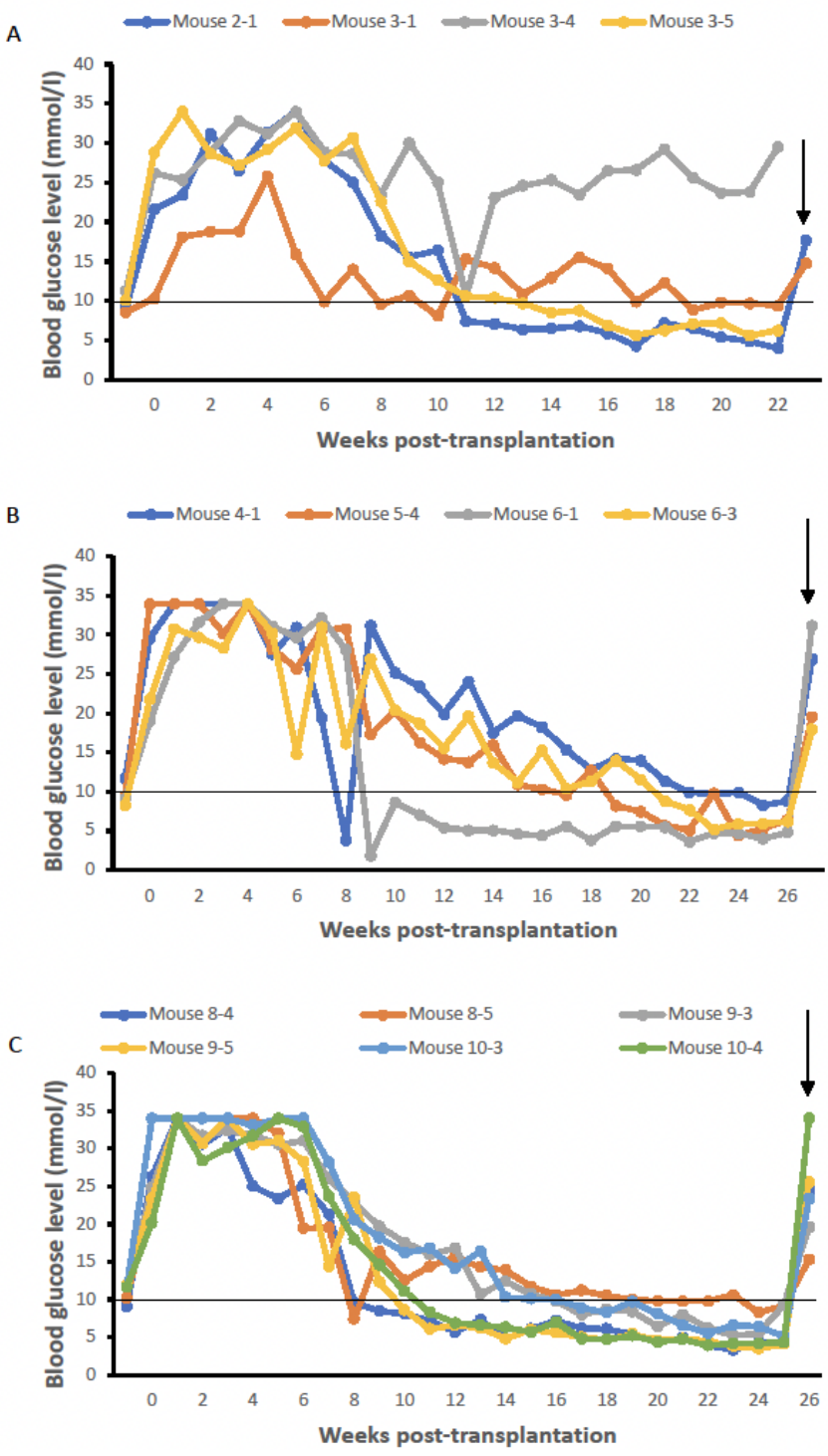

Figure 3.7: Blood glucose levels of B6 Rag -/- mice transplanted with 2000 IEQ of neonatal pig islets. (A) Recipients of islets from 1-day-old pigs (n=4), (B) recipients of islets from 3-day-old pigs (n=4), and (C) recipients of islets from 7-day-old pigs (n=6). Graph demonstrates blood glucose levels of mice that received 2000 IEQ of neonatal pig islets. Solid black arrow indicates blood glucose levels one day following survival nephrectomy demonstrating the reversal of diabetes.

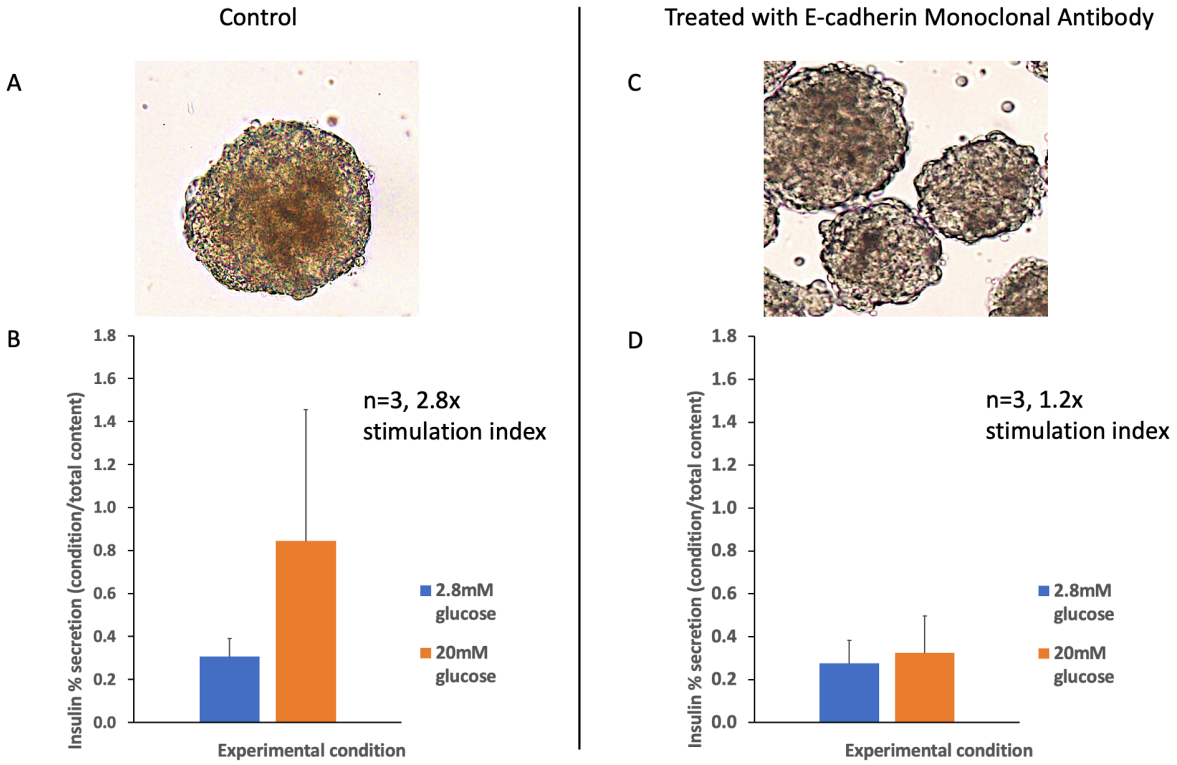

Figure 3.8: Qualitative and quantitative response of 3-day-old neonatal pig islets at 8 days of culture after treatment with anti E-cadherin monoclonal antibody. (A) Light microscopy image of control NPI not treated with monoclonal antibody. (B) In vitro insulin secretory capacity of untreated islets, obtained by GSIS assay. (C) Light microscopy image of NPI following treatment with 5µg/uL of anti-E-cadherin monoclonal antibody. (D) In vitro insulin secretory capacity of islets following treatment with 5µg/uL of anti-E-cadherin monoclonal antibody, obtained by GSIS assay. Stimulation index is calculated by insulin % secretion at the 20mM glucose condition divided by the insulin secretion at the 2.8mM glucose condition. Images at 20x objective magnification.

Supplementary Data

Supplementary Table 3.1: TaqMan real-time polymerase chain reaction primer details ordered off the shelf from ThermoFisher Scientific

Primer target molecule	ThermoFisher Scientific TaqMan primer ID	Efficiency (%)	Amplicon length (number of base pairs)
E (epithelial) cadherin	Ss03377287_u1	88.7	121
VE (vascular-endothelial) cadherin	Ss03378336_u1	92.6	105
GLUT2	Ss03385240_u1	95.7	79
RAC1	Ss06942696_m1	100.9	65
Beta actin	Ss03376563_uH	95.7	79
GAPDH	Ss03375629_u1	92.0	64
HPRT1	Ss03388273_m1	92.9	112

Supplementary Table 3.2: TaqMan real-time polymerase chain reaction primer details custom designed by our research team

Primer target molecule	Custom primer/probe sequence	Efficiency	Amplicon length (number of base pairs)
SNAP25	Forward primer - AATCAGGATGGAGTTGTGGCCA Reverse primer - CATGTGACGGAGGTTTCCAATGATG Probe - CATCAGTGGTGGCTTCATCCGCAGGGTAACAAATGATGC	83.8	168

Supplementary Table 3.3: KRBH Solution Recipe

Reagent	mM	Added for 1000mL KRBH
NaCl	115	6.720g
KCl	5	0.372g
$NaHCO_3$	24	2.016g
$CaCl_2 . 2H_2O$	2.5	0.368g
$MgCl_2 . 6H_2O$	1	0.203g
HEPES	10	2.383g
BSA	0.5%	5.0g
Deionized H_2O		1000mL

Ph to 7.32 at 37C

Add glucose & KCl as required for conditions of interest

Supplementary Table 3.4: Average RNA Integrity Number (RIN) values of RNA extracted from islets across various days of culture

Day of Culture	n	Average RIN +/- SD
Day 0	8	2.2 +/- 1.0
Day 1	7	3.2 +/- 2.9
Day 3	12	6.2 +/- 2.8
Day 5	12	7.5 +/- 2.3
Day 7	14	7.7 +/- 0.7

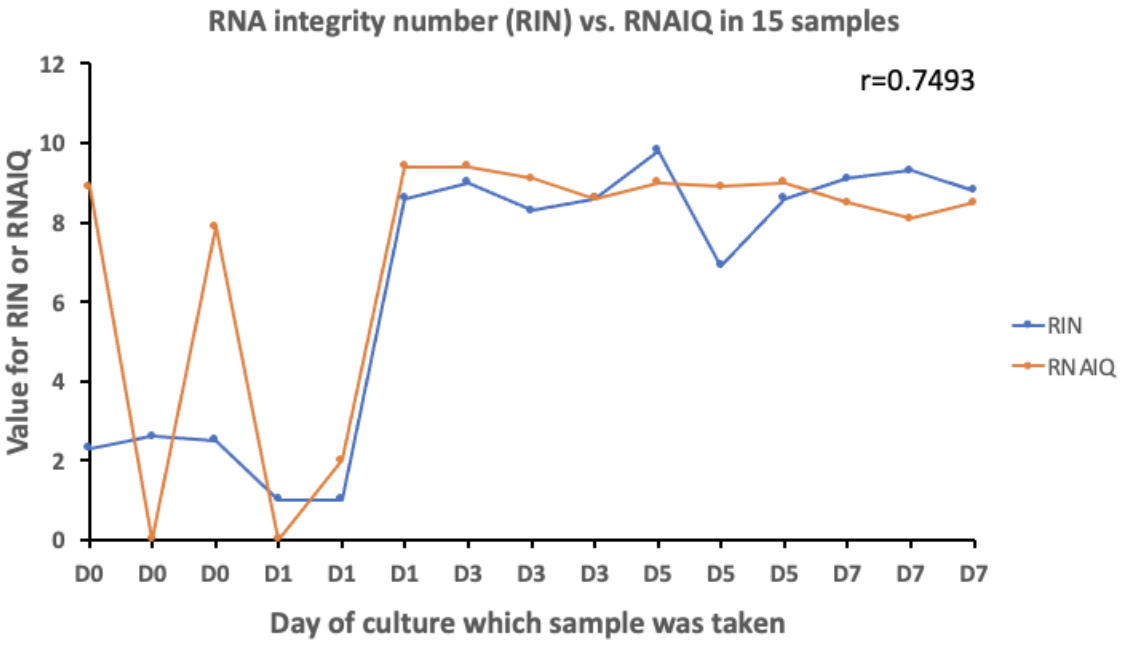

Supplementary Figure 3.9: Comparison of two independent assessments used to determine RNA quality across 15 samples. RNA Integrity Number (RIN) values, as determined by Agilent 2100 Bioanalyzer (Agilent) vs. RNAIQ values, as determined by Qubit fluorometer (ThermoFisher).

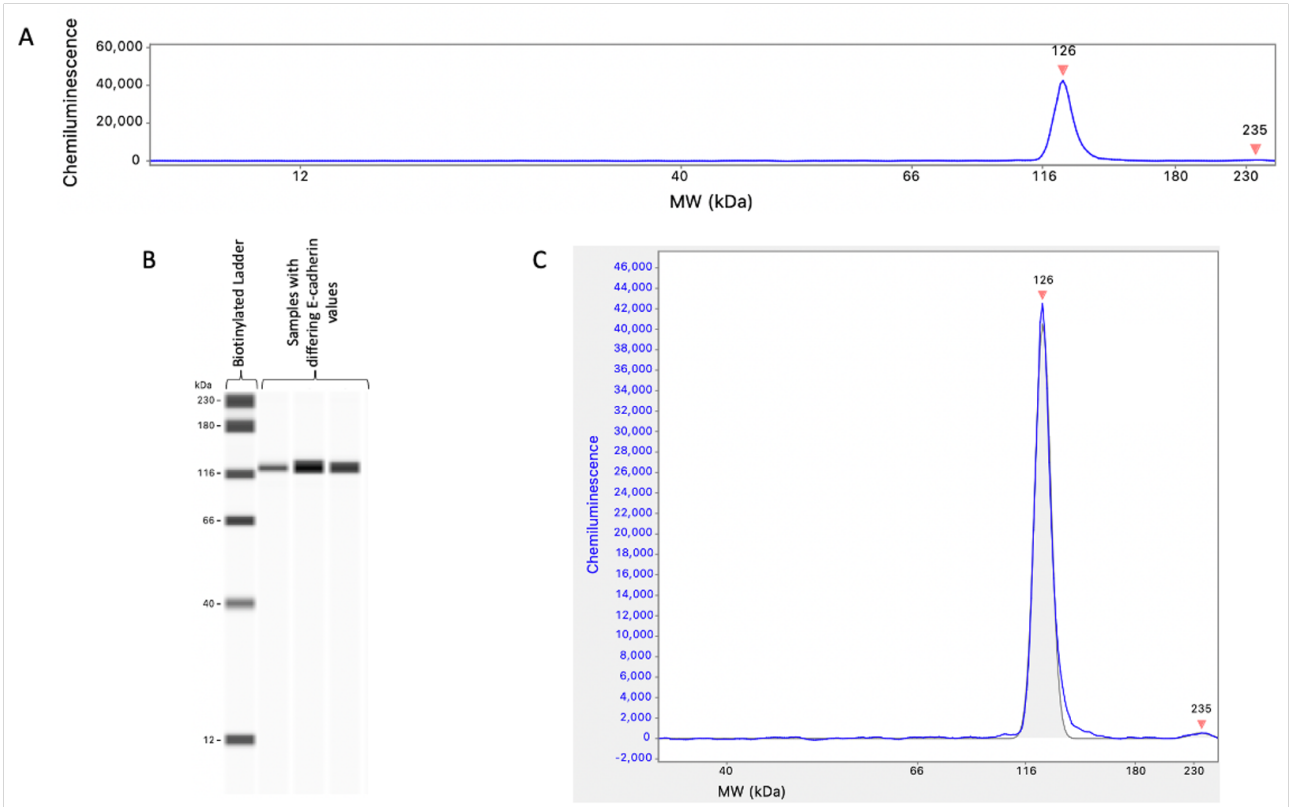

Supplementary Figure 3.10: Visual demonstration of the output and interpretation of the Simple Western WES machine results, interpreted with the use of Compass Software Version 5.0.1. (A) electropherogram produced by WES machine demonstrating single band for E-cadherin. (B) Results from WES demonstrated in classical Western Blot format, as rendered by Protein Simple's Compass Software. (C) Image demonstrating electropherogram, with light grey shading outlining the fitting of peaks, used to estimate area under the curve and protein quantification.

Chapter 4 Exploring the postnatal development of neonatal pig islets: an in vitro model, general discussion and conclusions

Type 1 diabetes mellitus (T1DM) is a common, chronic metabolic disorder defined by hyperglycemia due to the autoimmune destruction of the endocrine cells in the pancreas. The majority of T1DM patients are treated by exogenous insulin injection, which has turned diabetes from a fatal disease into a chronic disease; however, patients with diabetes still suffer various acute and chronic complications, and insulin therapy requires significant amounts of patient education and responsibility.

Alternative feasible treatment options include pancreas and islet transplantation, both of which have been proven to be able to reverse diabetes in the clinical setting. Multiple barriers currently hamper the expansion of islet transplantation including the limited number of pancreatic donors, the immune rejection of donor grafts by host immune systems necessitating the need for immune suppression as well as difficulty monitoring of islet grafts following transplantation. As is detailed throughout this thesis, pig islet xenotransplantation could serve as a solution to many of these problems and could provide access to an unlimited source of islets for transplantation and research.

To address two specific barriers faced by islet transplantation, these being the imaging of islets following transplantation and the understanding of pig islet biology, for which a better understanding is necessary for the translation of pig islet xenotransplantation to the clinical realm, we performed a variety of experiments as has been detailed in Chapters 2 and 3 of this thesis. In Chapter 2, we demonstrated the ability to use a novel polymer to coat iron oxide nanoparticles which were then used to label neonatal porcine islets. Our data demonstrates that our reagent of interest, polyvinylpyrrolidone (PVP), can be used to coat superparamagnetic iron oxide (SPIO) nanoparticles, allowing these islets to be visualized on MRI in a mouse model. Future research could explore the safety of this agent in large animal models.

In Chapter 3, we conduct an exploratory study looking at the gene and protein expression by pig islets, with special focus on molecules spanning cell-cell adhesion and insulin secretion pathways in the early post-natal phase. We identify trends in E and VE-cadherin protein expression which could be used as a starting point to determine the optimal age of neonatal pig islets for transplantation. Our experiments characterize a relationship between E-cadherin and the

insulin secretion pathway for the first time in neonatal pig islets by demonstrating the loss of islet function under high glucose conditions by pig islets which have been inhibited by anti E-cadherin antibodies. A better understanding of the biology and physiology of the tissue that we plan to use for transplantation is essential in the translation of pig islet xenotransplantation to the clinical realm. Future directions for this focus of study could include broad genome wide association type studies observing the overall trends of gene expression by techniques like RNA-Seq and further study regarding the specific impact of E-cadherin on the actin cytoskeleton to mechanistically define how it impacts stimulated insulin secretion.

In conclusion, pig islet xenotransplantation holds potential to solve many of the problems faced by the field of islet transplantation today. However, despite recurrent successes in large animal models including non-human primates, at this time it has not been proven successful in clinical use. We feel that a further understanding of pig islet biology will help advance the field, and a better understanding of the underlying physiologic pathways as well as the differences between these pathways in pigs and humans will help us be better able to optimize the tissue we plan to eventually transplant into humans. Research in this area will also uncover further knowledge that is necessary to have when manipulating pig tissue to try limit immune rejection and increase chance of graft success. We hope that this thesis and the papers contained within will provide insight and eventually help advance pig islet xenotransplantation to the clinical setting.

References

1. Thomas CC, Philipson LH. Update on Diabetes Classification. *Med Clin North Am*. 2015;99(1):1-16. doi:10.1016/j.mcna.2014.08.015
2. You WP, Henneberg M. Type 1 diabetes prevalence increasing globally and regionally: The role of natural selection and life expectancy at birth. *BMJ Open Diabetes Res Care*. 2016;4(1):1-7. doi:10.1136/bmjdrc-2015-000161
3. WHO. *Definition and Diagnosis of Diabetes Mellitus and Intermediate Hyperglycemia*.; 2006.
4. Bilandzic A, Rosella L. The cost of diabetes in Canada over 10 years: Applying attributable health care costs to a diabetes incidence prediction model. *Heal Promot Chronic Dis Prev Canada*. 2017;37(2):49-53. doi:10.24095/hpcdp.37.2.03
5. Augustyn Adam, Zeidan Adam ZA et al. Islets of Langerhans. In: *Encyclopædia Britannica*. ; 2020. https://www.britannica.com/science/islets-of-Langerhans.
6. Caglar V, Kumral B, Uygur R, Alkoc OA, Ozen OA, Demirel H. Study of Volume, Weight and Size of Normal Pancreas, Spleen and Kidney in Adults Autopsies. *Forensic Med Anat Res*. 2014;02(03):63-69. doi:10.4236/fmar.2014.23012
7. Nakamura, Hana, Satou A. *Pancreas : Anatomy, Diseases, and Health Implications*. New York: Nova Science Publishers, Inc; 2012. https://search-ebscohost-com.login.ezproxy.library.ualberta.ca/login.aspx?direct=true&db=e000xna&AN=548884&site=eds-live&scope=site.
8. Meier JJ, Köhler CU, Alkhatib B, et al. B-Cell Development and Turnover During Prenatal Life in Humans. *Eur J Endocrinol*. 2010;162(3):559-568. doi:10.1530/EJE-09-1053
9. Rayat GR, Rajotte R V., Hering BJ, Binette TM, Korbutt GS. In vitro and in vivo expression of Galα-(1,3)Gal on porcine islet cells is age dependent. *J Endocrinol*. 2003;177(1):127-135. doi:10.1677/joe.0.1770127
10. Criscimanna, Angela, Speicher, Julie Houshmand G. Duct Cells Contribute to Regeneration of Endocrine and Acinar Cells Following Pancreatic Damage in Adult Mice. *Gastroenterology*. 2015;141(4):1451-1462. doi:10.1053/j.gastro.2011.07.003.Duct
11. Jolles S. Paul Langerhans. *J Clin Pathol*. 2002;55:243.
12. Sakula A. Paul Langerhans (1847-1888): a centenary tribute. *J R Soc Med*. 1988;81(July):414-415.
13. Cabrera O, Berman DM, Kenyon NS, Ricordi C, Berggren PO, Caicedo A. The unique cytoarchitecture of human pancreatic islets has implications for islet cell function. *Proc Natl Acad Sci U S A*. 2006;103(7):2334-2339. doi:10.1073/pnas.0510790103
14. Atkinson MA, Eisenbarth GS. Type 1 diabetes: New perspectives on disease pathogenesis and treatment. *Lancet*. 2001;358(9277):221-229. doi:10.1016/S0140-6736(01)05415-0
15. Kahn, S., Cooper, M, Del Prato S. Pathophysiology and treatment of type 2 diabetes: perspectives on the past, present and future. *Lancet*. 2014;383(9922):1068-1083. doi:10.1201/9781420038798.sec2
16. Santamaria P. The Long and Winding Road to Understanding and Conquering Type 1 Diabetes. *Immunity*. 2010;32(4):437-445. doi:10.1016/j.immuni.2010.04.003
17. Weng J, Zhou Z, Guo L, et al. Incidence of type 1 diabetes in China, 2010-13: population based study. *BMJ*. 2018;360:j5295. doi:10.1136/bmj.j5295
18. Harjutsalo Valma, Sund Reijo, Knip Mikael GP-H. Incidence of Type 1 Diabetes in

Finland. *JAMA - J Am Med Assoc*. 2013;310(4):427-428. doi:10.1001/jama.2013.8739
19. Nistico L, Iafusco D, Galderisi A, et al. Emerging Effects of Early Environmental Factors over Genetic Background for Type 1 Diabetes Susceptibility : 2012;97(August):1483-1491. doi:10.1210/jc.2011-3457
20. Pociot F, Akolkar B, Concannon P, et al. Genetics of type 1 diabetes: What's next? *Diabetes*. 2010;59(7):1561-1571. doi:10.2337/db10-0076
21. Scott FW, Pound LD, Patrick C, Eberhard CE, Crookshank JA. Where genes meet environment—integrating the role of gut luminal contents, immunity and pancreas in type 1 diabetes. *Transl Res*. 2017;179:183-198. doi:10.1016/j.trsl.2016.09.001
22. Fløyel T, Kaur S, Pociot F. Genes Affecting β-Cell Function in Type 1 Diabetes. *Curr Diab Rep*. 2015;15(11). doi:10.1007/s11892-015-0655-9
23. Edamura K, Nasu K, Iwami Y, Ogawa H, Sasaki N, Ohgawara H. Effect of adhesion or collagen molecules on cell attachment, insulin secretion, and glucose responsiveness in the cultured adult porcine endocrine pancreas: A preliminary study. *Cell Transplant*. 2003;12(4):439-446. doi:10.3727/000000003108746867
24. Lysy PA, Weir GC, Bonner-Weir S. Concise Review : Pancreas Regeneration : Recent Advances and Perspectives. *Stem Cells Transl Med*. 2012;1:150-159.
25. Predieri B, Bruzzi P, Bigi E, et al. Endocrine disrupting chemicals and type 1 diabetes. *Int J Mol Sci*. 2020;21(8):1-21. doi:10.3390/ijms21082937
26. Stene LC, Rewers M. Immunology in the clinic review series; focus on type 1 diabetes and viruses: The enterovirus link to type 1 diabetes: Critical review of human studies. *Clin Exp Immunol*. 2012;168(1):12-23. doi:10.1111/j.1365-2249.2011.04555.x
27. Zhai N, Bidares R, Makoui MH, et al. Vitamin D receptor gene polymorphisms and the risk of the type 1 diabetes: A meta-regression and updated meta-analysis. *BMC Endocr Disord*. 2020;20(1):1-22. doi:10.1186/s12902-020-00575-8
28. Glaser N, Barnett P, McCaslin I et al. Risk factors for cerebral edema in children with diabetic Ketoacidosis. *N Engl J Med*. 2001;344(4):264-269.
29. Li S, Fant AL, McCarthy DM, Miller D, Craig J, Kontrick A. Gender Differences in Language of Standardized Letter of Evaluation Narratives for Emergency Medicine Residency Applicants. *AEM Educ Train*. 2017;1(4):334-339. doi:10.1002/aet2.10057
30. The Diabetes Control and Complications Trial Research Group. The Effect of Intensive Treatment of Diabetes on the Development and Progression of Long-term Complications In Insulin-Dependent Diabetes Mellitus. *N Engl J Med*. 1993;329(14):977-986.
31. Vergès B. Cardiovascular disease in type 1 diabetes: A review of epidemiological data and underlying mechanisms. *Diabetes Metab*. 2020;46:442-449. doi:10.1016/j.diabet.2020.09.001
32. Casqueiro Juliana, Casquerio Janine AC. Infections in patients with diabetes mellitus: A review of pathogenesis. *Indian J Endocrinol Metab*. 2012;16(Suppl1):S27-S36. doi:10.4103/2230-8210.94253
33. Banting FG, Best CH, Collip JB, Macleod JJR, Noble EC. The effect of pancreatic extract (insulin on normal rabbits. *Am J Physiol Content*. 1922;62(1):162-176.
34. Vargas E, Joy N, Sepulveda M. *Biochemistry, Insulin Metabolic Effects.* Treasure Island (FL): StatPearls Publishing; 2020. https://www.ncbi.nlm.nih.gov/books/NBK525983/.
35. Kathryn K. A history of insulin: from discovery to modern alternatives. *Br J Nurs*. 2003;12(19):1137-1141.
36. Wang Z, Thurmond DC. Mechanisms of biphasic insulin-granule exocytosis – roles of the

cytoskeleton, small GTPases and SNARE proteins. *J Cell Sci*. 2009;122:893-903. doi:10.1242/jcs.034355
37. Candido R, Wyne K, Romoli E. A Review of Basal-Bolus Therapy Using Insulin Glargine and Insulin Lispro in the Management of Diabetes Mellitus. *Diabetes Ther*. 2018;9(3):927-949. doi:10.1007/s13300-018-0422-4
38. Dissanayake WC, Sorrenson B, Shepherd PR. The role of adherens junction proteins in the regulation of insulin secretion. *Biosci Rep*. 2018;38(2):1-9. doi:10.1042/BSR20170989
39. Stettler C, Allemann S, Jüni P, et al. Glycemic control and macrovascular disease in types 1 and 2 diabetes mellitus: Meta-analysis of randomized trials. *Am Heart J*. 2006;152(1):27-38. doi:10.1016/j.ahj.2005.09.015
40. Ratzki-Leewing A, Harris SB, Mequanint S, et al. Real-world crude incidence of hypoglycemia in adults with diabetes: Results of the InHypo-DM Study, Canada. *BMJ Open Diabetes Res Care*. 2018;6(1). doi:10.1136/bmjdrc-2017-000503
41. Bosi E, Choudhary P, de Valk HW, et al. Efficacy and safety of suspend-before-low insulin pump technology in hypoglycaemia-prone adults with type 1 diabetes (SMILE): an open-label randomised controlled trial. *Lancet Diabetes Endocrinol*. 2019;7(6):462-472. doi:10.1016/S2213-8587(19)30150-0
42. Moscoso-Vasquez M, Colmegna P, Rosales N, Garelli F, Sanchez-Pena R. Control-Oriented Model with Intra-Patient Variations for an Artificial Pancreas. *IEEE J Biomed Heal Informatics*. 2020;24(9):2681-2689. doi:10.1109/JBHI.2020.2969389
43. Skyler JS. Prevention and reversal of type 1 diabetes-past challenges and future opportunities. *Diabetes Care*. 2015;38(6):997-1007. doi:10.2337/dc15-0349
44. Loretelli C, Assi E, Seelam AJ, Ben Nasr M, Fiorina P. Cell therapy for type 1 diabetes. *Expert Opin Biol Ther*. 2020;20(8):887-897. doi:10.1080/14712598.2020.1748596
45. Gruessner, Rainer, Sutherland D. *Transplantation of the Pancreas*. Vol 5.; 2004.
46. McCall M, Shapiro AMJ. Islet cell transplantation. *Semin Pediatr Surg*. 2014;23(2):83-90. doi:10.1053/j.sempedsurg.2014.03.006
47. PW W. Notes on diabetes treated with extract and by grafts of sheep's pancreas. *Br Med J*. 1894:1303–1304.
48. Shapiro A, Lakey J, Ryan E, et al. Islet Transplantation in seven patients with type 1 diabetes mellitus using a glucocorticoid-free immunosuppresive regimen. *N Engl J Med*. 2000;343(44):230-238.
49. Shapiro AMJ, Ricordi C, Hering BJ, et al. International trial of the Edmonton protocol for islet transplantation. *N Engl J Med*. 2006;355(13):1318-1330. doi:10.1056/NEJMoa061267
50. Hering BJ, Clarke WR, Bridges ND, et al. Phase 3 trial of transplantation of human islets in type 1 diabetes complicated by severe hypoglycemia. *Diabetes Care*. 2016;39(7):1230-1240. doi:10.2337/dc15-1988
51. Collaborative Islet Transplant Registry (CITR). CITR Tenth Annual Report. *https://citregistry.org/system/files/10th_AR.pdf*. 2017.
52. Robertson P. Islet transplantation as a treatment for diabetes— A Work in Progress. *N Engl J Med*. 2004;350(7):694-705. doi:10.1056/nejm200405133502022
53. Merani S, Toso C, Emamaullee J, Shapiro AMJ. Optimal implantation site for pancreatic islet transplantation. *Br J Surg*. 2008;95(12):1449-1461. doi:10.1002/bjs.6391
54. Pepper AR, Gala-Lopez B, Pawlick R, Merani S, Kin T, Shapiro AMJ. A prevascularized subcutaneous device-less site for islet and cellular transplantation. *Nat Biotechnol*.

2015;33(5):518-523. doi:10.1038/nbt.3211
55. Stokes RA, Cheng K, Lalwani A, et al. Transplantation sites for human and murine islets. *Diabetologia*. 2017;60(10):1961-1971. doi:10.1007/s00125-017-4362-8
56. Bottino R, Knoll MF, Knoll CA, Bertera S, Trucco MM. The future of islet transplantation is now. *Front Med*. 2018;5(JUL):1-13. doi:10.3389/fmed.2018.00202
57. Pepper AR, Bruni A, Shapiro AMJ. Clinical islet transplantation: Is the future finally now? *Curr Opin Organ Transplant*. 2018;23(4):428-439. doi:10.1097/MOT.0000000000000546
58. Abreu JRF, Roep BO. Immune monitoring of islet and pancreas transplant recipients. *Curr Diab Rep*. 2013;13(5):704-712. doi:10.1007/s11892-013-0399-3
59. Evgenov N V, Medarova Z, Dai G, Bonner-weir S, Moore A. In vivo imaging of islet transplantation. 2006;12(1):144-148. doi:10.1038/nm1316
60. Health Resources and Services Administration. Organdonor.gov. Published 2022. Accessed March 15, 2022.
61. Lablanche S, Borot S, Wojtusciszyn A, et al. Five-year metabolic, functional, and safety results of patients with type 1 diabetes transplanted with allogenic islets within the Swiss-French GRAGIL network. *Diabetes Care*. 2015;38(9):1714-1722. doi:10.2337/dc15-0094
62. Li X, Burlak C. Xenotransplantation literature update, March/April 2020. *Xenotransplantation*. 2020;27(3):1-3. doi:10.1111/xen.12607
63. Van Der Windt DJ, Bottino R, Kumar G, et al. Clinical islet xenotransplantation: How close are we? *Diabetes*. 2012;61(12):3046-3055. doi:10.2337/db12-0033
64. Goto M, Tjernberg J, Dufrane D, et al. Dissecting the instant blood-mediated inflammatory reaction in islet xenotransplantation. *Xenotransplantation*. 2008;15(4):225-234. doi:10.1111/j.1399-3089.2008.00482.x
65. Van Der Windt DJ, Bottino R, Casu A, Campanile N, Cooper DKC. Rapid loss of intraportally transplanted islets: An overview of pathophysiology and preventive strategies. *Xenotransplantation*. 2007;14(4):288-297. doi:10.1111/j.1399-3089.2007.00419.x
66. Lambris John, Ekdahl Kristina, Ricklin Daniela NB. *Immune Responses to Biosurfaces*.; 2015.
67. Mihalicz, D., Rajotte, RV. , & Rayat G. Porcine Islet Xenotransplantation for the Treatment of Type 1 Diabetes. In: *In (Ed.), Type 1 Diabetes - Pathogenesis, Genetics and Immunotherapy.* IntechOpen; 2011. doi:10.5772/22206
68. Rood PPM, Bottino R, Balamurugan AN, et al. Reduction of Early Graft Loss After Intraportal Porcine Islet Transplantation in Monkeys. *Transplantation*. 2007;83(2):202-210. doi:10.1097/01.tp.0000250680.36942.c6
69. Moberg L, Olsson A, Berne C, et al. Nicotinamide inhibits tissue factor expression in isolated human pancreatic islets: Implications for clinical islet transplantation. *Transplantation*. 2003;76(9):1285-1288. doi:10.1097/01.TP.0000098905.86445.0F
70. Jung DY, Park JB, Joo SY, et al. Effect of nicotinamide on early graft failure following intraportal islet transplantation. *Exp Mol Med*. 2009;41(11):782-792. doi:10.3858/emm.2009.41.11.084
71. Cabric S, Sanchez J, Lundgren T, et al. Islet surface heparinization prevents the instant blood-mediated inflammatory reaction in islet transplantation. *Diabetes*. 2007;56(8):2008-2015. doi:10.2337/db07-0358
72. Cooper D, Esker B, Tector AJ. Immunobiological barriers to Xenotransplantation. *Int J*

Surg. 2016;23(0 0):211-216. doi:10.1016/j.ijsu.2015.06.068.IMMUNOBIOLOGICAL
73. Lu T, Yang B, Wang R, Qin C. Xenotransplantation : Current Status in Preclinical Research. *Front Immunol*. 2020;10(January). doi:10.3389/fimmu.2019.03060
74. Cooper DKC, Good AH, Koren E, et al. Identification of α-galactosyl and other carbohydrate epitopes that are bound by human anti-pig antibodies: relevance to discordant xenografting in man. *Transpl Immunol*. 1993;1(3):198-205. doi:10.1016/0966-3274(93)90047-C
75. Cooper D, Human P, Lexer G, Al. E. Effects of cyclosporine and antibody adsorption on pig cardiac xenograft survival in the baboon. *J Heart Transplant*. 1988;7(3):238-246.
76. Phelps CJ, Koike C, Vaught TD, et al. Production of α1,3-Galactosyltransferase–Deficient Pigs. *Science (80-)*. 2003;299(5605):411-414. doi:10.1126/science.1078942.Production
77. Park CG, Shin JS, Min BH, Kim H, Yeom SC, Ahn C. Current status of xenotransplantation in South Korea. *Xenotransplantation*. 2019;26(1):1-11. doi:10.1111/xen.12488
78. Hering BJ, Wijkstrom M, Graham ML, et al. Prolonged diabetes reversal after intraportal xenotransplantation of wild-type porcine islets in immunosuppressed nonhuman primates. *Nat Med*. 2006;12(3):301-303. doi:10.1038/nm1369
79. Kirchhof N, Shibata S, Wijkstrom M, et al. Reversal of diabetes in non-immunosuppressed rhesus macaques by intraportal porcine islet xenografts precedes acute cellular rejection. *Xenotransplantation*. 2004;11(5):396-407. doi:10.1111/j.1399-3089.2004.00157.x
80. Cadili A, Kneteman N. The Role of Macrophages in Xenograft Rejection. *TPS*. 2008;40(10):3289-3293. doi:10.1016/j.transproceed.2008.08.125
81. Gill RG. Pancreatic islet xenotransplantation. *Autoimmunity*. 1993;15(s1):18-20. doi:10.3109/08916939309008855
82. Buhler L, Awwad M, Basker M, et al. High dose porcine hematopoietic cell transplantation combined with CD40 ligand blockade in baboons prevents and induced anti-pig humoral response. *Transplantation*. 2000;69(11):2296-2304.
83. Scalea J, Hanecamp I, Robson SC, Yamada K. T-cell-mediated immunological barriers to xenotransplantation. *Xenotransplantation*. 2012;19(1):23-30. doi:10.1111/j.1399-3089.2011.00687.x
84. Morris CF, Simeonovic CJ, Fung M, Wilson JD, Hapel AJ. Intragraft expression of cytokine transcripts during pig proislet xenograft rejection and tolerance in mice. *J Immunol*. 1995;154:2470-2482.
85. Purich K, Black A, Cai H, et al. MRI monitoring of transplanted neonatal porcine islets labeled with polyvinylpyrrolidone-coated superparamagnetic iron oxide nanoparticles in a mouse model. *Xenotransplantation*. 2022;(September 2021):1-16. doi:10.1111/xen.12720
86. Berney T, Toso C. Monitoring of the islet graft. *Diabetes Metab*. 2006;32(5 C2):503-512. doi:10.1016/s1262-3636(06)72803-8
87. Arifin DR, Bulte JWM. In Vivo Imaging of Pancreatic Islet Grafts in Diabetes Treatment. 2021;12(March):1-9. doi:10.3389/fendo.2021.640117
88. Estelrich J, Sanchez-Martin MJ, Busquets MA. Nanoparticles in magnetic resonance imaging : from simple to dual contrast agents. *Int J Nanomedicine*. 2015;10:1727-1741.
89. Juang J, Wang J, Shen C, et al. Magnetic Resonance Imaging of Transplanted Porcine Neonatal Pancreatic Cell Clusters Labeled with Chitosan-Coated Superparamagnetic Iron Oxide Nanoparticles in Mice. *Polymers (Basel)*. 2021;13.

90. Borot S, Crowe LA, Parnaud G, et al. Quantification of islet loss and graft functionality during immune rejection by 3-tesla MRI in a rat model. *Transplantation*. 2013;96(5):438-444. doi:10.1097/TP.0b013e31829b080f
91. Huang H, Xie Q, Kang M, et al. Labeling transplanted mice islet with polyvinylpyrrolidone coated superparamagnetic iron oxide nanoparticles for in vivo detection by magnetic resonance imaging. *Nanotechnology*. 2009;20(36). doi:10.1088/0957-4484/20/36/365101
92. Smith RM, Mandel TE. Pancreatic islet xenotransplantation: The potential for tolerance induction. *Immunol Today*. 2000;21(1):42-48. doi:10.1016/S0167-5699(99)01554-6
93. Cooper D, Ekser B, Tector J. A brief history of clinical xenotransplantation. *Int J Surg*. 2015;23:205-210. doi:10.1016/j.ijsu.2015.06.060.A
94. Ekser B, Cooper DKC, Tector AJ. The need for xenotransplantation as a source of organs and cells for clinical transplantation. *Int J Surg*. 2015;23:199-204. doi:10.1016/j.ijsu.2015.06.066
95. Weiss Michael, Steiner Donald PL. Insulin Biosynthesis, Secretion, Structure, and Structure-Activity Relationships. In: *Endotext [Internet]*. ; 2014. https://www.ncbi.nlm.nih.gov/books/NBK279029/.
96. Dhanasekaran M, George JJ, Loganaan G, et al. Pig islet xenotransplantation. *Curr Opin Organ Transplant*. 2017;22(5):452-462. doi:10.1097/MOT.0000000000000455
97. Hering BJ, Cooper DKC, Cozzi E, et al. The International Xenotransplantation Association consensus statement on conditions for undertaking clinical trials of porcine islet products in type 1 diabetes-Executive summary. *Xenotransplantation*. 2009;16(4):196-202. doi:10.1111/j.1399-3089.2009.00547.x
98. Hering BJ, Cozzi E, Spizzo T, et al. First update of the International Xenotransplantation Association consensus statement on conditions for undertaking clinical trials of porcine islet products in type 1 diabetes - Executive summary. *Xenotransplantation*. 2016;23(1):3-13. doi:10.1111/xen.12231
99. Samy K, Martin B, Turgeon N, Kirk A. Islet Cell Xenotransplantation: A Serious Look Towards the Clinic. *Xenotransplantation*. 2014;21(3):221-229. doi:10.1111/xen.12095.Islet
100. Dufrane D, Gianello P. Pig islet xenotransplantation into non-human primate model. *Transplantation*. 2008;86(6):753-760. doi:10.1097/TP.0b013e3181840f55
101. Liu Z, Hu W, He T, et al. Pig-to-primate islet xenotransplantation: Past, present, and future. *Cell Transplant*. 2017;26(6):925-947. doi:10.3727/096368917X694859
102. Shin JS, Kim JM, Kim JS, et al. Long-term control of diabetes in immunosuppressed nonhuman primates (NHP) by the transplantation of adult porcine islets. *Am J Transplant*. 2015;15(11):2837-2850. doi:10.1111/ajt.13345
103. Sgroi A, Bühler LH, Morel P, Sykes M, Noel L. International human xenotransplantation inventory. *Transplantation*. 2010;90(6):597-603. doi:10.1097/TP.0b013e3181eb2e8c
104. Groth CG, Korsgren O, Tibell A, Al. E. Transplantation of porcine fetal pancreas to diabetic patients. *Lancet*. 1994;344:1402-1404. doi:10.1007/s001090050325
105. Rood PPM, Cooper DKC. Islet xenotransplantation: Are we really ready for clinical trials? *Am J Transplant*. 2006;6(6):1269-1274. doi:10.1111/j.1600-6143.2006.01336.x
106. Organization WH. *Fifty-Seventh World Health Assembly Resolution WHA57.18*.; 2004.
107. Zhu HT, Yu L, Lyu Y, Wang B. Optimal pig donor selection in islet xenotransplantation: Current status and future perspectives. *J Zhejiang Univ Sci B*. 2014;15(8):681-691.

doi:10.1631/jzus.B1400120
108. Bellin MD, Dunn TB. Transplant strategies for type 1 diabetes: whole pancreas, islet and porcine beta cell therapies. *Diabetologia*. 2020;63(10):2049-2056. doi:10.1007/s00125-020-05184-7
109. Dufrane D, Gianello P. Pig islet for xenotransplantation in human: Structural and physiological compatibility for human clinical application. *Transplant Rev*. 2012;26(3):183-188. doi:10.1016/j.trre.2011.07.004
110. Shimoda M, Matsumoto S. Update regarding xenotransplantation in Japan. *Xenotransplantation*. 2019;26(1):1-4. doi:10.1111/xen.12491
111. Denner J. Why was PERV not transmitted during preclinical and clinical xenotransplantation trials and after inoculation of animals ? *Retrovirology*. 2018:1-9. doi:10.1186/s12977-018-0411-8
112. Moran C. Xenotransplantation: Benefits, risks and relevance of reproductive technology. *Theriogenology*. 2008;70(8):1269-1276. doi:10.1016/j.theriogenology.2008.06.019
113. Yang L, Güell M, Niu D, et al. Genome-wide inactivation of porcine endogenous retroviruses (PERVs). *Science (80-)*. 2015;350(6264):1101-1104. doi:10.1126/science.aad1191
114. Niu Dong, Wei Hong-Jiang LL et al. Inactivation of porcine endogenous retrovirus in pigs using CRISPR-Cas9, editorial commentary. *Science (80-)*. 2017;357:1303-1307. doi:10.1111/xen.12363
115. Morozov VA, Wynyard S, Matsumoto S, Abalovich A, Denner J, Elliott R. No PERV transmission during a clinical trial of pig islet cell transplantation. *Virus Res*. 2017;227:34-40. doi:10.1016/j.virusres.2016.08.012
116. Wynyard S, Nathu D, Garkavenko O, Denner J, Elliott R. Microbiological safety of the first clinical pig islet xenotransplantation trial in New Zealand. *Xenotransplantation*. 2014;21(4):309-323. doi:10.1111/xen.12102
117. Krüger L, Kristiansen Y, Reuber E, et al. A comprehensive strategy for screening for xenotransplantation-relevant viruses in a second isolated population of Göttingen minipigs. *Viruses*. 2019;12(1). doi:10.3390/v12010038
118. Wolf E, Kemter E, Klymiuk N, Reichart B. Genetically modified pigs as donors of cells, tissues, and organs for xenotransplantation. *Anim Front*. 2019;9(3):13-20. doi:10.1093/af/vfz014
119. Rayat GR, Johnson ZA, Beilke JN, Korbutt GS, Rajotte R V, Gill RG. The Degree of Phylogenetic Disparity of Islet Grafts Dictates the Reliance on Indirect CD4 T-Cell Antigen Recognition for Rejection. :1433-1440.
120. Meda P. Protein-Mediated Interactions of Pancreatic Islet Cells. *Scientifica (Cairo)*. 2013;2013:1-22. doi:10.1155/2013/621249
121. Steiner DJ, Kim A, Miller K, Hara M. Pancreatic islet plasticity: Interspecies comparison of islet architecture and composition Donald. *Islets*. 2010;2(3):135-145.
122. Halban PA, Powers SL, George KL, Bonner-Weir S. Spontaneous reassociation of dispersed adult rat pancreatic islet cells into aggregates with three-dimensional architecture typical of native islets. *Diabetes*. 1987;36(7):783-790. doi:10.2337/diab.36.7.783
123. Kim A, Miller K, Jo J, Kilimnik G, Wojcik P. Islet architecture:A comparative study. *Islets*. 2009;1(2):129-136. doi:doi:10.4161/isl.1.2.9480.
124. Wieczorek G, Pospischil A, Perentes E. A comparative immunohistochemical study of

pancreatic islets in laboratory animals (rats, dogs, minipigs, nonhuman primates). *Exp Toxicol Pathol*. 1998;50(3):151-172. doi:10.1016/S0940-2993(98)80078-X
125. Brereton MF, Vergari E, Zhang Q, Clark A. Alpha-, Delta- and PP-cells: Are They the Architectural Cornerstones of Islet Structure and Co-ordination? *J Histochem Cytochem*. 2015;63(8):575-591. doi:10.1369/0022155415583535
126. Jansson L, Barbu A, Bodin B, et al. Pancreatic islet blood flow and its measurement. *Ups J Med Sci*. 2016;121(2):81-95. doi:10.3109/03009734.2016.1164769
127. Citro A, Ott HC. Can We Re-Engineer the Endocrine Pancreas? *Curr Diab Rep*. 2018;18(11):1-7. doi:10.1007/s11892-018-1072-7
128. Geron E, Boura-Halfon S, Schejter ED, Shilo BZ. The Edges of Pancreatic Islet β Cells Constitute Adhesive and Signaling Microdomains. *Cell Rep*. 2015;10(3):317-325. doi:10.1016/j.celrep.2014.12.031
129. Takeichi Masatoshi. The cadherins: Cell-cell adhesion molecules controlling animal morphogenesis. *Development*. 1988;102(4):639-655.
130. Johansson JK, Voss U, Kesavan G, et al. N-cadherin is dispensable for pancreas development but required for β-cell granule turnover. *Genesis*. 2010;48(6):374-381. doi:10.1002/dvg.20628
131. Wakae-Takada N, Xuan S, Watanabe K, Meda P, Leibel RL. Molecular basis for the regulation of islet beta cell mass in mice: The role of E-cadherin. *Diabetologia*. 2013;56(4):856-866. doi:10.1007/s00125-012-2824-6
132. Bosco D, Rouiller DG, Halban PA. Differential expression of E-cadherin at the surface of rat β-cells as a marker of functional heterogeneity. *J Endocrinol*. 2007;194(1):21-29. doi:10.1677/JOE-06-0169
133. Parnaud G, Lavallard V, Bedat B, et al. Cadherin engagement improves insulin secretion of single human β-cells. *Diabetes*. 2015;64(3):887-896. doi:10.2337/db14-0257
134. Dahl U, Sjödin A, Semb H. Cadherins regulate aggregation of pancreatic β-cells in vivo. *Development*. 1996;122(9):2895-2902.
135. Gottardi CJ, Gumbiner BM. Adhesion signaling: How β-catenin interacts with its partners. *Curr Biol*. 2001;11(19):792-794. doi:10.1016/S0960-9822(01)00473-0
136. Hartsock A, Nelson J. Adherens and Tight Junctions: Structure, Function and Connections to the Actin Cytoskeleton. *Biochim Biophys Acta*. 2008;1778(3):660-669. doi:10.1016/j.bbamem.2007.07.012.Adherens
137. Nelson WJ. Regulation of cell-cell adhesion by the cadherin-catenin complex. *Biochem Soc Trans*. 2008;36(2):149-155. doi:10.1042/BST0360149
138. Takeichi M. Dynamic contacts: rearranging adherens junctions to drive epithelial remodelling. *Nat Rev Mol Cell Biol*. 2014;15:397. https://doi.org/10.1038/nrm3802.
139. Jaques F, Tomas A, Prost A, et al. Dual Effect of Cell-Cell Contact Disruption on Cytosolic. 2008;149(5):2494-2505. doi:10.1210/en.2007-0974
140. Yamagata K, Nammo T, Moriwaki M, et al. Overexpression of Dominant-Negative Mutant Hepatocyte Nuclear Factor-1 in Pancreatic B-Cells Causes Abnormal Islet Architecture With DecreasedExpression of E-Cadherin, Reduced B-cell Proliferation and Diabetes. *Diabetes*. 2002;51:114-123.
141. Carvell MJ, Marsh PJ, Persaud SJ, Peter M. Cellular Physiology and Biochemistr y Biochemistry E-cadherin Interactions Regulate Proliferation in Islet-like Structures β -Cell. 2007.
142. Giannotta M, Trani M, Dejana E. VE-cadherin and endothelial adherens junctions: Active

guardians of vascular integrity. *Dev Cell*. 2013;26(5):441-454. doi:10.1016/j.devcel.2013.08.020
143. Bentley K, Franco CA, Philippides A, et al. The role of differential VE-cadherin dynamics in cell rearrangement during angiogenesis. *Nat Cell Biol*. 2014;16(4):309-321. doi:10.1038/ncb2926
144. Falcão VTFL, Maschio DA, de Fontes CC, et al. Reduced insulin secretion function is associated with pancreatic islet redistribution of cell adhesion molecules (CAMs) in diabetic mice after prolonged high-fat diet. *Histochem Cell Biol*. 2016;146(1):13-31. doi:10.1007/s00418-016-1428-5
145. Rorsman P, Braun M. Regulation of insulin secretion in human pancreatic islets. *Annu Rev Physiol*. 2013;75(August 2012):155-179. doi:10.1146/annurev-physiol-030212-183754
146. Rorsman P, Ashcroft FM, Trube G. Single Ca channel currents in mouse pancreatic B-cells. *Pflügers Arch Eur J Physiol*. 1988;412(6):597-603. doi:10.1007/BF00583760
147. Rorsman P, Eliasson L, Renström E, Gromada J, Barg S, Göpel S. The cell physiology of biphasic insulin secretion. *News Physiol Sci*. 2000;15(2):72-77. doi:10.1152/physiologyonline.2000.15.2.72
148. Ashcroft F, Harrison D, Ashcroft S. Glucose induces closure of single potassium channels in isolated rat pancreatic p-cells. *Nature*. 1984;312:446-448.
149. Kalwat MA, Thurmond DC. Signaling mechanisms of glucose-induced F-actin remodeling in pancreatic islet β cells. *Exp Mol Med*. 2013;45(8). doi:10.1038/emm.2013.73
150. Pittman ME, Brunt EM. Anatomic Pathology of Hepatocellular Carcinoma: Histopathology Using Classic and New Diagnostic Tools. *Clin Liver Dis*. 2015;19(2):239-259. doi:10.1016/J.CLD.2015.01.003
151. Swanston-Flatt SK, Carlsson L, Gylfe E. Actin filament formation in pancreatic B-cells during glucose stimulation of insulin secretion. *FEBS Lett*. 1980;117(I):299-302.
152. McCulloch LJ, van de Bunt M, Braun M, Frayn KN, Clark A, Gloyn AL. GLUT2 (SLC2A2) is not the principal glucose transporter in human pancreatic beta cells: Implications for understanding genetic association signals at this locus. *Mol Genet Metab*. 2011;104(4):648-653. doi:10.1016/j.ymgme.2011.08.026
153. Gould GW, Holmant GD. The glucose transporter family : structure , function and tissue-specific expression. 1993;295:329-341.
154. Nolan CJ, Prentki M. The islet β-cell: fuel responsive and vulnerable. *Trends Endocrinol Metab*. 2008;19(8):285-291. doi:10.1016/j.tem.2008.07.006
155. De Vos A, Heimberg H, Quartier E, et al. Human and rat beta cells differ in glucose transporter but not in glucokinase gene expression. *J Clin Invest*. 1995;96(5):2489-2495. doi:10.1172/JCI118308
156. Kramer J, Moeller EL, Hachey A, Mansfield KG WL. Differential expression of GLUT2 in pancreatic islets and kidneys of New and Old World nonhuman primates. *Am J Physiol Regul Integr Comp Physiol*. 2009;296(3):R786-R793. doi:10.1152/ajpregu.90694.2008
157. Graham ML, Mutch LA, Rieke EF, et al. Refining the high-dose streptozotocin-induced diabetic non-human primate model: An evaluation of risk factors and outcomes. *Exp Biol Med*. 2011;236(10):1218-1230. doi:10.1258/ebm.2011.011064
158. Zuo J, Huang Z, Zhi A, et al. Cloning and distribution of facilitative glucose transporter 2 (SLC2A2) in pigs. *Asian-Australasian J Anim Sci*. 2010;23(9):1159-1165. doi:10.5713/ajas.2010.90551

159. Dufrane D, Van Steenberghe M, Guiot Y, Goebbels RM, Saliez A, Gianello P. Streptozotocin-induced diabetes in large animals (pigs/primates): Role of GLUT2 transporter and β-cell plasticity. *Transplantation*. 2006;81(1):36-45. doi:10.1097/01.tp.0000189712.74495.82
160. Asahara S, Shibutani Y, Teruyama K, et al. Ras-related C3 botulinum toxin substrate 1 (RAC1) regulates glucose-stimulated insulin secretion via modulation of F-actin. *Diabetologia*. 2013;56(5):1088-1097. doi:10.1007/s00125-013-2849-5
161. Hall A. Rho GTPases and the Actin Cytoskeleton. 1998;279(January).
162. Ridley AJ. Rho GTPases and actin dynamics in membrane protrusions and vesicle trafficking. *Trends Cell Biol*. 2006;16(10):522-529. doi:10.1016/j.tcb.2006.08.006
163. Nozaki S, Ueda S, Takenaka N, Kataoka T, Satoh T. Role of RalA downstream of Rac1 in insulin-dependent glucose uptake in muscle cells. *Cell Signal*. 2012;24(11):2111-2117. doi:10.1016/j.cellsig.2012.07.013
164. Ueda S, Kataoka T, Satoh T. Activation of the small GTPase Rac1 by a specific guanine-nucleotide-exchange factor suffices to induce glucose uptake into skeletal-muscle cells. *Biol Cell*. 2008;100(11):645-661. doi:10.1042/bc20070160
165. Li J, Luo R, Kowluru A, Li GD. Novel regulation by Rac1 of glucose- and forskolin-induced insulin secretion in INS-1 β-cells. *Am J Physiol - Endocrinol Metab*. 2004;286(5 49-5):818-827. doi:10.1152/ajpendo.00307.2003
166. Wang Z, Oh E, Thurmond DC. Glucose-stimulated Cdc42 signaling is essential for the second phase of insulin secretion. *J Biol Chem*. 2007;282(13):9536-9546. doi:10.1074/jbc.M610553200
167. Song SJ, Wang QC, Jia RX, Cui XS, Kim NH, Sun SC. Inhibition of Rac1 GTPase activity affects porcine oocyte maturation and early embryo development. *Sci Rep*. 2016;6(September):1-9. doi:10.1038/srep34415
168. Ducummon CC, Berger T. Localization of the Rho GTPases and some Rho effector proteins in the sperm of several mammalian species. *Zygote*. 2006;14(3):249-257. doi:10.1017/S0967199406003790
169. Söllner T, Bennett MK, Whiteheart SW, Scheller RH, Rothman JE. A protein assembly-disassembly pathway in vitro that may correspond to sequential steps of synaptic vesicle docking, activation, and fusion. *Cell*. 1993;75(3):409-418. doi:10.1016/0092-8674(93)90376-2
170. Wheeler B, Sheu L, Beaudoin R, et al. Characterization of SNARE Protein Expression in p Cell Lines and Pancreatic Islets. *Endocrinology*. 1996;137(4):1340-1348.
171. Rizo J, Südhof TC. Snares and munc18 in synaptic vesicle fusion. *Nat Rev Neurosci*. 2002;3(8):641-653. doi:10.1038/nrn898
172. Scales SJ, Chen YA, Yoo BY, Patel SM, Doung YC, Scheller RH. SNAREs contribute to the specificity of membrane fusion. *Neuron*. 2000;26(2):457-464. doi:10.1016/S0896-6273(00)81177-0
173. Söllner T, Whiteheart SW, Brunner M, et al. SNAP receptors implicated in vesicle targeting and fusion. *Nature*. 1993;362(March):318-323.
174. Liang T, Qin T, Kang F, et al. SNAP23 depletion enables more SNAP25/calcium channel excitosome formation to increase insulin exocytosis in type 2 diabetes. *JCI Insight*. 2020;5(3). doi:10.1172/jci.insight.129694
175. Rouiller DG, Cirulli V, Halban PA. Uvomorulin mediates calcium-dependent aggregation of islet cells, whereas calcium-independent cell adhesion molecules distinguish between

islet cell types. *Dev Biol*. 1991;148(1):233-242. doi:10.1016/0012-1606(91)90332-W
176. Andersen DK. The practical importance of recognizing pancreaticogenic or type 3c diabetes. *Diabetes Metab Res Rev*. 2012;28:326-328. doi:10.1002/dmrr.2285
177. Wang P, Schuetz C, Vallabhajosyula P, et al. Monitoring of allogeneic islet grafts in nonhuman primates using magnetic resonance imaging. *Transplantation*. 2015;99(8):1574-1581. doi:10.1016/j.physbeh.2017.03.040
178. Gray DW r., Titus N, Badet L. Islet cell transplantation for insulin-dependent diabetes mellitus: Perspectives from the present and prospects for the future. *Expert Rev Mol Med*. 2000;2(6):1-28. doi:10.1017/S1462399400001861
179. Pileggi A, Ricordi C, Alessiani M, Inverardi L. Factors influencing islet of Langerhans graft function and monitoring. *Clin Chim Acta*. 2001;310(1):3-16. doi:10.1016/S0009-8981(01)00503-4
180. Emamaullee JA, Shapiro AMJ. Factors influencing the loss of β-cell mass in islet transplantation. *Cell Transplant*. 2007;16(1):1-8. doi:10.3727/000000007783464461
181. Sakata N, Yoshimatsu G, Tsuchiya H, et al. Imaging of transplanted islets by positron emission tomography, magnetic resonance imaging, and ultrasonography. *Islets*. 2013;5(5):179-187. doi:10.4161/isl.26980
182. Paty BW, Bonner-Weir S, Laughlin MR, McEwan AJ, Shapiro AMJ. Toward development of imaging modalities for islets after transplantation: Insights from the National Institutes of Health workshop on beta cell imaging. *Transplantation*. 2004;77(8):1133-1137. doi:10.1097/01.TP.0000113231.90613.0E
183. Evgenov N V., Medarova Z, Pratt J, et al. In vivo imaging of immune rejection in transplanted pancreatic islets. *Diabetes*. 2006;55(9):2419-2428. doi:10.2337/db06-0484
184. Thorek DLJ, Chen AK, Czupryna J, Tsourkas A. Superparamagnetic iron oxide nanoparticle probes for molecular imaging. *Ann Biomed Eng*. 2006;34(1):23-38. doi:10.1007/s10439-005-9002-7
185. Arbab AS, Wilson LB, Ashari P, Jordan EK, Lewis BK, Frank JA. A model of lysosomal metabolism of dextran coated superparamagnetic iron oxide (SPIO) nanoparticles: Implications for cellular magnetic resonance imaging. *NMR Biomed*. 2005;18(6):383-389. doi:10.1002/nbm.970
186. Jung MJ, Lee SS, Hwang YH, et al. MRI of transplanted surface-labeled pancreatic islets with heparinized superparamagnetic iron oxide nanoparticles. *Biomaterials*. 2011;32(35):9391-9400. doi:10.1016/j.biomaterials.2011.08.070
187. Delcroix GJR, Jacquart M, Lemaire L, et al. Mesenchymal and neural stem cells labeled with HEDP-coated SPIO nanoparticles: In vitro characterization and migration potential in rat brain. *Brain Res*. 2009;1255:18-31. doi:10.1016/j.brainres.2008.12.013
188. Kriz J, Jirak D, Berkova Z, et al. Detection of pancreatic islet allograft impairment in advance of functional failure using magnetic resonance imaging. *Transpl Int*. 2012;25(2):250-260. doi:10.1111/j.1432-2277.2011.01403.x
189. Malosio ML, Esposito A, Brigatti C, et al. MR imaging monitoring of iron-labeled pancreatic islets in a small series of patients: Islet fate in successful, unsuccessful, and autotransplantation. *Cell Transplant*. 2015;24(11):2285-2296. doi:10.3727/096368914X684060
190. Jirák D, Kríz J, Herynek V, et al. MRI of transplanted pancreatic islets. *Magn Reson Med*. 2004;52(6):1228-1233. doi:10.1002/mrm.20282
191. Wang P, Goodwill PW, Pandit P, et al. Magnetic particle imaging of islet transplantation

in the liver and under the kidney capsule in mouse models. *Quant Imaging Med Surg*. 2018;8(2):114-122. doi:10.21037/qims.2018.02.06
192. Toso C, Vallee JP, Morel P, et al. Clinical magnetic resonance imaging of pancreatic islet grafts after iron nanoparticle labeling. *Am J Transplant*. 2008;8(3):701-706. doi:10.1111/j.1600-6143.2007.02120.x
193. Kim SH, Kim H, Park KS, Moon WK. Evaluation of porcine pancreatic islets transplanted in the kidney capsules of diabetic mice using a clinically approved super paramagnetic iron oxide (SPIO) and a 1.5t MR scanner. *Korean J Radiol*. 2010;11(6):673-682. doi:10.3348/kjr.2010.11.6.673
194. Juang JH, Shen CR, Wang JJ, et al. Magnetic Resonance Imaging of Mouse Islet Grafts Labeled with Novel Chitosan-Coated Superparamagnetic Iron Oxide Nanoparticles. *PLoS One*. 2013;8(4). doi:10.1371/journal.pone.0062626
195. Ris F, Lepetit-Coiffe M, Meda P, et al. Assessment of human islet labeling with clinical grade iron nanoparticles prior to transplantation for graft monitoring by MRI. *Cell Transplant*. 2010;19(12):1573-1585. doi:10.3727/096368910X515863
196. Saudek F, Jirák D, Girman P, et al. Magnetic resonance imaging of pancreatic islets transplanted into the liver in humans. *Transplantation*. 2010;90(12):1602-1606. doi:10.1097/TP.0b013e3181ffba5e
197. Kriz J, Jirák D, Girman P, et al. Magnetic resonance imaging of pancreatic islets in tolerance and rejection. *Transplantation*. 2005;80(11):1596-1603. doi:10.1097/01.tp.0000183959.73681.b9
198. Ryan EA, Paty BW, Senior PA, et al. Five-year follow-up after clinical islet transplantation. *Diabetes*. 2005;54(7):2060-2069. doi:10.2337/diabetes.54.7.2060
199. Alejandro R, Barton FB, Hering BJ, Wease S. 2008 Update from the collaborative islet transplant r. *Transplantation*. 2008;86(12):1783-1788. doi:10.1097/TP.0b013e3181913f6a
200. MacKenzie DA, Hullett DA, Sollinger HW. Xenogeneic transplantation of porcine islets: An overview. *Transplantation*. 2003;76(6):887-891. doi:10.1097/01.TP.0000087114.18315.17
201. Emamaullee JA, Shapiro AMJ, Rajotte R V., Korbutt G, Elliott JF. Neonatal porcine islets exhibit natural resistance to hypoxia-induced apoptosis. *Transplantation*. 2006;82(7):945-952. doi:10.1097/01.tp.0000238677.00750.32
202. Korbutt GS, Elliott JF, Ao Z, Smith DK, Warnock GL, Rajotte R V. Large scale isolation, growth, and function of porcine neonatal islet cells. *J Clin Invest*. 1996;97(9):2119-2129. doi:10.1172/JCI118649
203. Joo HT, Foster P, Rosales A, et al. Imaging islets labeled with magnetic nanoparticles at 1.5 Tesla. *Diabetes*. 2006;55(11):2931-2938. doi:10.2337/db06-0393
204. Rayat GR, Gill RG. Indefinite survival of neonatal porcine islet xenografts by simultaneous targeting of LFA-1 and CD154 or CD45RB. *Diabetes*. 2005;54(2):443-451. doi:10.2337/diabetes.54.2.443
205. Arefanian H, Tredget EB, Rajotte R V., Gill RG, Korbutt GS, Rayat GR. Short-term administrations of a combination of anti-LFA-1 and anti-CD154 monoclonal antibodies induce tolerance to neonatal porcine islet xenografts in mice. *Diabetes*. 2010;59(4):958-966. doi:10.2337/db09-0413
206. Arefanian H, Tredget EB, Rajotte R V., Korbutt GS, Gill RG, Rayat GR. Combination of anti-CD4 with anti-LFA-1 and anti-CD154 monoclonal antibodies promotes long-term survival and function of neonatal porcine islet xenografts in spontaneously diabetic NOD

mice. *Cell Transplant*. 2007;16(8):787-798. doi:10.3727/000000007783465244
207. Zhang B, Jiang B, Chen Y, et al. Detection of viability of transplanted beta cells labeled with a novel contrast agent - Polyvinylpyrrolidone-Coated superparamagnetic iron oxide nanoparticles by magnetic resonance imaging. *Contrast Media Mol Imaging*. 2012;7(1):35-44. doi:10.1002/cmmi.461
208. Smood B, Bottino R, Hara H, Cooper DKC. Is the renal subcapsular space the preferred site for clinical porcine islet xenotransplantation? Review article. *Int J Surg*. 2019;69(July):100-107. doi:10.1016/j.ijsu.2019.07.032
209. Zacharovová K, Berková Z, Jirák D, et al. Processing of superparamagnetic iron contrast agent ferucarbotran in transplanted pancreatic islets. *Contrast Media Mol Imaging*. 2012;7(6):485-493. doi:10.1002/cmmi.1477
210. Osch MJP Van, Webb AG, Static Á. Safety of Ultra-High Field MRI : What are the Specific Risks ? 2014. doi:10.1007/s40134-014-0061-0
211. Weissleder R, Stark DD, Engelstad BL, et al. Superparamagnetic iron oxide: Pharmacokinetics and toxicity. *Am J Roentgenol*. 1989;152(1):167-173. doi:10.2214/ajr.152.1.167
212. Itescu S, Kwiatkowski P, Artrip JH, et al. Role of natural killer cells, macrophages, and accessory molecule interactions in the rejection of pig-to-primate xenografts beyond the hyperacute period. *Hum Immunol*. 1998;59(5):275-286. doi:10.1016/S0198-8859(98)00026-3
213. Huo Q, Zhou M, Cooper DKC, Dai Y, Xie N, Mou L. Circulating miRNA or circulating DNA—Potential biomarkers for organ transplant rejection. *Xenotransplantation*. 2019;26(1):1-12. doi:10.1111/xen.12444
214. Zhou M, Lu Y, Zhao C, et al. Circulating pig-specific DNA as a novel biomarker for monitoring xenograft rejection. *Xenotransplantation*. 2019;26(4):1-12. doi:10.1111/xen.12522
215. Dinnyes A, Schnur A, Muenthaisong S, et al. Integration of nano- and biotechnology for beta-cell and islet transplantation in type-1 diabetes treatment. *Cell Prolif*. 2020;53(5):1-9. doi:10.1111/cpr.12785
216. Hering BJ, Wijkstrom M, Graham ML, et al. intraportal xenotransplantation nonhuman primates. 2006;12(3):301-303. doi:10.1038/nm1369
217. Cardona K, Russell M, Badell IR, et al. CD40-Specific Costimulation Blockade Enhances. doi:10.1111/j.1600-6143.2011.03509.x
218. Coe TM, Markmann JF, Rickert CG. Current status of porcine islet xenotransplantation. *Curr Opin Organ Transplant*. 2020;25(5):449-456. doi:10.1097/MOT.0000000000000794
219. Mueller KR, Balamurugan AN, Cline GW, et al. Differences in glucose-stimulated insulin secretion in vitro of islets from human, nonhuman primate, and porcine origin. *Xenotransplantation*. 2013;20(2):75-81. doi:10.1111/xen.12022
220. Kim S, Whitener RL, Peiris H, et al. Molecular and genetic regulation of pig pancreatic islet cell development. 2020. doi:10.1242/dev.186213
221. Lamb M, Laugenour K, Liang O, Alexander M, Iii CEF, Lakey JRT. In Vitro Maturation of Viable Islets From Partially Digested Young Pig Pancreas. 2014;23(714):263-272. doi:10.3727/096368912X662372
222. Jia D, Dajusta D, Foty RA. Tissue Surface Tensions Guide In Vitro Self- Assembly of Rodent Pancreatic Islet Cells. 2007;(June):2039-2049. doi:10.1002/dvdy.21207
223. Jain R, Lammert E. Cell – cell interactions in the endocrine pancreas. 2009;11:159-167.

doi:10.1111/j.1463-1326.2009.01102.x
224. Dufrane D, Goebbels RM, Fdilat I, Guiot Y, Gianello P. Impact of Porcine Islet Size on Cellular Structure and Engraftment After Transplantation Adult Versus Young Pigs. *Pancreas*. 2005;30(2):138-147.
225. Strober W. Trypan Blue Exclusion Test of Cell Viability. 2015;(November):3-5. doi:10.1002/0471142735.ima03bs111
226. Bustin SA, Benes V, Garson JA, et al. The MIQE Guidelines : M inimum I nformation for Publication of Q uantitative Real-Time PCR E xperiments SUMMARY : 2009;622:611-622. doi:10.1373/clinchem.2008.112797
227. Vandesompele J, Preter K De, Poppe B, Roy N Van, Paepe A De. Accurate normalization of real-time quantitative RT -PCR data by geometric averaging of multiple internal control genes. *Genome Biol*. 2002;3(7).
228. Bonner-Weir S. The islets of Langerhans continue to reveal their secrets. *Nat Rev Endocrinol*. 2020;16(2):73-74. doi:10.1038/s41574-019-0296-1
229. Rafati S, Le C, Rajotte R V, Rayat GR. Cell Separation , Perfusion from Tissue , Organelle Fractionation A Comparison of the Methods Used for Porcine Islet Isolation for Transplantation as a Treatment for Type 1 Diabetes Mellitus. 2012;3:33-51. doi:10.1016/B978-0-12-381373-2.10067-5
230. Montesano R, Mouron P, Amherdt M, Orci L. Collagen matrix promotes reorganization of pancreatic endocrine cell monolayers into islet-like organoids. *J Cell Biol*. 1983;97(3):935-939. doi:10.1083/jcb.97.3.935
231. Pipeleers D, Maes E, Winkel MVANDE. Glucose-induced insulin release depends on functional cooperation between islet cells Cell Biology : 1982;79(December):7322-7325.
232. Stützer I, Esterházy D, Stoffel M. The pancreatic beta cell surface proteome. 2012:1877-1889. doi:10.1007/s00125-012-2531-3
233. Cirulli V, Baetens D, Rutishauser U, Halban PA, Orci L, Rouiller DG. Expression of neural cell adhesion molecule (N-CAM) in rat islets and its role in islet cell type segregation. 1994;1436:1429-1436.
234. Esni F, Täljedal I, Perl A, Cremer H, Christofori G, Semb H. Neural Cell Adhesion Molecule (N-CAM) Is Required for Cell Type Segregation and Normal Ultrastructure in Pancreatic Islets. 1999;144(2):325-337.
235. Mullin AE, Soukatcheva G, Verchere CB, Chantler JK. Application of in situ ductal perfusion to facilitate isolation of high-quality RNA from mouse pancreas. 2006:617-620. doi:10.2144/000112146
236. Fleige S, Pfaffl MW. RNA integrity and the effect on the real-time qRT-PCR performance. 2006;27:126-139. doi:10.1016/j.mam.2005.12.003
237. Butler AE, Matveyenko A V, Kirakossian D, et al. microdissected human and rodent pancreas Recovery of high-quality RNA from laser capture microdissected human and rodent pancreas. 2016;8885. doi:10.1080/01478885.2015.1106073
238. ThermoFisher Scientific I. *Qubit ™ RNA IQ Assay Kits, User Guide*.; 2017.
239. ThermoFisher Scientific I. *Qubit RNA IQ Assay : A Fast and Easy Fluorometric RNA Quality Assessment*.; 2018.
240. ThermoFisher Scientific I. Fast, reliable detection of viable RNA.
241. Hao JC, Salem N, Peng X, Kelly RB, Bennett MK. Effect of Mutations in Vesicle-Associated Membrane Protein (VAMP) on the Assembly of Multimeric Protein Complexes. 1997;17(5):1596-1603.

242. Poirier MA, Hao JC, Malkus PN, et al. Protease Resistance of Syntaxin SNAP-25-VAMP Complexes. *J Biol Chem*. 1998;273(18):11370-11377. doi:10.1074/jbc.273.18.11370
243. Rogers GJ, Hodgkin MN, Squires PE. Cellular Physiology and Biochemistr y Biochemistry E-Cadherin and Cell Adhesion : a Role in Architecture and Function in the Pancreatic Islet. 2007:0-7.
244. Kelly C, Mcclenaghan NH, Flatt PR, et al. Role of islet structure and cellular interactions in the control of insulin secretion. *Islets*. 2011;3(2):41-47. doi:10.4161/isl.3.2.14805
245. Konstantinova I, Nikolova G, Ohara-imaizumi M, et al. EphA-Ephrin-A-Mediated b Cell Communication Regulates Insulin Secretion from Pancreatic Islets. 2007:359-370. doi:10.1016/j.cell.2007.02.044
246. Orsulic S, Kemler R. Expression of Eph receptors and ephrins is differentially regulated by. 2000;1802:1793-1802.